NTNU – Trondheim
Norwegian University of
Science and Technology

Metal-producing Mechanisms in the Carbothermic Silicon Process

Jørund Vangskåsen

Materials Science and Engineering
Submission date: June 2012
Supervisor: Merete Tangstad, IMTE

Norwegian University of Science and Technology
Department of Materials Science and Engineering

I hereby declare that this work has been carried out independently and in compliance with the examination regulations of the Norwegian University of Science and Technology, NTNU.

Jørund Vangskåsen

Trondheim, June 2012

Preface

This master thesis has been written as a part of the evaluation in the course TMT 4905. It is the final course of a five year long journey at NTNU in Trondheim. A lot of good memories have accumulated throughout the time spent with the class of 2012 at materials science and technology.

This master thesis would not be the same without the cooperation with SINTEF, by letting me investigate their remains of a pilot scale furnace for silicon production. I wish to thank my supervisor Merete Tangstad, not only for the support during the master work, but also as a good mentor and rolemodel during the time here at NTNU. The exchange of knowledge as well as the social activities with the ReSiNa group has been really useful. I hope that this tradition where master student get to interact with the PhD students will become a tradition for years to come.

At last I wish to thank the fellow students in my class for a eventful and memorable time at the universtity.

Jørund Vangskåsen

Trondheim, June 2012

Abstract

The mechanisms in the carbothermic production of silicon have been examined in this report. Through the investigation of a pilot scale furnace as well as five small scale induction furnace experiments, a better understanding of this comlex process has been obtained. Especially the silicon producing reactions and mechanisms have been studied.

Samples of all raw material as they travelled downwards in the pilot scale furnace was investigated along with samples from the induction furncace. SiO gas formed in the hot zone (∼2000 °C) travelled upwards and deposited as a condensate mixture of SiO_2 and Si. In the pilot scale furnace this condensate went back down with raw material as the furnace was stoked or the raw materials slowly melted. The condensate decomposed as the temperatures increased; silicon accumulated and escaped from the SiO_2-matrix in the condensate.

A typical experiment conducted in the induction furnace had a specific power consumption of roughly 62 MWh per ton silicon produced, far more than normal industrial power consumption of 11-13 MWh per ton Si produced. The material consumption (SiO_2+SiC) was very low for temperatures below 1820 °C as no SiO gas was produced. At 1900 °C, 9.6 % of the initial charge mass had been consumed. The consumption increased to 13.8 % when the temperature was raised to 1980 °C and further to 15.0 % at 2000 °C. The reaction rate between SiO_2 and SiC increased significantly from 1980 °C to 2000 °C.

Mass balance demonstrated that just over half of the silicon produced were left in the silicon pool in the bottom of the crucible. ∼44% of the total amount had to end up as silicon particles in the condensate deposited in the upper portion of the crucible.

The main silicon producing reaction is: $SiO(g) + SiC(s) = 2Si(s,l) + CO(g)$, but the findings in this thesis have shown that the perspiration of silicon from the condensate is very important. A significant contribution to the total amount of silicon produced can therefore come from the following reaction: $2SiO(g) = SiO_2(s,l) + Si(s,l)$

Compression tests have been made on the agglomerate caused by the deposits of condensate (SiO_2+Si). The compression strength varied from 115 to 396 MPa. Samples exposed to temperatures above 1670 °C had the lowest strenght, while those exposed to lower temperatures were the strongest.

Sammendrag

Den karbotermiske produksjonsprosessen og dens mekanismer har blitt etterforsket i denne rapporten. Gjennomgående undersøkelser av en pilot-skala silisiumovn samt fem små-skala induksjonseksperimenter har blitt gjennomført for å bedre kunnskapen om denne komplekse prosessen. Spesielt har produksjonsmekanismene og reaksjonene blitt studert.

Prøver av råmaterialer som bevegde nedover i pilot-skala forsøket ble analysert sammen med prøver fra induksjonsforsøkene. SiO-gass som ble produsert i den varme delen av ovnene (∼2000 °C) steg oppover og avla seg som et kondensat bestående av SiO_2 og Si. Kondensatet fulgte med råmaterialene nedover i pilot-forsøket etter at ovnen ble staket, eller når råmaterialene gradvis smeltet. Når temperaturen økte, dekomponerte kondensatet seg, slik at silisiumet akkumulerte og forsvant fra den omliggende SiO_2-strukturen.

Et typisk induksjonsforsøk resulterte i et energiforbruk på ca. 62 MWh per tonn silisium produsert, mye mer enn normalt forbruk industrielt sett som ligger rundt 11-13 MWh per ton Si produsert. Forbruket av råmaterialene (SiO_2+SiC) var veldig lavt ved temperaturer under 1820 °C, og SiO-gass ble ikke produsert. Rundt 1900 °C, hadde 9.6 % av den opprinnelige tilstatsen av materiale blitt konsumert. Konsumet økte til 13.8 % når temperaturen ble økt til 1980 °C og videre til 15.0 % ved 2000 °C. Reaksjonshastigheten for SiO_2 og SiC hadde en signifikant økning fra 1980 °C til 2000 °C.

Massebalanse viste at drøyt halvparten av den produserte massen med silisium var å finne i metallbadet nederst i digelen. Den andre knappe halvdelen var dermed forventet å befinne seg som silisium partikler i kondensatet som ble avsatt i de øvre delene av digelen.

$SiO(g) + SiC(s) = 2Si(s,l) + CO(g)$ er den viktigste silisiumproduserende reaksjonen, men funnene i denne oppgaven har vist at utsvetting av silisium fra kondensatet også spiller en viktig rolle. Reaksjonen: $2SiO(g) = SiO_2(s,l) + Si(s,l)$ kan derfor bidra med en vesentlig andel av totalt produsert silisium.

Kompresjonstester har blitt utført på materialet som har blitt sementert av kondensat (SiO_2+Si). Trykkfastheten varierte fra 115 til 396 MPa. Prøvene eksponert for temperaturer over 1670 °C hadde lavest trykkfasthet, mens de eksponert for lavere temperaturer hadde høyest fasthet.

Contents

Chapter 1

Introduction

Metallurgical grade silicon (MG-Si) consists of approximately 98% silicon, and this thesis will mainly be focused on the production process of this kind of metal. Industrial MG-Si is produced in submerged arc furnaces, where the power input can be as high as 45 MW. Good supply of cheap electrical energy has made Norway one of the leading stars of this energy demanding process.

To get a better understanding of any process, it is essential to understand every singel part of it. The carbothermic production of silicon is a very energy demanding and complex process with unknown reaction mechanisms and many intermediate reactions. The complexity of this process has made it keep many of its secrets from the industry, even though a lot of research has been made. This work is part of the "ReSiNa" project under the auspices of SINTEF and NTNU in Trondheim, Norway. The project is mainly funded by the Research Council of Norway and deals with the process from quartz to silicon.

Crust formation due to condensate in the upper part of the furnace, and the silicon producing reactions and mechanisms are examples of topics which this thesis will deal with. A pilot scale furnace experiment as well as five small scale induction furnace experiments have been conducted and investigated to put light on these issues.

One of the three main objectives of this thesis has been to reveal some of the secrets concerning the silicon producing reactions. This includes the traditionally well known reaction where SiO gas reacts with SiC and forms Si metal and CO gas, but also the less invastigated mechanism, where Si perspire from the condensate (Si + SiO_2) produced in the upper parts of the furnace and ends up in the metal bath. The second objective was to find the temperature dependence of the reaction between SiO_2 and SiC. Finally, the last objective was to examine the crust formation in the furnace mainly caused by this aforementioned condensate which is a mixture of Si and SiO_2.

Observations during the induction furnace experiments, SEM studies of the samples taken from the furnaces, as well as compression strength tests have been examined in this work to reveal some of the secrets which the metallurgical silicon process is holding on to.

Chapter 2

Theory

2.1 General

The metallurgical production of silicon is a high temperature process where quartz (SiO_2) is reduced with carbon (C) to silicon (Si) and carbon monoxide gas (CO(g)). Typical consumption of electrical energy is 11-13 MWh per ton silicon metal produced. A full description of the process can be seen in Schei et al. (2000). The overall reaction of the process can be written as: (The $\triangle H$ values are from HSC (2012)).

$$SiO_2(s,l) + 2C(s) = Si(l) + 2CO(g) \qquad \triangle H_{2000^\circ C} = 687 \text{ kJ/mol} \qquad (1)$$

The total description of the process involves many intermediate reactions, and complicates the situation significantly from what reaction (1) describes. The internals of a submerged arc silicon furnace can be divided into a high and low temperature zone, where different reactions dominates. A description of the different zones in the silicon process is displayed in figure 2.1.

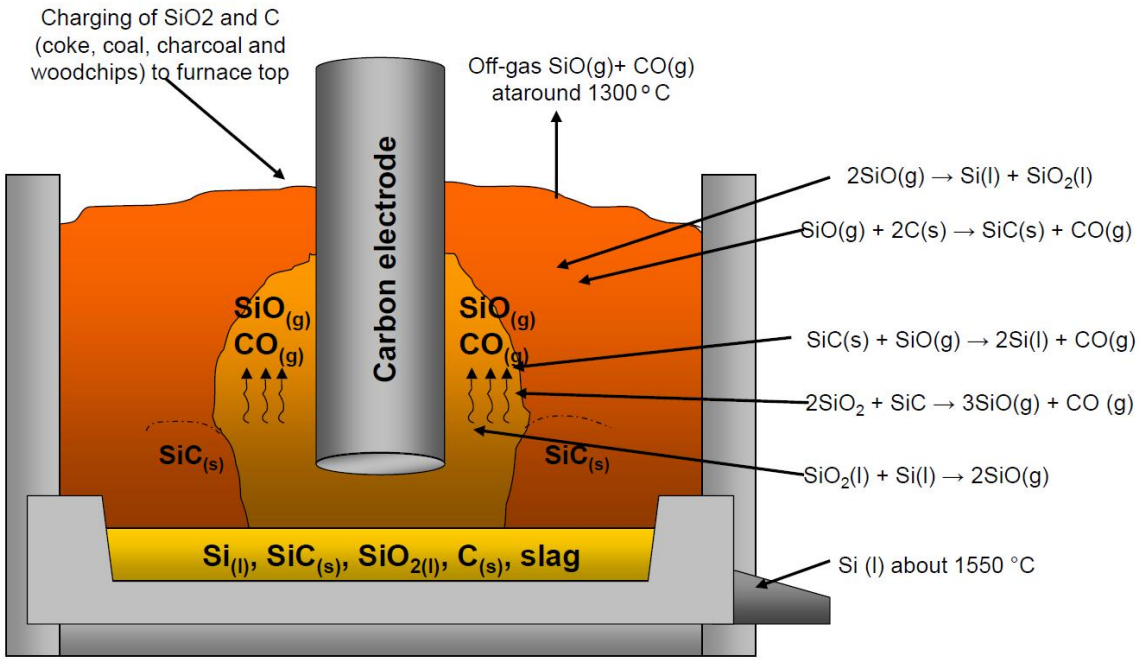

Figure 2.1: Sketch of the silicon furnace with important reactions. (Kvande 2008)

The following three ractions (2), (3) and (4) occurs in the lower parts of the furnace, where the temperature of the condensed phases is around 2000 °C.

$$2SiO_2(s,l) + SiC(s) = 3SiO(g) + CO(g) \qquad \triangle H_{2000^\circ C} = 1364 \text{ kJ/mol} \qquad (2)$$

$$SiO_2(s,l) + Si(s,l) = 2SiO(g) \qquad \triangle H_{2000^\circ C} = 599 \text{ kJ/mol} \qquad (3)$$

$$SiO(g) + SiC(s) = 2Si(s,l) + CO(g) \qquad \triangle H_{2000^\circ C} = 167 \text{ kJ/mol} \qquad (4)$$

The slowest of these three reactions are probably the strongly endothermic silicon monoxide gas (SiO(g)) producing reactions (2) and (3) and consume most of the heat from the furnace. As seen in figure 2.2 a high SiO content in the gas is necessary to produce silicon through reaction (4).

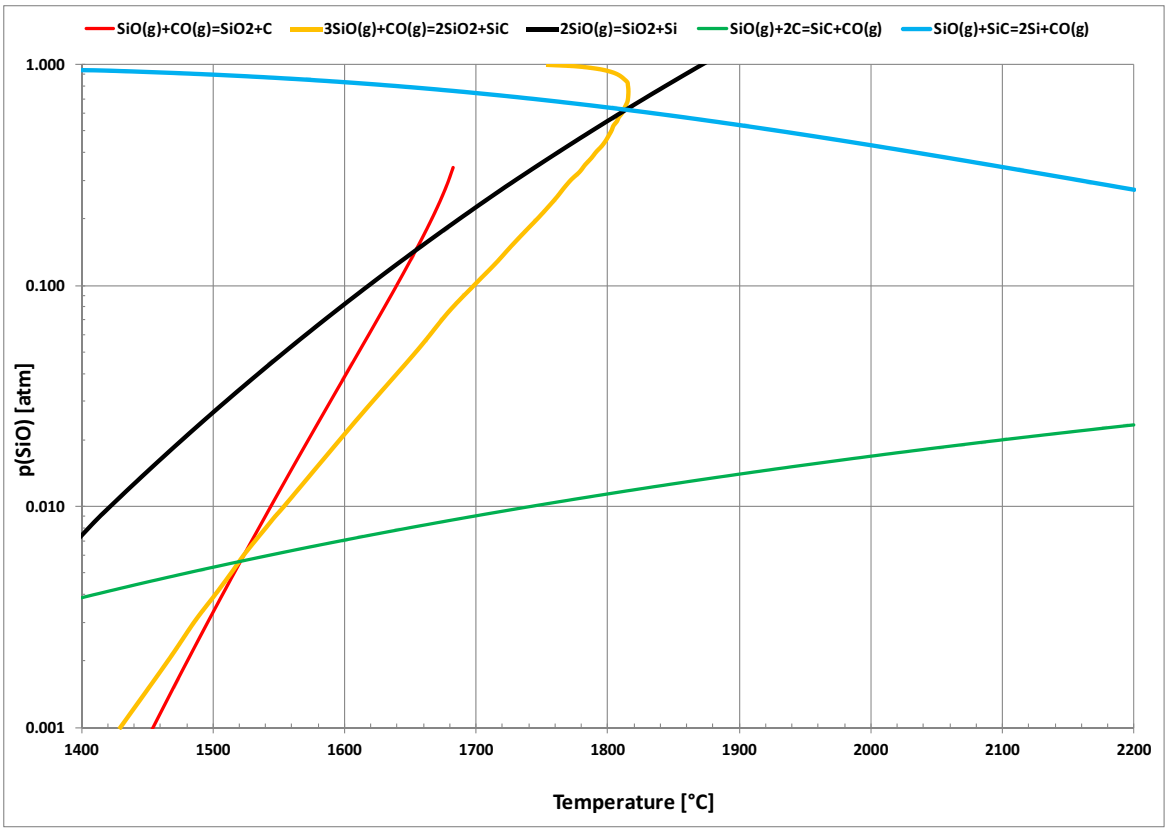

Figure 2.2: Partial pressure of SiO(g) in equilibrium with SiO_2, SiC and C. Total pressure of SiO(g) and CO(g) are 1 atm. (HSC Chemistry 6.1)

The reaction between SiO_2 and C (reaction (5)) goes through the CO-CO_2 system. The intermediate reactions are: $SiO_2 + CO(g) = SiO(g) + CO_2(g)$ and $CO_2(g) + C(s) = 2CO(g)$ with the expected overall reaction:

$$SiO_2(s,l) + C(s) = SiO(g) + CO(g) \qquad \triangle H_{2000^\circ C} = 643 \text{ kJ/mol} \qquad (5)$$

This reaction will run until the SiO pressure is sufficient to produce SiC, and then SiO reacts with C according to reaction (6).

The SiO gas produced from the high temperature zone is travelling upwards through the charge and reacts either with carbon material (reaction (6)) or condenses through reaction (-2) or (-3). Figure 2.2 show that (-2) are thermodynamically more favourable than (-3), but practical observations show that reaction (-3) dominates. This may beacause of the slow kinetics of reaction (-2) where four gas molecules have to collide. Condensation of SiO gas occurs generally below 1811 °C according to figure 2.2. Reaction (6) will go to the right only at temperatures above 1535 °C. Below this temperature, SiO gas will only be recovered by reaction (-2) or (-3).

$$SiO(g) + 2C(s) = SiC(s) + CO(g) \qquad \triangle H_{1800^\circ C} = \text{-78 kJ/mol} \qquad (6)$$

$$3SiO(g) + CO(g) = 2SiO_2(s,l) + SiC(s) \qquad \triangle H_{1800^\circ C} = \text{-1380 kJ/mol} \qquad (-2)$$

$$2SiO(g) = SiO_2(s,l) + Si(s,l) \qquad \triangle H_{1800^\circ C} = \text{-606 kJ/mol} \qquad (-3)$$

The condensate producing reactions (-2) and (-3) are strongly heat-producing, and are the main factor how heat is transported upwards in the furnace. Measurements in industrial furnaces have shown that the temperatures in the top charge layer can reach ∼1300 °C . Reaction (-3) will for 1300 °C have an equilibrium pressure of SiO below 0.01 atm, giving Si losses to off-gas less than one 1%. This results in a theoretical Si yield of more than 99%, significantly higher than the typical industrial Si yield of 80-90%. Non equilibrium conditions are therefore considered to dominate at the furnace top. (Ringdalen & Tangstad 2012)

Andersen (2010) investigated in his master thesis the kinetics for reaction (2) and (3). The rate of reaction (2) (between SiO_2 and SiC) was generally faster than reaction (3) (between SiO_2 and Si) in the temperature range from 1450 °C to 2000 °C. He discovered that the rate of reaction (3) dropped significantly after the melting of SiO_2(˜1725 °C) and stayed nearly constant for a fairly long temperature range. The reaction rates for these two reactions are graphically presented in figure 2.3.

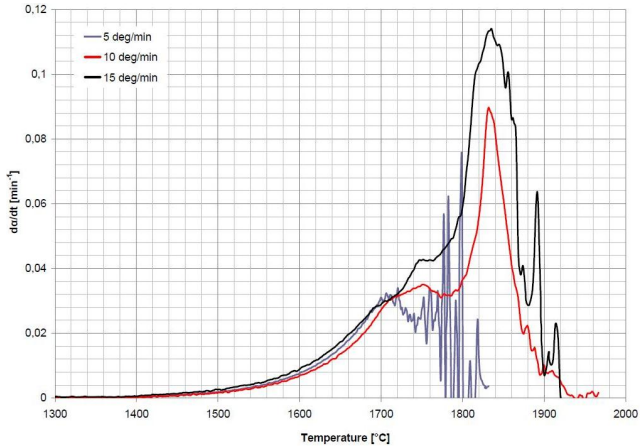

(a) Rate of conversion of SiO_2 + SiC mixture versus temperature.

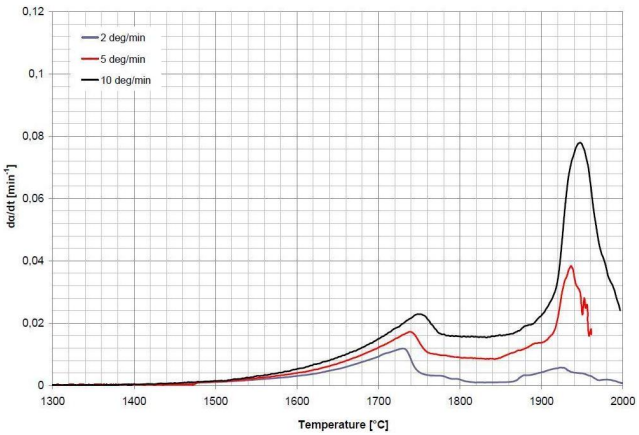

(b) Rate of conversion of SiO_2 + Si mixture versus temperature.

Figure 2.3: Conversion rates of the reactants used in Andersen's experiments. (Andersen 2010)

2.2 Condensate formation

CO(g) and SiO(g) produced in the inner zone will travel upwards to the colder outer zone of the furnace. To ensure a high Si-yield in the process, SiO(g)-recovery is imperative. Recovery of SiO(g) can occur either by reaction with free C in the cold zone (reaction (6)) or by condensation of SiO(g) when the temperature is below 1800°C. The condensation reactions in the system are the reverse of reaction (2) and (3). Reaction (-2) carries more heat to the outer zone per mole SiO than reaction (-3), and the gasified condensate is less efficient in producing Si since it contains CO. The most favourable mechanism for recovery of SiO(g) through condensation would therefore be reaction (-3).

$$3SiO(g) + CO(g) = 2SiO_2(s,l) + SiC(s) \tag{-2}$$

$$2SiO(g) = SiO_2(s,l) + Si(s,l) \tag{-3}$$

The amount of SiO(g) that can be recovered is limited because the condensation reaction is exothermic, which in turn may raise the temperature above the condensation temperature. The remaining SiO(g) will pass through the charge and burn above it producing amorphous silica. The product of reaction (-3) is a mixture of Si and SiO_2. In this mixture, Si droplets will agglomerate and fall down from the SiO_2 on the cavity roof. The inner zone consists of a gas-filled cavity with a solid roof. With carbon-deficiency we may observe a complete vaporization of SiO_2 through reaction (2) and (3). But normally a cave-in or a stoking of the furnace will interrupt the reaction before it completes so that more SiO_2 is added to the hot zone. (Schei et al. 2000)

Excavations of 50kW furnaces done by Schei et al. in the 1960s, lead to the discovery of a dense, brown substance which glued the the upper charge layers together. This substance was after further investigations in electron microscope identified as Si droplets in a SiO_2 matrix. On the outer surface of the brown layer there was also found a green substance, which was identified as SiC in a SiO_2 matrix. Schei pointed out that reaction (-2) and (-3) are very important for describing the thermodynamics of SiO(g)-condensation.

Tangstad et al. (2010) described what they called white and brown condensate in their report. A sample covered with condensate was investigated in the electron probe micro-analyzer (EPMA). The sample had been extracted from the cooler parts of a crucible held at 1600°C for 60 minutes. A 15 kVA induction furnace was used in this experiment. The condensate was divided into a white and a brown layer. The white condensate was closest to the substrate particles, and the brown condensate was layered outside of this. The brown condensate appeared as spherical metal droplets of diameter between 0.1µm and 0.5µm in a matrix assumed to be SiO_2. The difference in silicon particle size can be seen in figure 2.4.

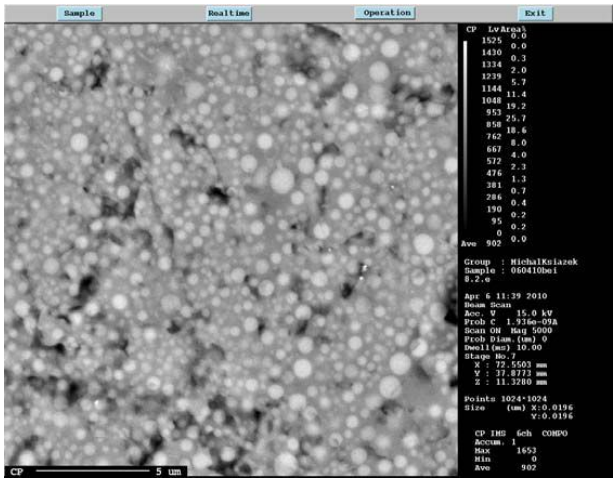

(a) Brown condesate (next to the white condesate)

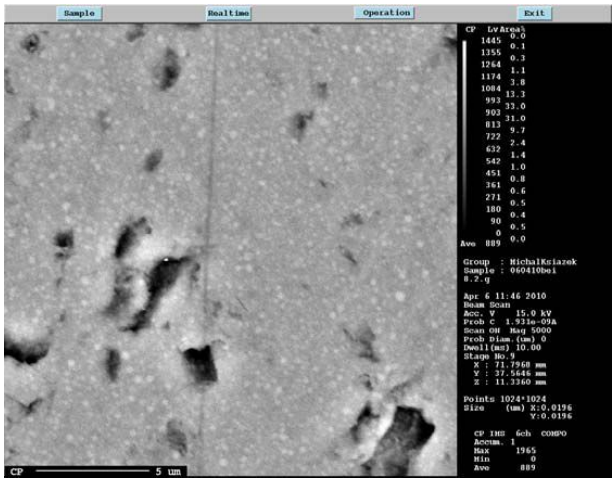

(b) The outer brown condensate

Figure 2.4: Comparison of size between the condensate formed first relative to the condensate formed last. (Tangstad & Ksiazek 2010)

Different shades of brown condensate could be seen. The white condensate was more or less homogenous; no silicon particles could be spotted. The reason for this can either be resolution limitations of the electron probe micro-analyzer (EPMA), or that the silicon has reacted with CO gas to form SiO and SiC. The white condensate were investigated in the EPMA, and they found that the average molar ratio $\frac{Si}{O}$ was equal to 0.67. (Tangstad & Ksiazek 2010)

Mølnås (2010) performed experiments using the vertical tube furnace, and observed pale-blue condensate in addition to the brown and white condensate as seen in figure 2.5. The pale-blue condensate is similar to the white, and can on some particles, particularly SiC, be found as a thin layer closest to the particle. In addition he found that condensate formed at ∼1100 °C contained ∼50% crystalline polymorphs of SiO_2 and SiC. Condensate formed in the temperature area ∼1311 °C to ∼1434 °C did not contain SiC. There was expected a transition zone between the two reaction regimes (reaction -2 and -3) between 1100 °C and 1300 ^{o}C.

(a) White and blue condensate formed at temperatures between 1100°C and 1430°C.

(b) Brown and white condensate formed at ∼1650^{o}C.

Figure 2.5: Condensate types observed by Mølnås (2010).

Vangskåsen & Høgsand (2011) found in their report that the white condensate contained more carbon than the brown. This carbon will be in the form of SiC, indicating that reaction -2 is more active for the white condensate. The brown condensate will mainly be a product of reaction (-3). They investigated the element distribution of the brown and white condensate taken from four different samples. The data was obtained by EPMA and is presented in table 2.1. From these results, the following $\frac{Si}{O}$ molar ratios could be calculated:

- $\frac{Si}{O}_{brown} = \frac{42.2}{47.1} = 0.90$
- $\frac{Si}{O}_{white} = \frac{36.6}{46.9} = 0.78$

Table 2.1: Element distribution in the condensate types. (Vangskåsen & Høgsand 2011)

(a) Brown condensate.

	Si	O	C	Tot
wt%	60.8	38.7	6.6	105.5
at%	42.2	47.1	10.7	100

(b) White condensate.

	Si	O	C	Tot
wt%	53.7	39.2	10.5	103.4
at%	36.6	46.9	16.7	100.2

An image illustrating the distribution of C, O and Si in the condensate layer is shown in figure 2.6. Different color gradients gives the relative content for each element. Blue represent low amount and purple high. The white condensate is next to the SiC particle on the inside of the brown condensate. The brown condensate was most likely produced by gas created at temperatures around 2000 ^{o}C. The white condensate on the other hand was probably created by gas produced at lower temperatures during initial heating of the crucible. (Vangskåsen & Høgsand 2011)

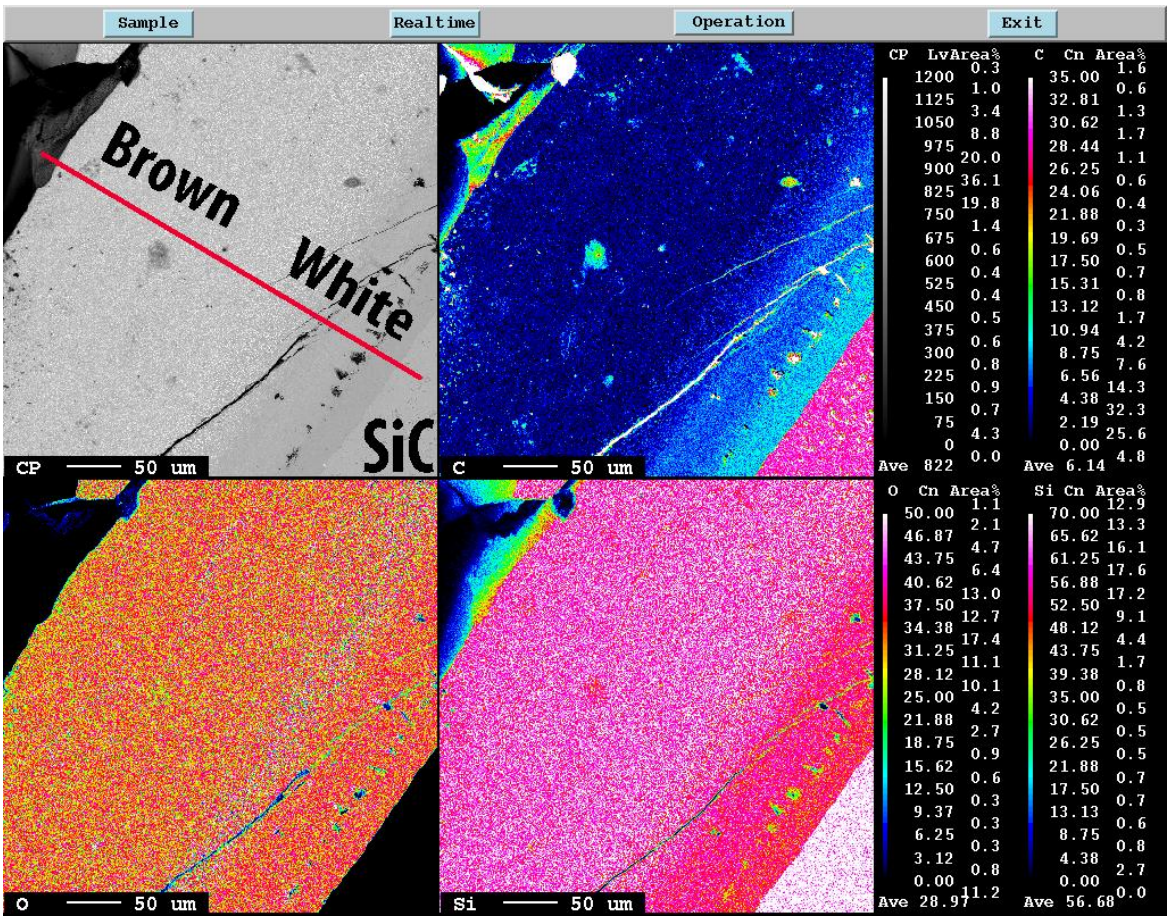

Figure 2.6: EPMA mapping of the condensate products layered next to a SiC particle in the charge. (Vangskåsen & Høgsand 2011)

In addition, Vangskåsen & Høgsand did some topographic investigations on the different condensate types. This resulted in many interesting SEM-images, several types of structures could be observed. In figure 2.7 the topography of both white and brown condensate can be seen.

The latest work on this condensate formation was made int the fall of 2011 by Vangskåsen (2011*a*). The report confirmed that that the brown condensate is mainly a product of reaction (-3) and the white condensate corresponds to reaction (-2). The different condensates were studied in the EPMA, and gave the following $\frac{Si}{O}$ molar ratios:

- $\frac{Si}{O}_{brown} = 1.014 \iff \frac{Si}{O}_{reaction(-3)} = 1$
- $\frac{Si}{O}_{white} = 0.764 \iff \frac{Si}{O}_{reaction(-2)} = 0.75$

The measured values fitted well with the values from the reaction products from reactions (-2) and (-3). Hence, the brown condensate consisted of SiO_2 and Si, while the white consisted of SiO_2 and SiC.

By using a sessile drop furnace, Vangskåsen also found that the silicon in the brown condensate melted away from the surrounding SiO_2 at temperatures above 1395 °C. The separation of silicon happened most rapidly above ∼1700 °C. The remaining amorphous SiO_2 retained its shape up to the maximum temperature of the furnace at about 1850 °C and showed no signs of melting. The remaining SiO_2 of the heat-treated brown condensate changed color to pale grey, which somewhat resembled the white condensate. The white condensate behaved different, it softened at 1515 °C and eventually melted to a round lump at 1850 °C. The difference between the brown and white condensate can be seen in figure 2.8 and figure 2.9 (Vangskåsen 2011*a*)

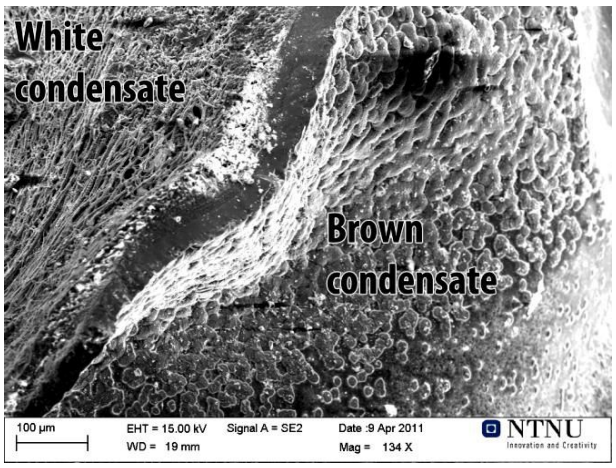

Figure 2.7: Transition zone between white and brown condensate. (Vangskåsen & Høgsand 2011)

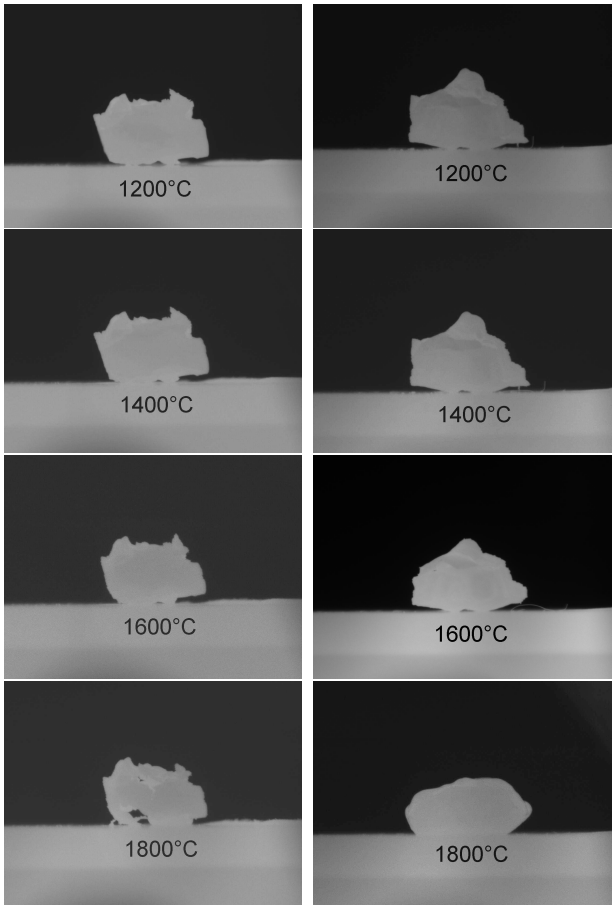

Figure 2.8: Heating of brown condensate

Figure 2.9: Heating of white condensate

2.3 Dynamics of the inner structure

A description of the structure of a silicon furnace shortly before it is ripe for stoking is displayed in figure 2.10. Schei et al. (2000) stated that the electrode in a submerged arc furnace is surrounded by a gas-filled cavity. The bottom of the cavity consists of a slurry of molten Si and SiC, and possibly a layer of relatively pure Si. SiC crystals are sintered along the furnace lining, creating a solid wall along the sides. Highly viscous SiO_2 (silica) may flow down these walls and react with the SiC.

SiO gas flowing upwards through the charge will condense according to reaction (-3) and create a sticky layer gluing the particles together. The condensate mixture of Si and SiO_2 will form a roof above the cavity, and the charge is then consumed from below as the quartz melts and sink down with other materials. The size of the cavity increases gradually. When cavity roof has lost its ability to capture SiO gas, it is time to stoke the furnace. The operator breaks it down and fills the furnace up with new charge. The process will then repeat itself.

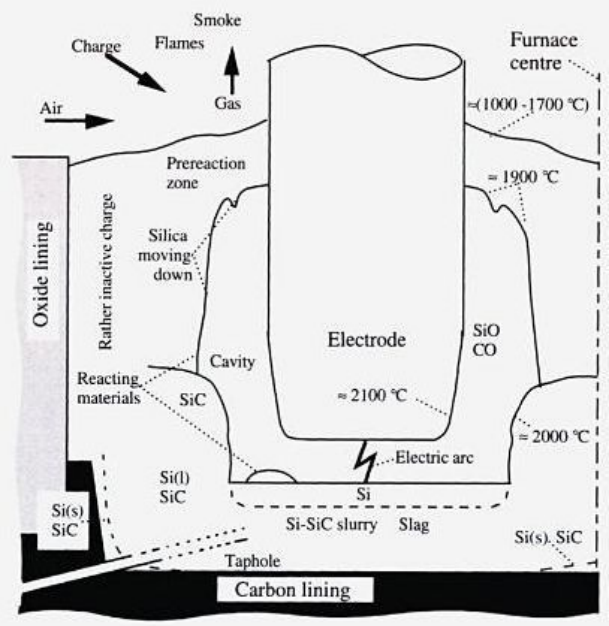

Figure 2.10: The inner structure of a submerged arc furnace, producing silicon metal. The image represents the internals of a furnace shortly before stoking. (Schei et al. 2000)

The stoking interval is somewhere between 30 and 75 minutes industrially. Crust formation due to condensation of SiO gas can be a big problem, and may hinder the stoking process. (Schei et al. 2000) Furnace stoking will create new equilibrium conditions, but it is not established how quickly these new conditions are established.

The silicon process is based on non-equilibrium conditions. Therefore, understanding the reaction mechanisms and kinetics is critical in understanding the Si recovery process. (Ringdalen & Tangstad 2012)

Optimally the $\frac{C}{SiO_2}$ molar ratio in the charge will be 2, and in accordance with the overall reaction $SiO_2 + 2C = Si + 2CO$. In operation with excess C in the charge, the surplus will be deposited as SiC. This situation is known as overcoking, and can be described by the reaction: $SiO_2 + 3C = SiC + 2CO$. Undercoking occurs if the charge consists of insuffiecent amounts of C, and can be represented by the reaction: $SiO_2 + C = SiO + CO$. This will cause the furnace to produce a lot of gas.

Through eight small scale induction furnace experiments, Vangskåsen (2011*b*) studied the dynamics of the cavity inside a silicon furnace. The cross-sections from the experiments are displayed in figure 2.11. The raw materials were SiO_2 and SiC in crucible 1 to 5, while the last three had additions of respectively coke, coal and woodchips to imitate an industrial furnace. The temperature in the crucibles was approximately 2000°C for each experiment (measured in the bottom). The holding times varied from 10 to 40 minutes in the order from left to right among the first five crubles.

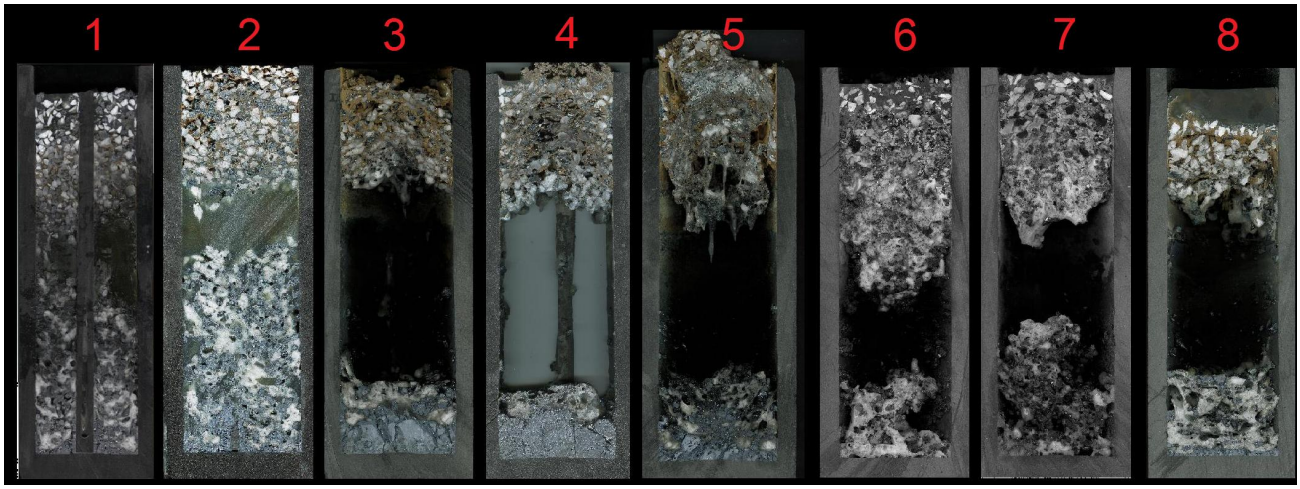

Figure 2.11: Cross-sections from eight small scale induction furnace experiments simulating the silicon process. (Vangskåsen 2011*b*)

Cavities were formed in the crucibles where the charge had been consumed, and the interesting factor was that the cavity roof was positioned in approximately the same height in all experiments. Deposits of condensate glued the charge in the upper part of the crucible together. The material beneath this point will melt and sink down and ultimatelly be consumed in the hottest part of the furnace. A description of this dynamic process is illustrated in figure 2.12.

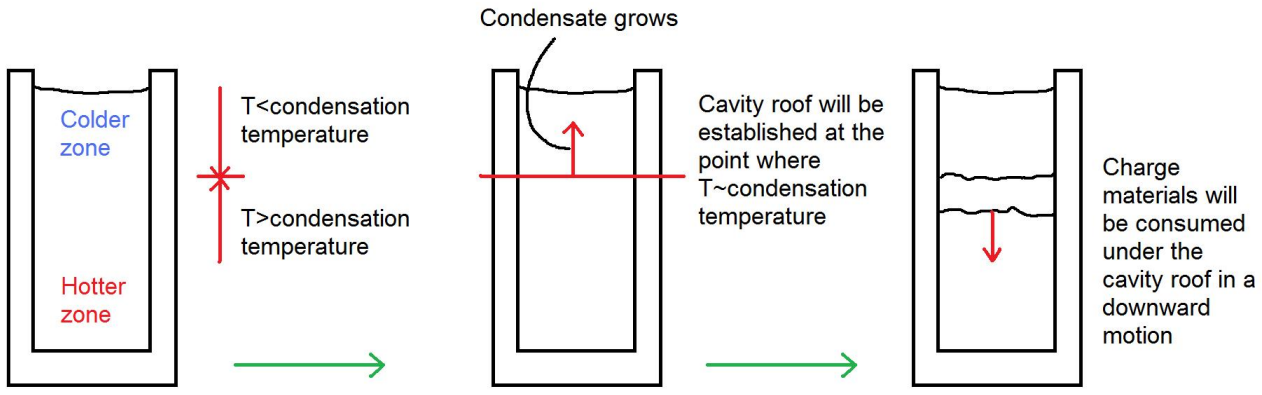

Figure 2.12: Dynamics of the cavity formation in the silicon process. (Vangskåsen 2011*b*)

2.4 Industrial excavation at Finnfjord AS

In April 2009 a submerged arc furnace producing FeSi75 was excavated at Finnfjord AS. The furnace stopped during normal operating procedure when the electrical input was 17.5 MW. The outside diameter was 7 meters, making it the smallest of their three furnaces. (Tranell et al. 2010)

The principles for producing high silicon ferrosilicon alloy and metallurgical silicon are very similar. They both involve the reduction of SiO_2 with carbon in an electrical arc furnace. The main difference is that iron ore is added to the charge in the ferrosilicon process.

With systematic core drilling, Tranell et al. (2010) performed an thorough investigation of this furnace. Samples taken from the different reaction zones were characterized and analyzed by optical microscopy, EPMA and XRD. Development of the reaction zones and the metal forming mechanisms were discussed, and an overview of the these zones can be seen in figure 2.13. A review of the work is also presented by Ringdalen & Tangstad (2012).

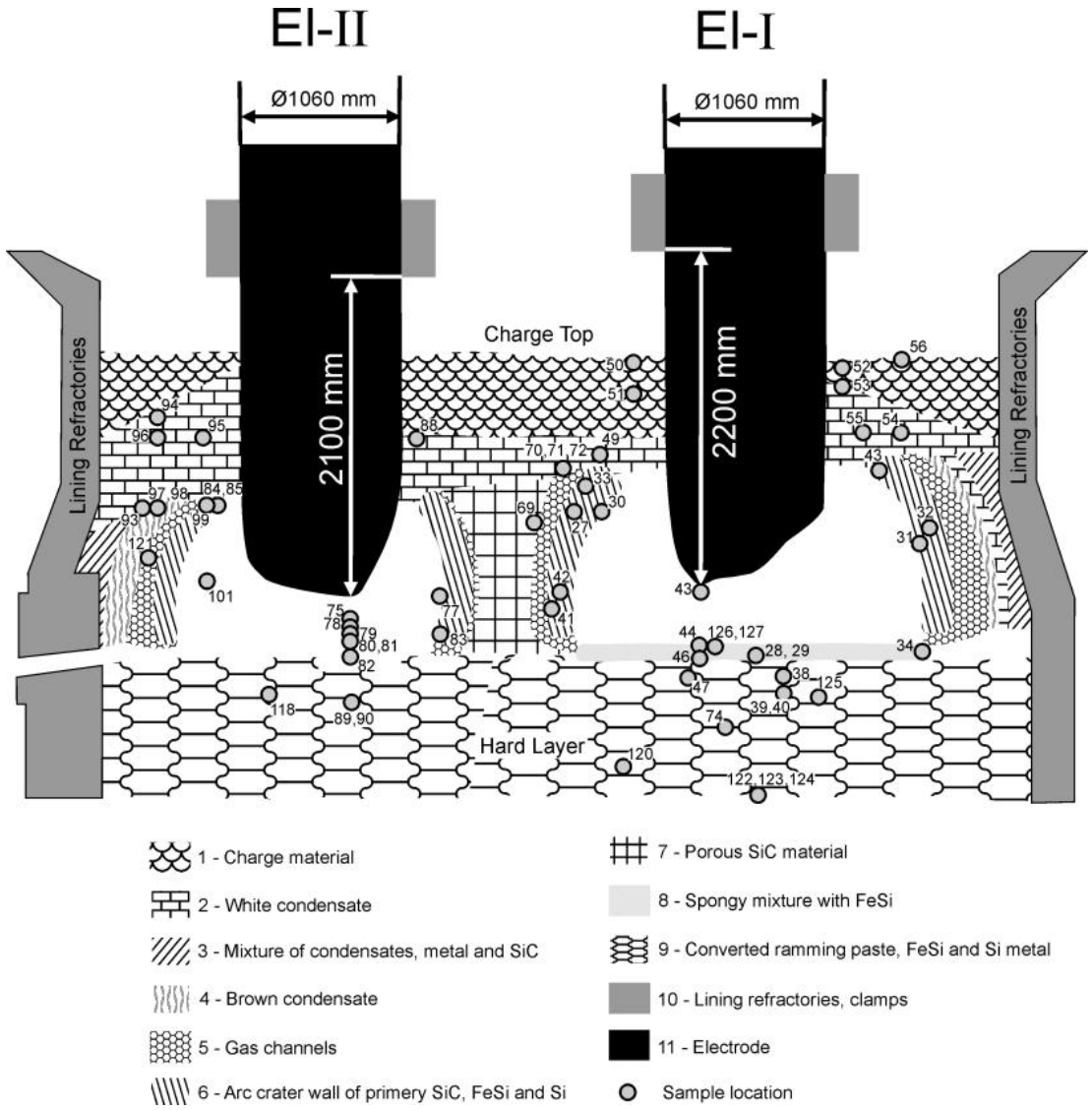

Figure 2.13: Sketch of the furnace excavated at Finnfjord. Different reaction zones are are described with their associated patterns. (Ringdalen & Tangstad 2012)

Studies from similar FeSi furnaces (Grådahl et al. 2007) and (Hjartarson 2009) have found that the off gases emerges from the furnace at an average temperature of ∼700 °C.

Raw materials on the top were loosely packed and appeared unreacted in the top layer (20-30 cm). Partly reacted raw materials were held together by glassy condensates in a 50 cm thick layer beneath the top layer. XRD analysis revealed the presence of metallic silicon, confirming the condensation reaction (-3): $2SiO(g) = SiO_2(s,l) + Si(s,l)$.

A macrograph of this condensate can be seen in figure 2.14.

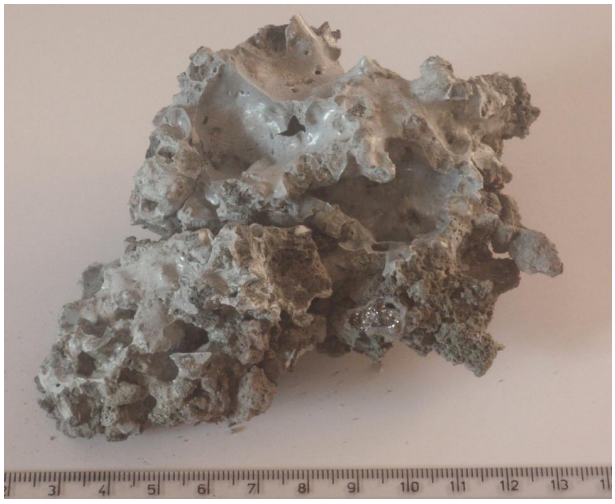

Figure 2.14: Sample taken from the "condensate zone" - raw material held together by condensate. (Tranell et al. 2010)

The crater walls around the electrodes consisted mainly of SiC and Si/FeSi metal as well as small amounts of SiO_2. Having a layered structure, these walls suggests a dynamic interaction between solid wall phases and gases. Outside of the crater walls vertical layers of brown and white condensates could be found. This indicates the presence of radial temperature zones in the furnace.

An almost pure silicon phase were found relatively high up in the furnace (40 cm below the charge top) in the crater walls. The origin of silicon this far up in the furnace is not obvious. Silicon may be generated from the condensation reaction (-3) at temperatures below 1811 °C, but since very small amounts of SiO_2 were found in the crater walls, this mechanism is questionable. The temperature may have been sufficient to produce silicon through reaction (4): $SiO(g) + SiC(s) = 2Si(s,l) + CO(g)$.

Under the electrodes a spongy mixture of SiC soaked with FeSi metal were found. The excavation revealed metal at levels beneath the tap hole. A thick SiC slab on the furnace floor obstructed metal tapping at the end of the furnace campaign. (Tranell et al. 2010)

Chapter 3

Experimental

3.1 Pilot scale experiment

In 2011, SINTEF in Trondheim conducted a pilot scale experiment on the the silicon process. The main focus of this experiment was to copy and manipulate the mechanisms for NO_x-formation by controlling the flow of false air through the off-gas system. The NO_x-content was then measured using different air inlets. The results gave significant differences for the various air inlet geometries. (Kamfjord et al. 2012)

The experiment was carried out using a 400 kVA furnace operated at 160 kW. A sketch of the furnace and an image of it in operation can be seen in figure 3.1. It was a single electrode submerged arc furnace with adjustable current and voltage supply. Power supply could be operated by either AC and DC. AC was chosen for this experiment. Maximum AC current was 5700 V and max AC voltage was 215. The furnace was connected to an off-gas system monitoring composition and temperature of the gas, and with filter collecting coarse and fine particles.

Raw material used for this experiment was quartz (3-25 mm) and coke (3-15 mm). Wood chips (20-50 mm), was added to increase the charge permeability. The raw material mix started with a carbon cover of 80 %, and was gradually increased to 97 %.

The pilot furnace was operating for 44 hours and tapped 13 times. 87 kg of metal was produced with a silicon yield of 62%. The furnace was stoked after each tapping, giving an average stoking cycle of 200 minutes.

After the experiment was finished, two component epoxy was poured into the furnace top fixing the charge together. The molded mass was removed in one piece and then cut in the vertical axis leaving the cut in figure 3.2 representing a quarter of the furnace. Samples was then drilled out and analyzed in the Scanning Electron Microscope (SEM). (Solheim et al. 2012)

The main purpose of this experiment was to investigate the NO_x-emission not the silicon production. Excavation of the furnace was therefore not of particular interest for SINTEF, but contained lots of valuable information for the reaction mechanisms in the silicon process. The information from the samples was to be examined in this thesis.

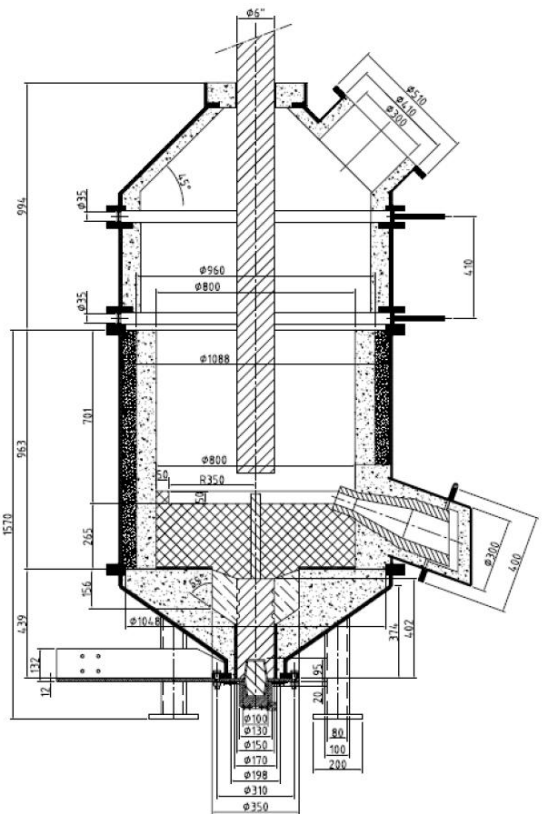

(a) Dimensions of pilot furnace in [mm]. (Kamfjord et al. 2012)

(b) Pilot scale furnace in operation. (Solheim et al. 2012)

Figure 3.1: Pilot scale furnace experiment conducted in 2011 by Solheim et al.

Samples were taken from positions in the cross-section as displayed in figure 3.2. The electrode can be seen to the right in this image. A large cavity has formed around the lower section of this electrode where the temperature was highest.

The internals of the furnace could be divided into different areas. Samples in position 1 to 4 represents the upper and partially unreacted part of the charge as well as the cavity roof where SiO has condensed. This zone is considered to be static before the furnace is stoked.

From 5 to 12 charge materials and condensate from the cavity roof is melting and slowly flowing downwards to the hottest zone. These positions makes up a dynamic zone.

13 and 14 is the metal bath, where you can see two distinctive phases. The upper phase (light gray) is probably silicon metal and the lower phase (dark gray) is silicon carbide, since ρ_{Si}=2.57 g/cm^3 and ρ_{SiC}=3.21 g/cm^3.

Position 15 to 17 constitutes a zone where gas have forced its way between the charge and the inside of the lining, leaving gas channels filled with condensate. This zone on the outside of the charge is considered to be inactive.

Figure 3.2: Sample extraction from the pilot scale experiment. The cross-section was taken from the side of a quarter piece cut from the furnace.

3.2 Induction furnace (IF75) experiments

To investigate the inner dynamics of the silicon furnace, series of induction furnace experiments was conducted. Four experiments was conducted with same charge composition and holding times, but at different temperatures. These were done to find the relation between temperature and reaction kinetics, amount of produced silicon, type of condensate produced (white or brown) etc. In addition one experiment was conducted to determine the strength of the cavity roof, ie. the charge material above the cavity which is held together by condensate and melted quartz. A summary of the experiments, their charge mixtures and other details is listed in table 3.1. The main charge mixture was 1 mole SiO_2 and 2 moles SiC. From this we get the following total reaction: $SiO_2 + 2SiC = 3Si + 2CO(g)$. This mixture will cut the reaction path from C to SiC, reducing the reaction time significantly.

Table 3.1: Summary of experiments

Exp.	Charge mixture (molar ratio)	Crucible weight (empty)	Crucible weight (full)
1	$\frac{SiC}{SiO_2} = 2$	6004 g	11311 g
2	$\frac{SiC}{SiO_2} = 2$	6005 g	11320 g
3	$\frac{SiC}{SiO_2} = 2$	6035 g	11352 g
4	$\frac{SiC}{SiO_2} = 2$	5981 g	11320 g
5	$\frac{C(coke)}{SiO_2} = 2$ in the upper $\frac{1}{3}$ of the crucible $\frac{SiC}{SiO_2} = 2$ in the lower $\frac{2}{3}$ of the crucible	6009 g	10920 g

The furnace used had a max effect of 75kW and is hereby reffered to as IF75. The manufacturer was "Inductotherm", and the power supply model was called "VIP POWER-TRAK". It had induction coils which went 300 mm up from the furnace bottom. The height of the furnace hole was 400 mm. This resulted in a big temperature difference between the bottom and top of the furnace. This property was utilized to imitate an industrial scale metallurgical silicon furnace, where the temperature in the bottom is ∼2000 °C while the temperature on the top of the charge burden is ∼1000→1700 °C (Schei et al. 2000).

Graphite crucibles were loaded to the brim with charge material and lifted down in the furnace hole. A graphite wool sheet was wrapped around the crucible to protect the furnace lining.

The set up with the furnace and the thermocouples for the experiments is shown in figure 3.3a. The crucible top can be seen in the middle of the furnace body, while the thermocouples are sticking out from their protective graphite tubes. The thermocouples were connected to a Campbell 21x micrologger.

(a) Experimental setup for induction furnace experiments.

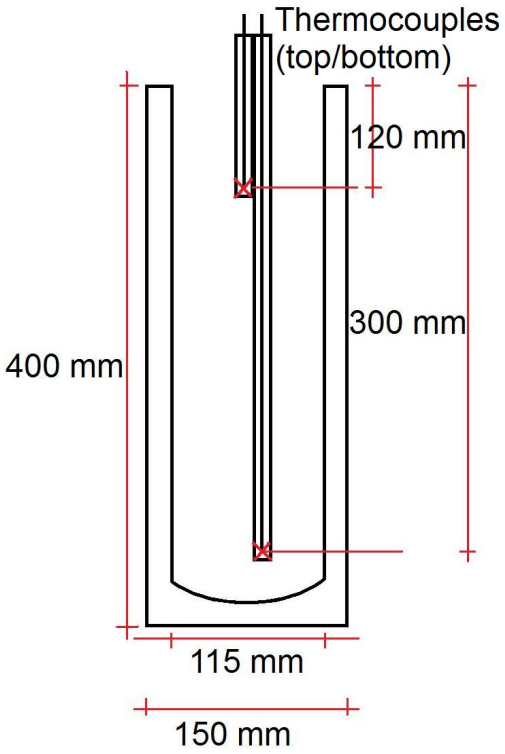

(b) Crucible dimension and thermocouple position.

Figure 3.3: Experimental setup for the small scale induction furnace experiments.

Two thermocouples were used, and their position, as well as the crucible dimensions can be seen in figure 3.3b. The bottom thermocouple were positioned at the furnace "hot spot" 100 mm above the bottom of the furnace (or 300 mm down in the crucible). This "hot spot" is a result of induction coil position. The upper thermocouple was positioned 120 mm below the crucible top, and was designed to measure the temperature around the cavity roof. The position of the cavity roof has previously been indicated by Vangskåsen (2011*b*).

After each experiment the crucibles were lifted out, cooled and weighed. Crucible 1 through 4 was filled with two component epoxy to fix the internals of the remaining charge material. Crucible number 5 was not filled with epoxy, since the purpose of this experiment was to determine the strength of the cavity roof.

When the epoxy had solidified, the crucibles were cut at "Nidaros Domkirkes Restaureringsarbeider" (Bispegata 11 Trondheim). Crucible 1 to 4 were cut in the longitudal axis, resulting in 20 mm thick, 150 mm wide and 400 mm tall plates. Cylindrical samples with diameter 25 mm could be drilled out from these plates. Some issues were experienced when drilling out the samples from crucible 3 and 4 since the epoxy did not go through the thick condensate layer which formed around the cavity roof area.

After extraction of the samples, they were embedded in epoxy (if necessary), grinded and polished down to 1µm. To avoid electrical charging of the sample surface in the SEM, good electric conductivity is required. Since the mixture of condensate, SiC and quartz is a poor conductor, a thin layer of carbon was added to the surface. This was done by carbon vapor deposition.

Crucible 5 was horizontally cut at the level where the cavity roof was anticipated to be. Cores were drilled out from the upper part of the crucible, cut into ∼25 mm thick slices and organized after position upwards from the cavity roof. The samples contained melted or unmelted quartz, coke partially reacted to SiC and condensate which glued the material together.

3.3 Pressure tests of samples from IF75 experiment

The samples taken from the area above the cavity roof in crucible 5 were positioned in a pressure machine as shown in figure 3.4. Mechanical data was recorded as the pressure on the cylindrical samples increased.

Compressing the samples ∼4 mm was sufficient to get the obtain the breaking strength. The samples were porous and brittle, so the resulting pressure - compression curves became somewhat jagged.

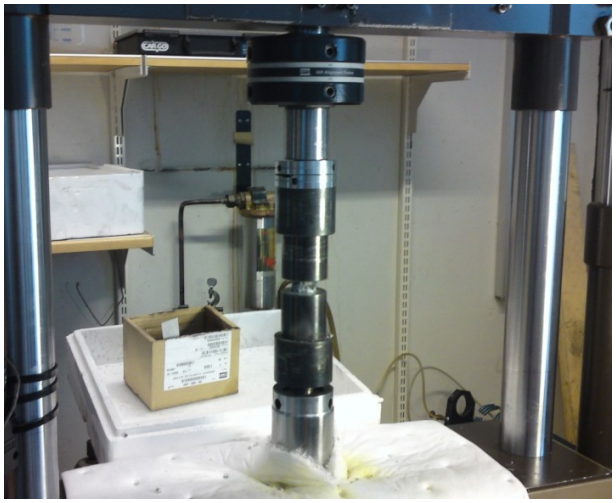

Figure 3.4: Sample positioned in compression machine.

3.4 Scanning Electron Microscope (SEM)

The SEM is an excellent tool for investigation of material surfaces. In addition to topographic studies, the SEM can be equipped with several detectors in order to provide additional information about the sample. In the work done in this report, two types of signals were of particular interest.

Backscatter electrons (BSE) are used to investigate surfaces containing phases with different compositions. Phases with high mean atomic number will appear brighter than phases containing lighter elements.

X-ray signals are emitted from the electron orbitals due to the energy of the electron beam. The energies from these x-rays are characteristical for the different elements, and can be used to obtain quantitative information about the sample. The x-ray signal can be detected either in a electron diffraction spectrometer (EDS) or a wavelength diffraction spectrometer (WDS). The WDS is also called the electron probe micro-analyzer (EPMA). The EDS is a quick and easy way of getting an overview of the elements in the samples. The EPMA on the other hand is more time consuming but more accurate than the EDS. (Hjelen 1989)

Chapter 4

Results

In this chapter, a thorough investigation of the samples extracted from both the pilot scale experiment, as well as the small scale induction furnace experiments will be presented. The main objectives of the investigation was to explain how the raw material behaved in an silicon furnace, which reactions occured where, as well as to clarify the silicon-producing mechanisms.

4.1 Pilot scale experiment

In this section, results from the excavations of a pilot scale experiment will be investigated. The experiment which focused on the emissions from the metallurgical production of silicon, was conducted by SINTEF in 2011. The focus in this investigation will be on the condensate as well as the silicon producing mechanisms.

Samples 1 to 14 has been investigated to figure out what happened to the different material as it moved down in the furnace. The material in question was carbon material as well as the produced condensate in the cooler part of the furnace. In figure 4.1 the cross-section representing the quarter piece of the furnace is shown, and in figure 4.2 with numbering of sample positions. The temperature in the furnace was not measured for the experiment. The cross-section describes the left hand half of the furnace. For convenience, the other half is not taken included since it it was almost identical. Samples in position 15 to 17 are not discussed, as it is most likely to be a static area in the furnace sintered together by condensate.

The quartz in the upper two sample positions was unreacted, but started to soften and melt below this point. Some unmelted quartz can be seen beside the tip of the graphite electrode, and this was probably just caused by materials falling from the top after the furnace was shut down. The big area to the left of the electrode is the cavity area. Right above this cavity, was the cavity roof which was mainly held up of the melted quartz and condensate gluing the material together (sample position 1-4). The condensate above the cavity had a brown color. The cavity wall is positioned to the left of the cavity between sample position 5-12. The condensate in the cavity wall had a pale brown color. Further to the left towards the furnace lining, partially unreacted material and condensate are present. In the pale brown condensate, visibly large droplets of silicon metal could be seen. These droplets were found high up in the furnace, around sample position 5. The size and occurence of these silicon drops increased with position downwards in the furnace.

The metal bath below the electrode consist of two phases, one Si-rich phase with SiC-particles, and one SiC-rich phase with some liquid silicon. The Si-rich phase was light gray and was posisitioned above the SiC-rich phase (dark gray).

Figure 4.1: Picture of the cross-section taken from the SINTEF pilot experiment.

Figure 4.2: Picture of the cross-section taken from the SINTEF pilot experiment, with sample numbering.

4.1.1 EPMA maps

The electron probe micro-analyzer (EPMA) was used to identify the various phases in the different material investigated in this thesis. Three elements: Si, O and C were quantified in the images by color intensities. From the different colors, it was possible to tell if the phases were C, SiO_2, SiC or Si.

A carbon particle relatively high up in the furnace (sample position 4) is imaged in fig. 4.3. SiO gas have reacted with the particle, converting the C into channels of SiC going fairly far under the surface. Condensate (SiO_2+Si) has also deposited outside the particle clogging further flow of SiO towards the C-particle.

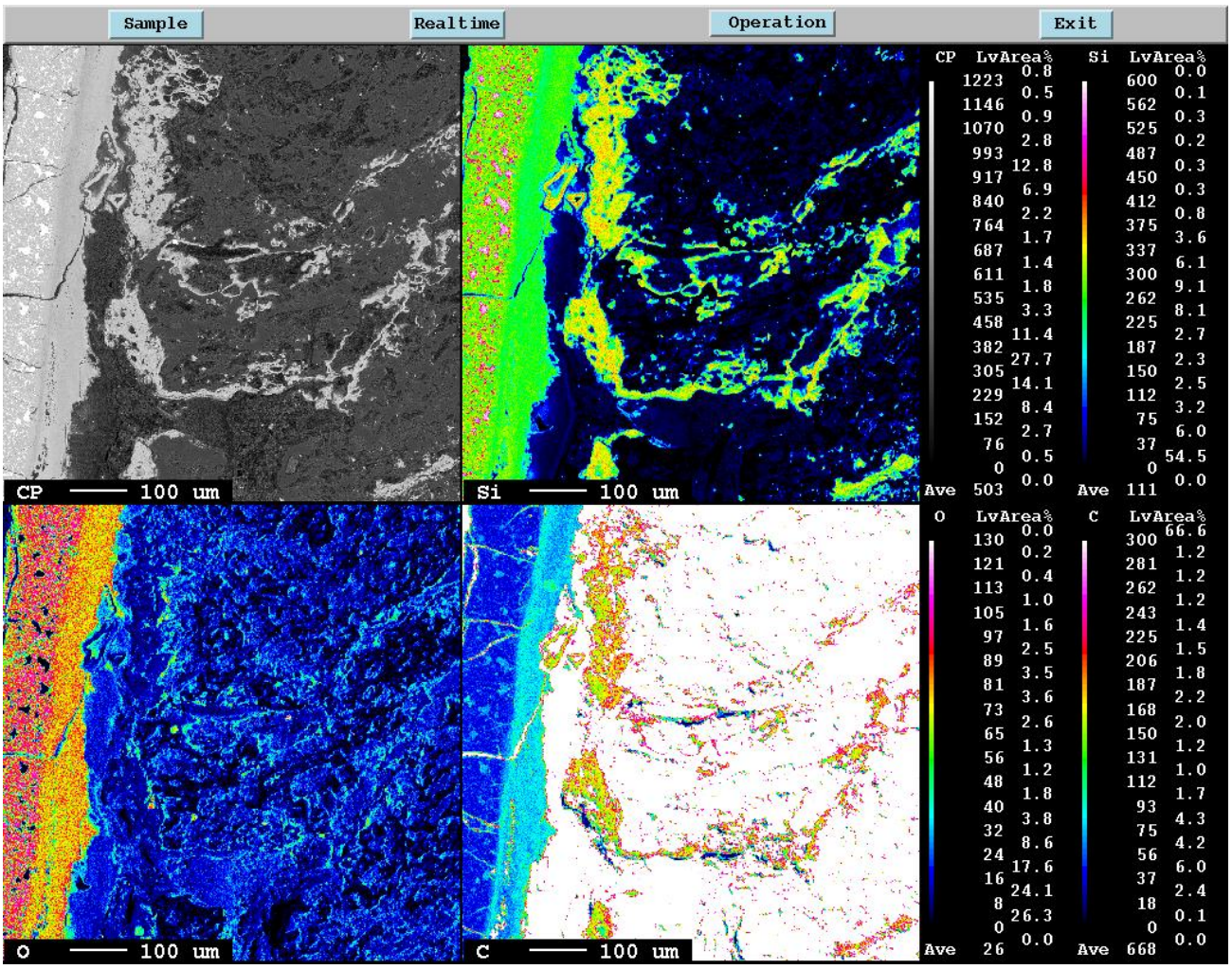

Figure 4.3: EPMA image of a carbon particle exposed to SiO gas. The sample was taken from position 2 in fig. 4.1.

Condensate which was exposed to higher temperatures would start too perspire the Si-phase. In fig. 4.4 an image of brown condensate (SiO_2+Si) taken from position 9 (relatively deep in the furnace) is displayed. Characteristic "rivers" of Si were flowing together, creating larger lumps of Si. In this image a large droplet ($\sim 100\mu$m) have been formed by the surrounding silicon.

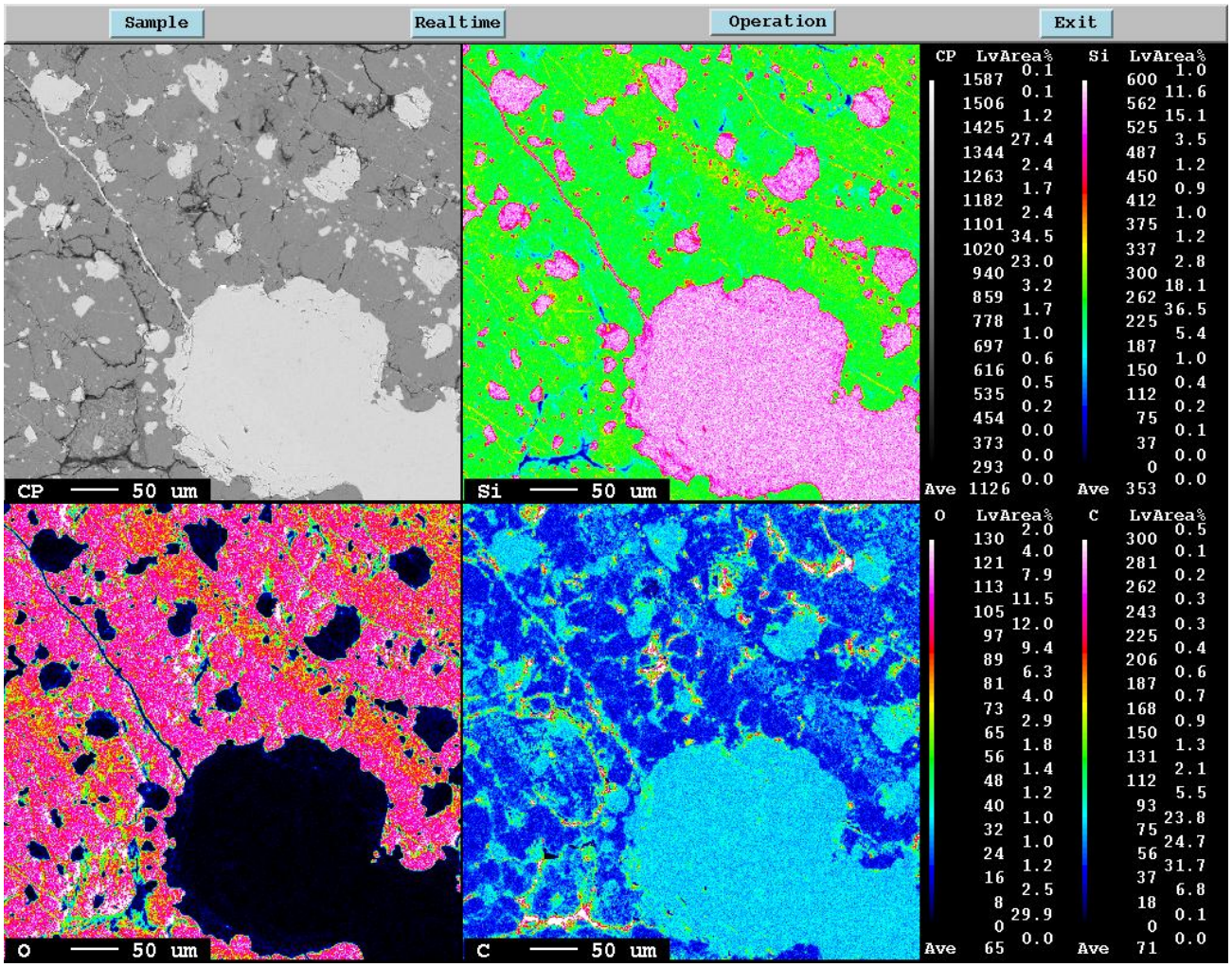

Figure 4.4: EPMA image of a condensate (SiO_2+Si) exposed to high temperature. The sample was taken from position 9 in fig. 4.1.

Right above the metal bath (position 11) a carbon particle has partially reacted to SiC and Si. In the upper part of the image in fig. 4.5 the composition is mostly C and SiC, while further down more and more SiC are converting to Si.

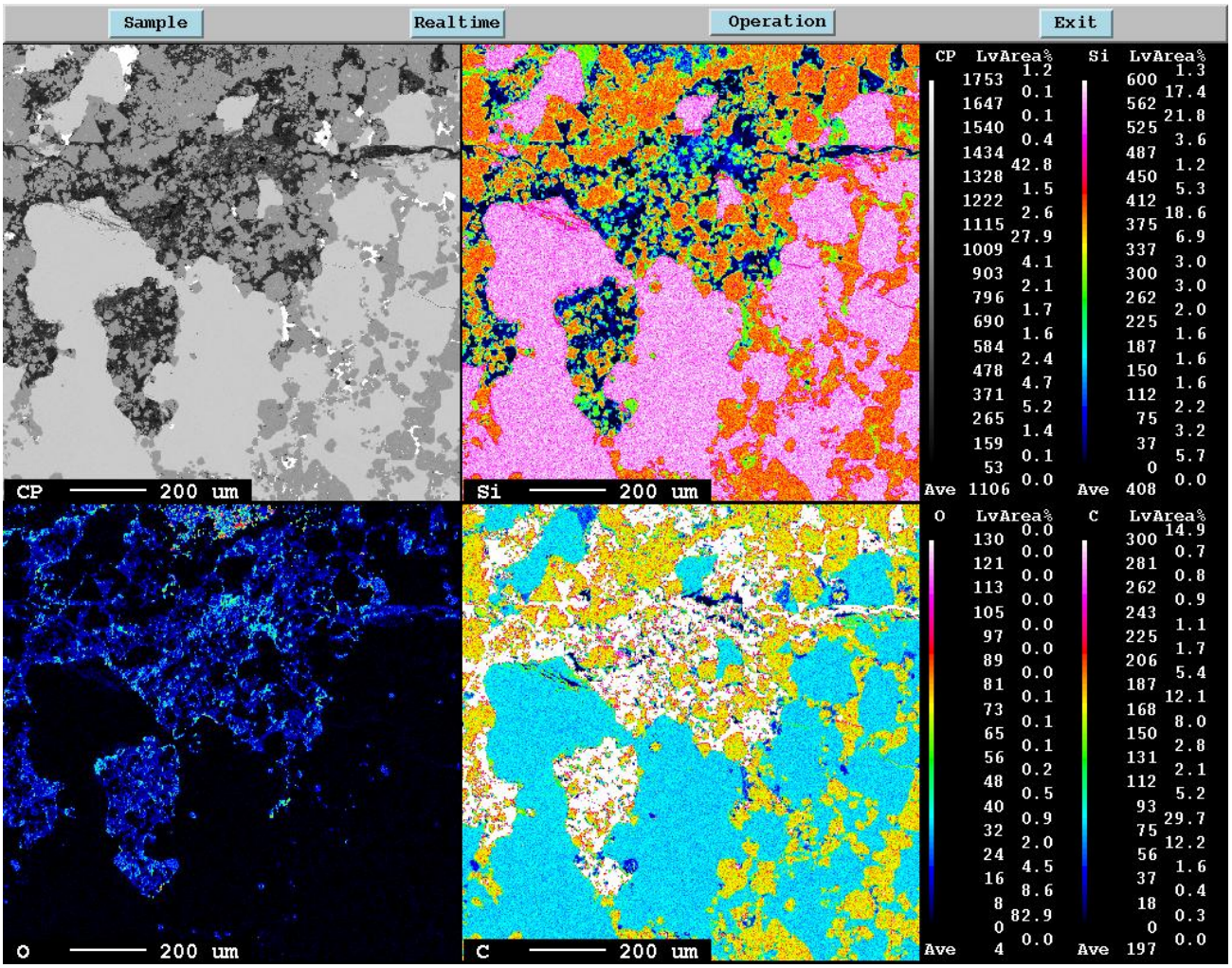

Figure 4.5: EPMA image of a partially reacted carbon particle. The sample was taken from position 11 in fig. 4.1.

4.1.2 SEM images - Condensate in pilot experiment

Here, the microstructure of the condensate as it moves down in the furnace will be presented. The silicon metal in these images can be seen as the light phase, while the surrounding SiO_2 will be darker. This is a result of the phenomenom called atomic contrast, where phases with high mean atomic number will appear brighter than the phases with lower mean atomic number. The possible phases listed from dark to light: C, SiO_2, SiC and Si.

The image sets is composed by a a low and a high magnified version of the same area. The high magnified image is zoomed in from the center of the low magnified one. The images are shown in figure 4.6 to 4.17. The images will be thouroghly analyzed in the discussion chapter.

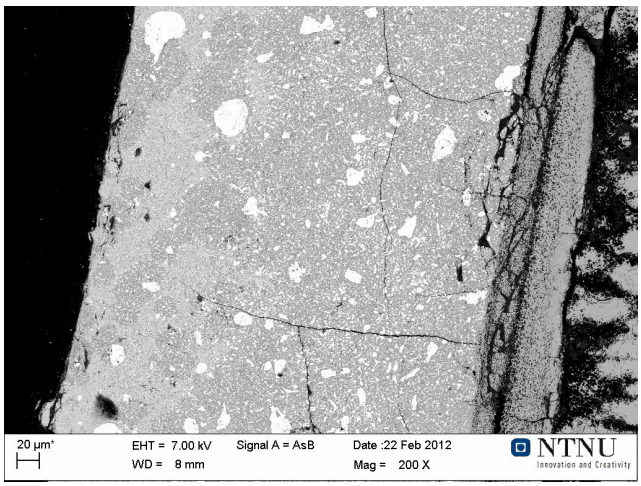

(a) 200X

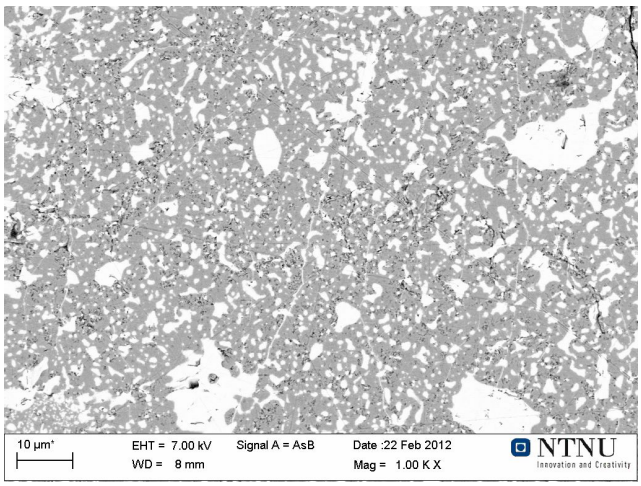

(b) 1000X

Figure 4.6: Brown condensate taken from sample position 1

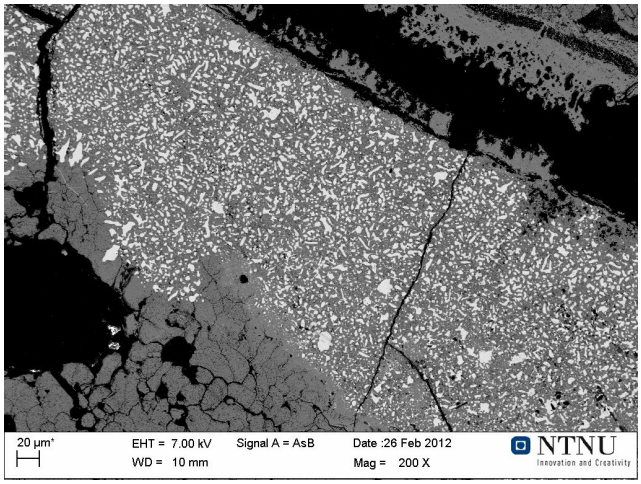

(a) 200X

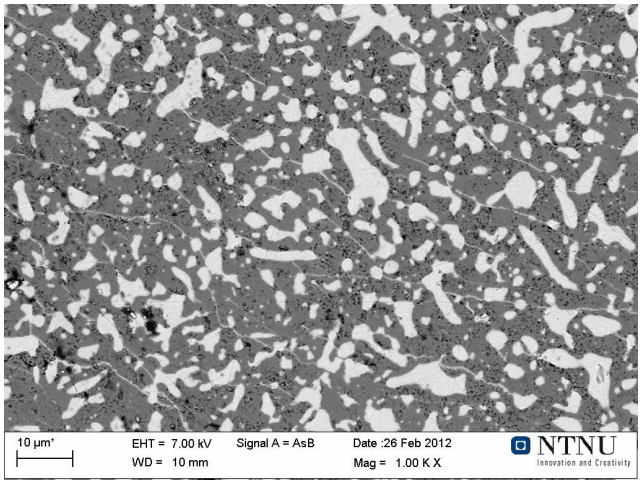

(b) 1000X

Figure 4.7: Brown condensate taken from sample position 2

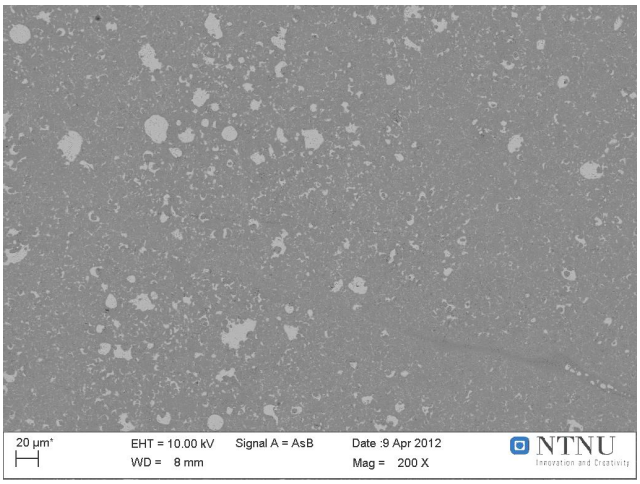

(a) 200X

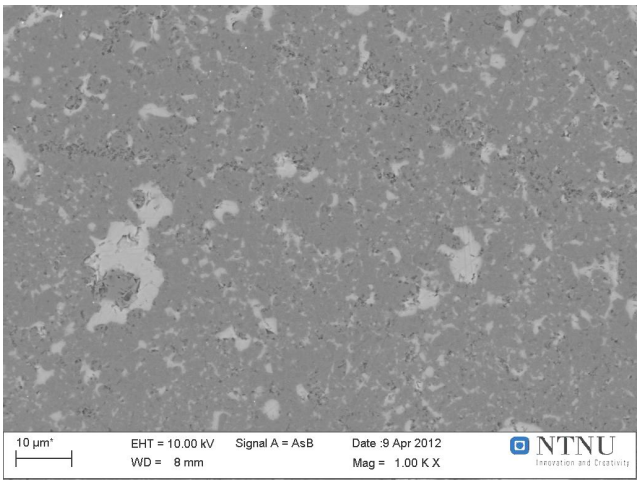

(b) 1000X

Figure 4.8: Brown condensate taken from sample position 3

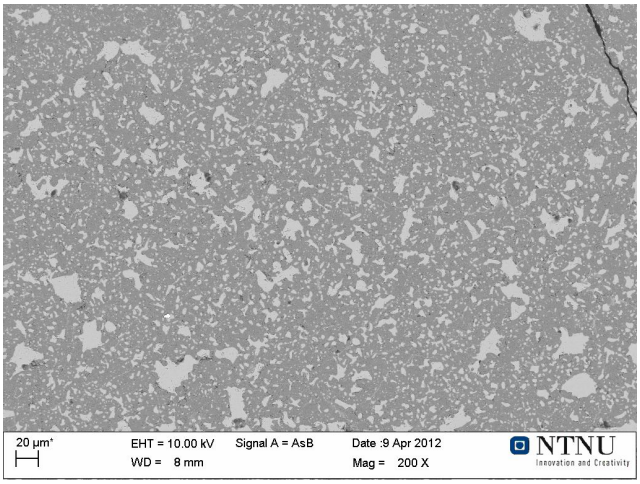

(a) 200X

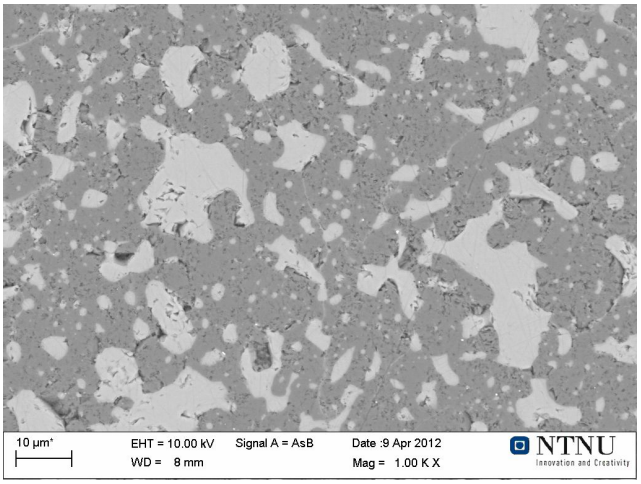

(b) 1000X

Figure 4.9: Brown condensate taken from sample position 4

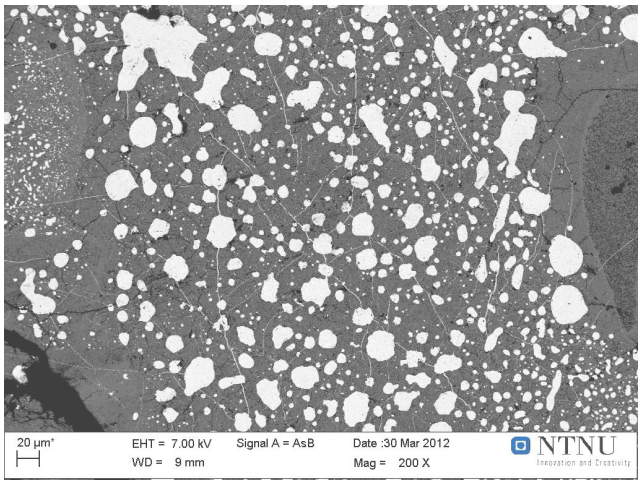

(a) 200X

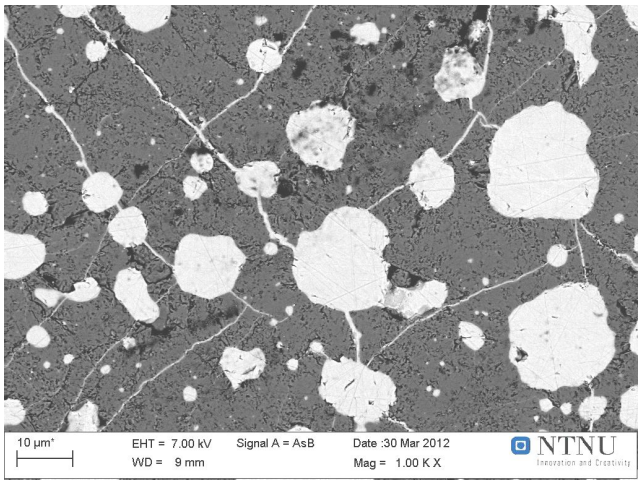

(b) 1000X

Figure 4.10: Pale brown condensate taken from sample position 5

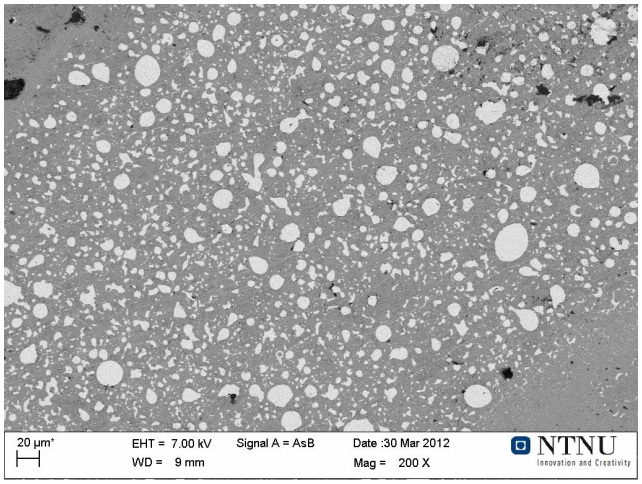

(a) 200X

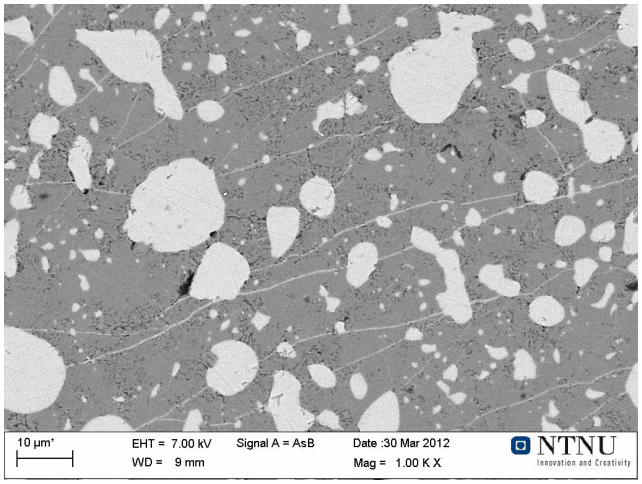

(b) 1000X

Figure 4.11: Pale brown condensate taken from sample position 6

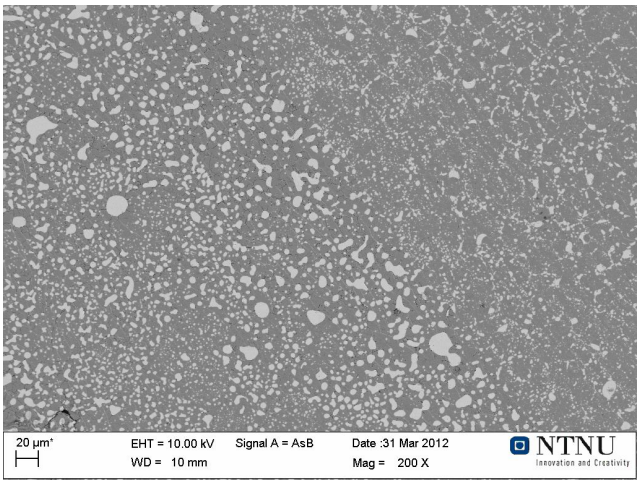

(a) 200X

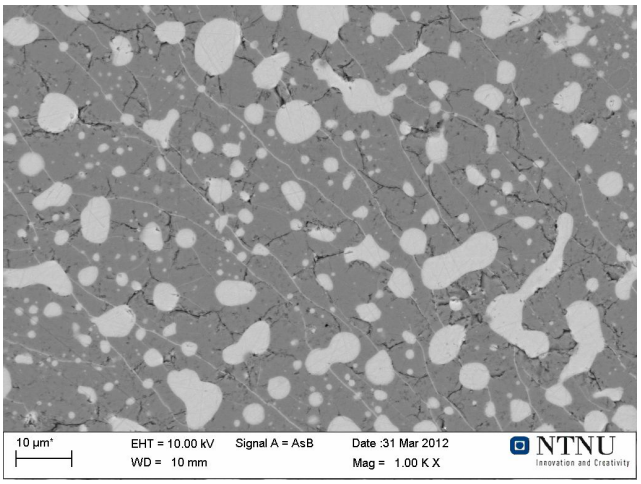

(b) 1000X

Figure 4.12: Pale brown condensate taken from sample position 7

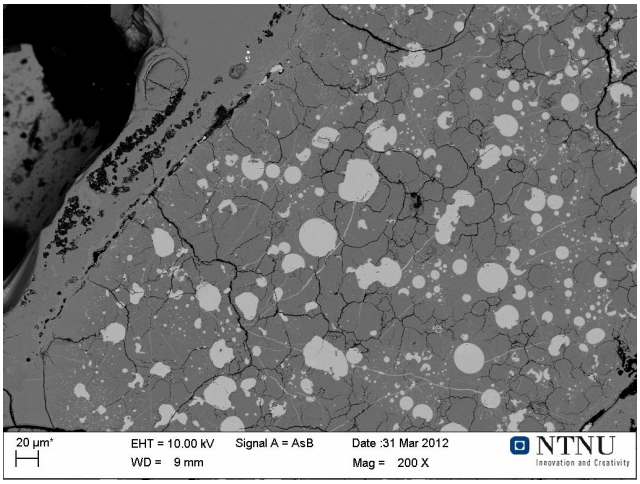

(a) 200X

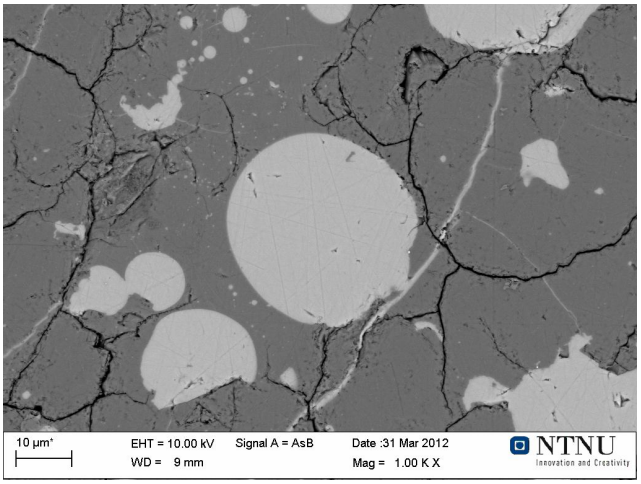

(b) 1000X

Figure 4.13: Pale brown condensate taken from sample position 8

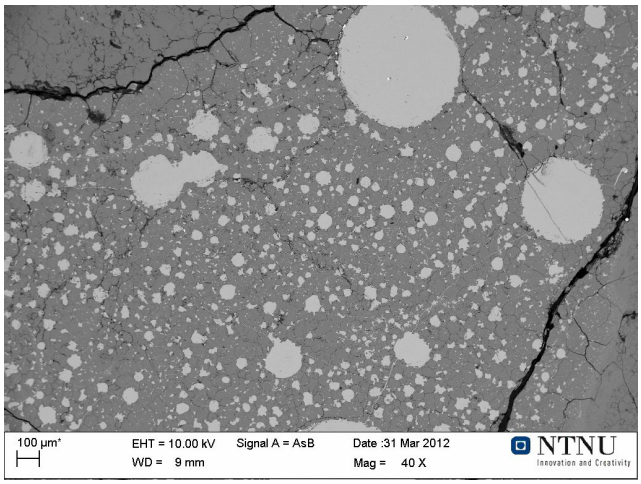

(a) 40X

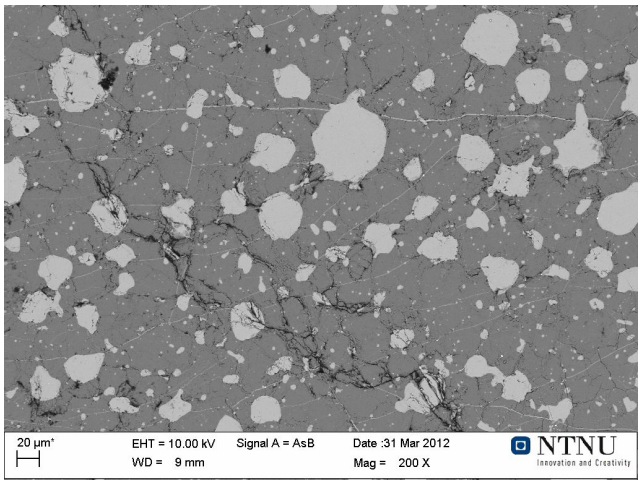

(b) 200X

Figure 4.14: Pale brown condensate taken from sample position 9

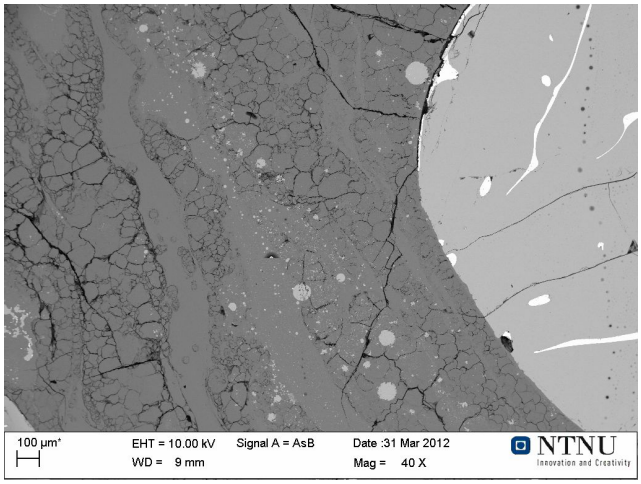

(a) 40X

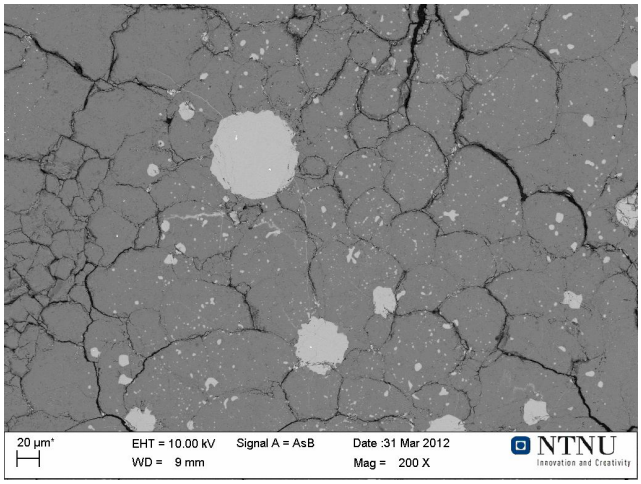

(b) 200X

Figure 4.15: Pale brown condensate taken from sample position 10

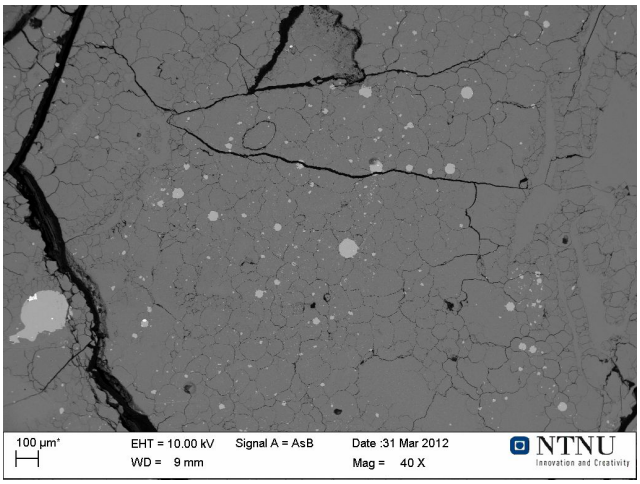

(a) 40X

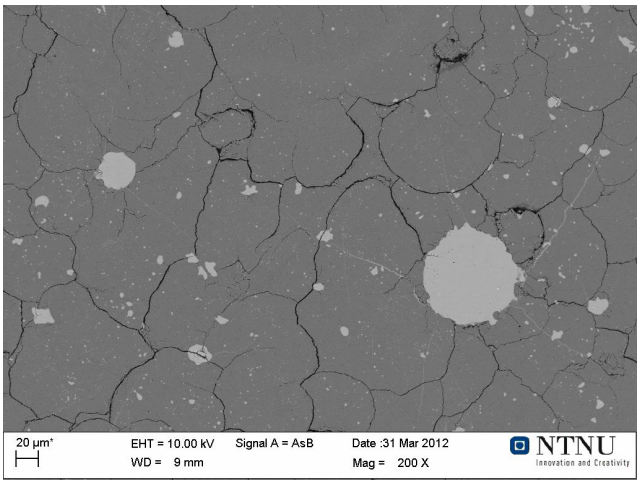

(b) 200X

Figure 4.16: Pale brown condensate taken from sample position 11

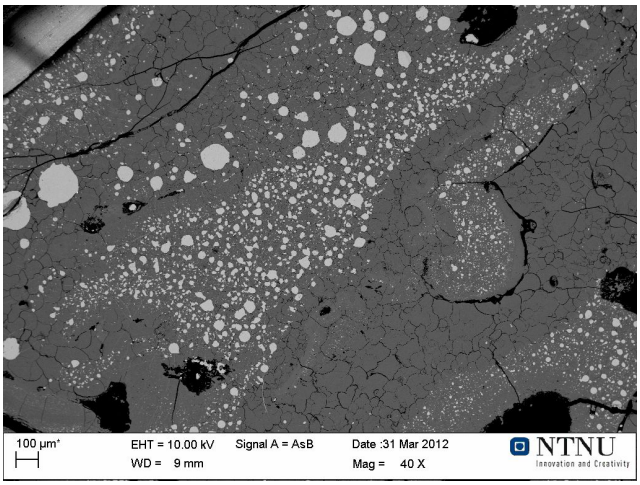

(a) 40X

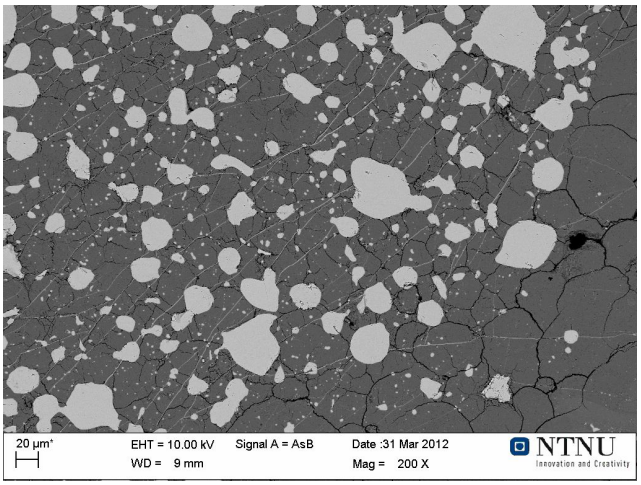

(b) 200X

Figure 4.17: Pale brown condensate taken from sample position 12

Weight fraction of the silicon content in the condensate was also calculated by image-analysis of the SEM-images. Two images from each sample position (1-12) were used as a basis to measure the area fractions using an image software called "ImageJ". The images analyzed was taken with 1000X magnification in relatively homogeneous areas. Big pits and other impurities were avoided to obtain comparable results. Knowing the densities of Si and SiO_2 it was possible to find the weight fraction of silicon in the surrounding SiO_2 matrix. The results are presented in figure 4.18, and shows the silicon content in the different sample positions downwards in the furnace. Sample position 1 is from the top of the charge while position 12 is just above the metal bath. The overall trend is that the silicon content in the condensate is dropping going downwards in the furnace.

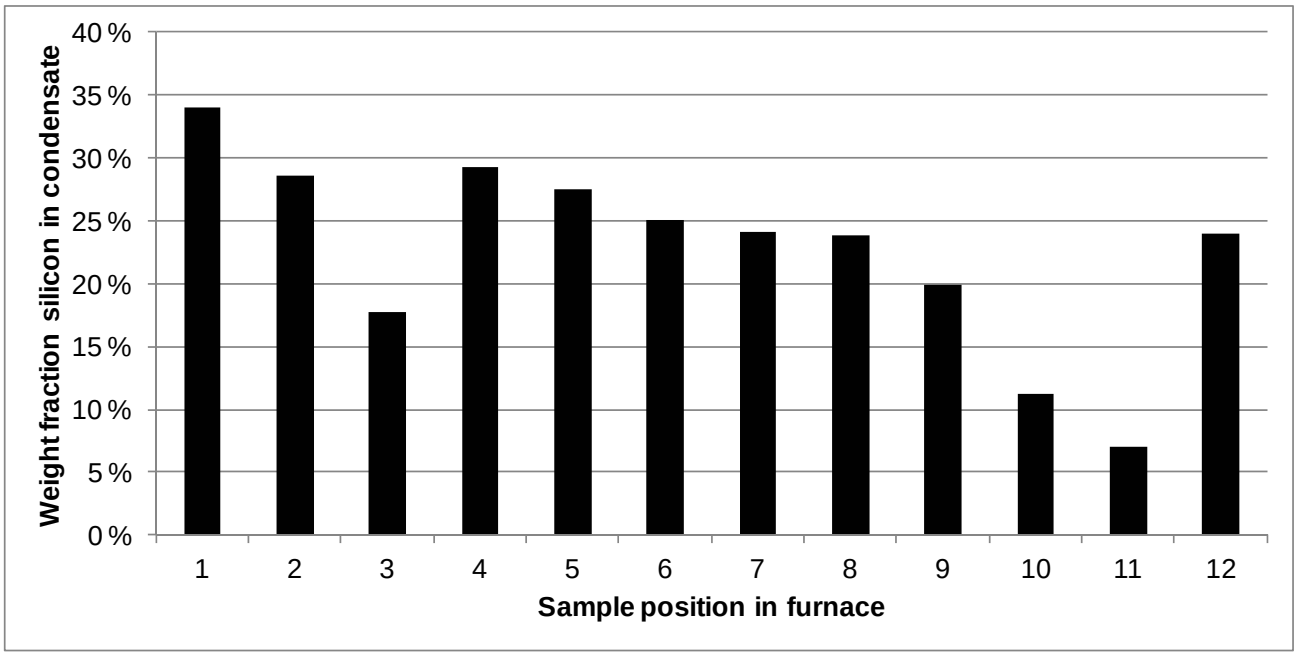

Figure 4.18: Silicon content in the condensate from the samples taken from the pilot scale furnace. Based on image analysis from the SEM-images taken.

4.1.3 SEM images - C→SiC→Si in pilot experiment

The route from carbon through SiC to Si was also studied for the material as it moved downwards in the furnace. The images describing the transformation from carbon particle to silicon metal can be seen in figure 4.19 to 4.29. Images of the two distinct metal phases in the bottom of the furnace can be seen in figure 4.31 and 4.32. The images will be thouroghly analyzed in the discussion chapter.

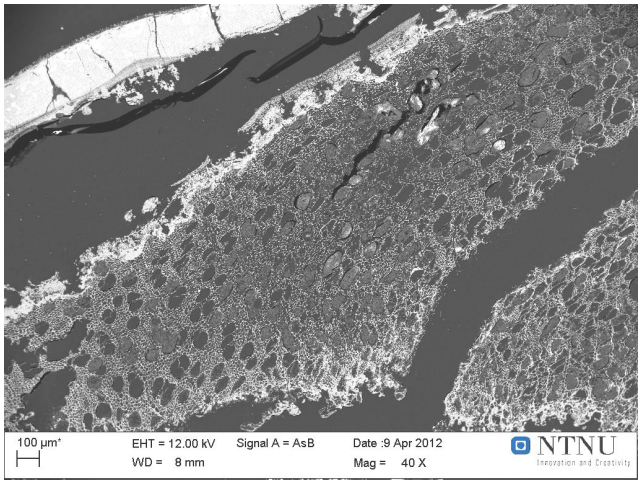

(a) 40X

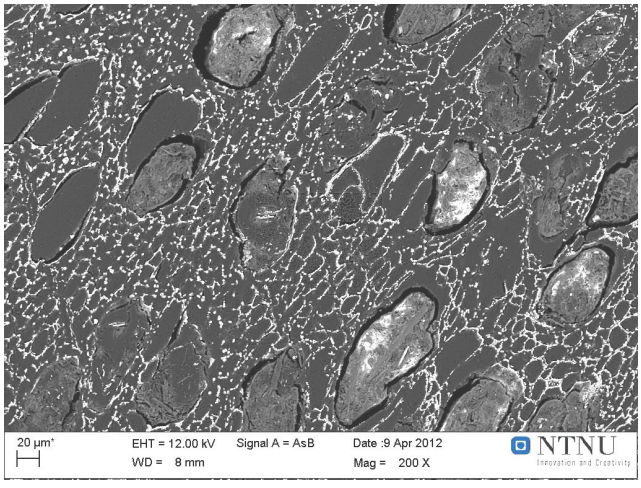

(b) 200X

Figure 4.19: Carbon particle exposed to SiO gas in sample position 1. Initial convertion to SiC.

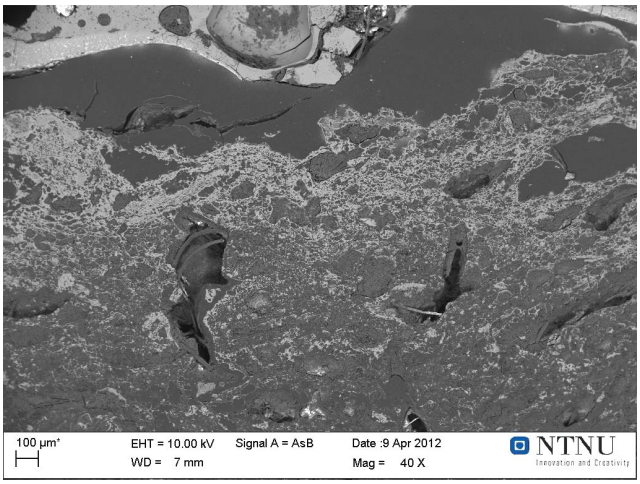

(a) 40X

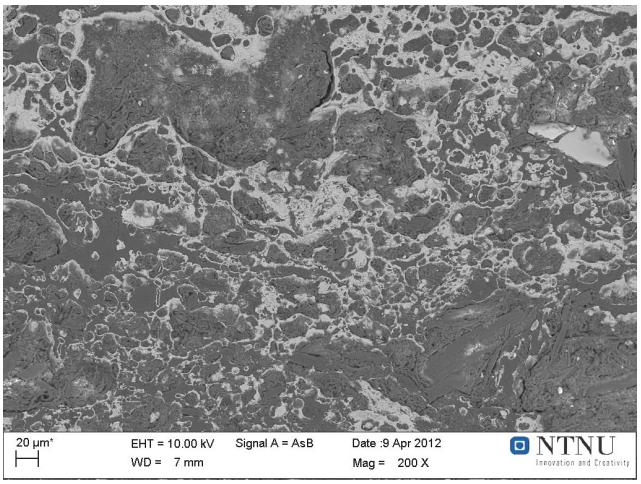

(b) 200X

Figure 4.20: Carbon particle exposed to SiO gas in sample position 2. Initial convertion to SiC.

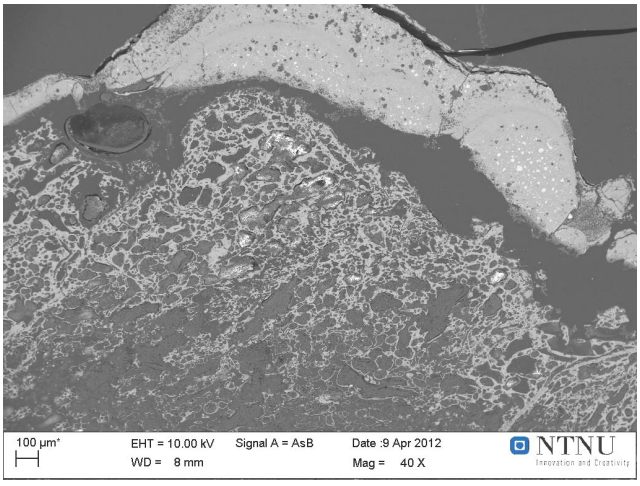

(a) 40X

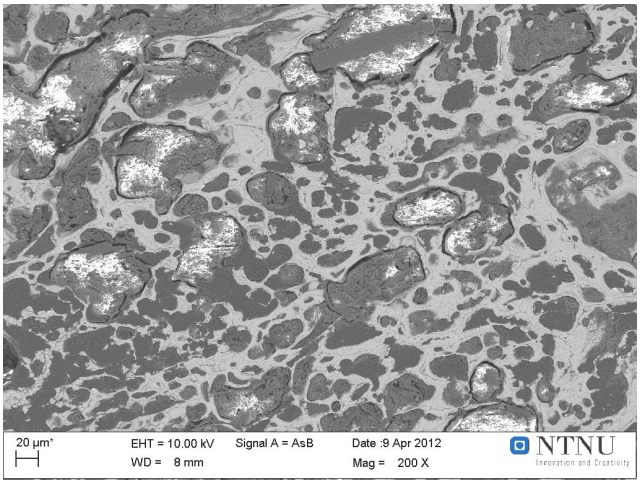

(b) 200X

Figure 4.21: Carbon particle exposed to SiO gas in sample position 3. Partially converted to SiC.

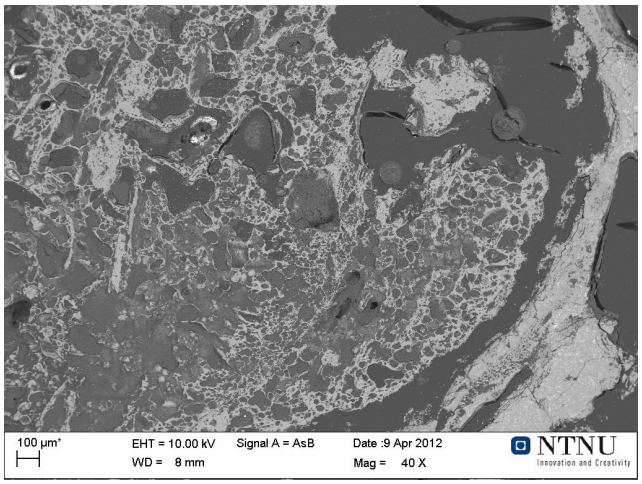

(a) 40X

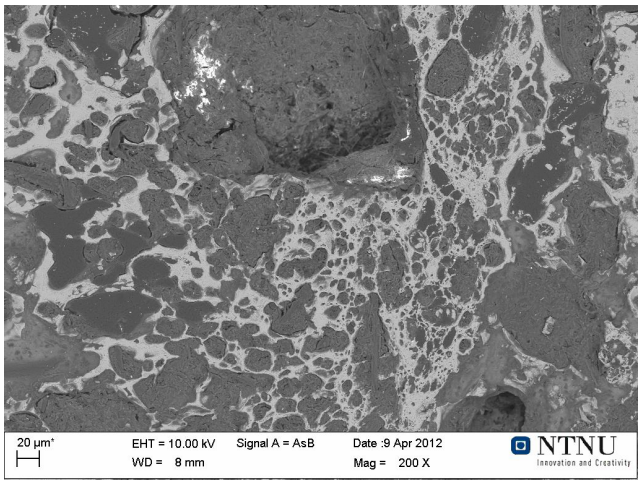

(b) 200X

Figure 4.22: Carbon particle exposed to SiO gas in sample position 4. Partially converted to SiC.

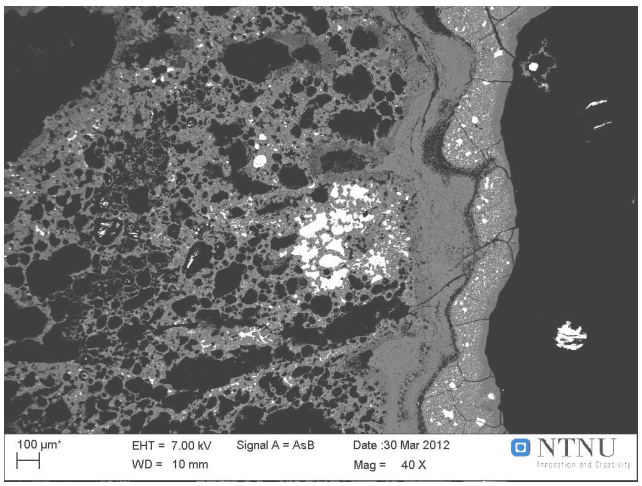

(a) 40X

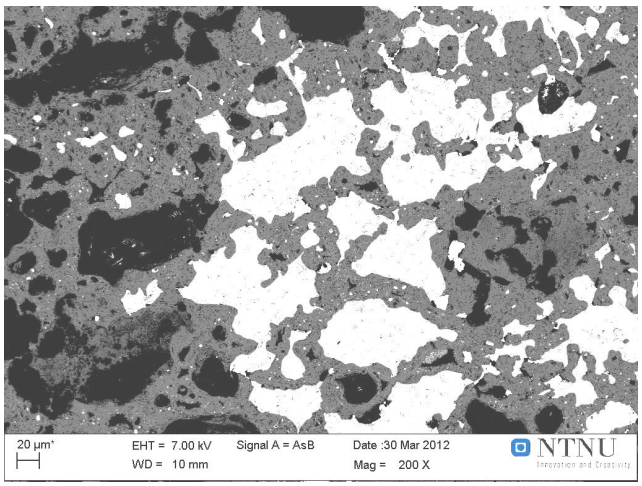

(b) 200X

Figure 4.23: Carbon particle exposed to SiO gas in sample position 5. Partially converted to SiC. A cluster of metal silicon can also be seen.

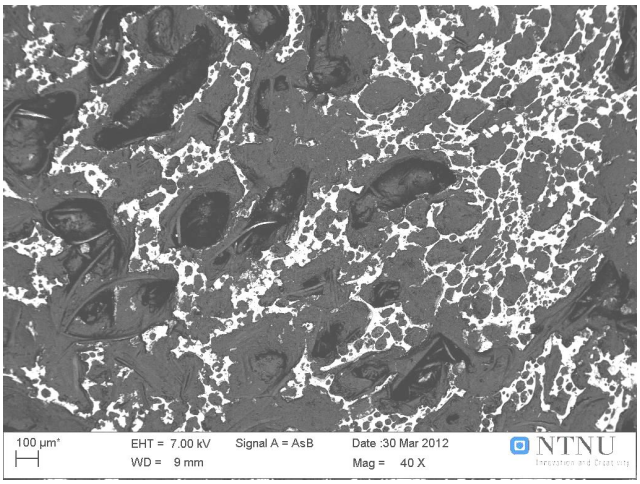

(a) 40X **(b)** 200X

Figure 4.24: Carbon particle partially converted to SiC in sample position 6.

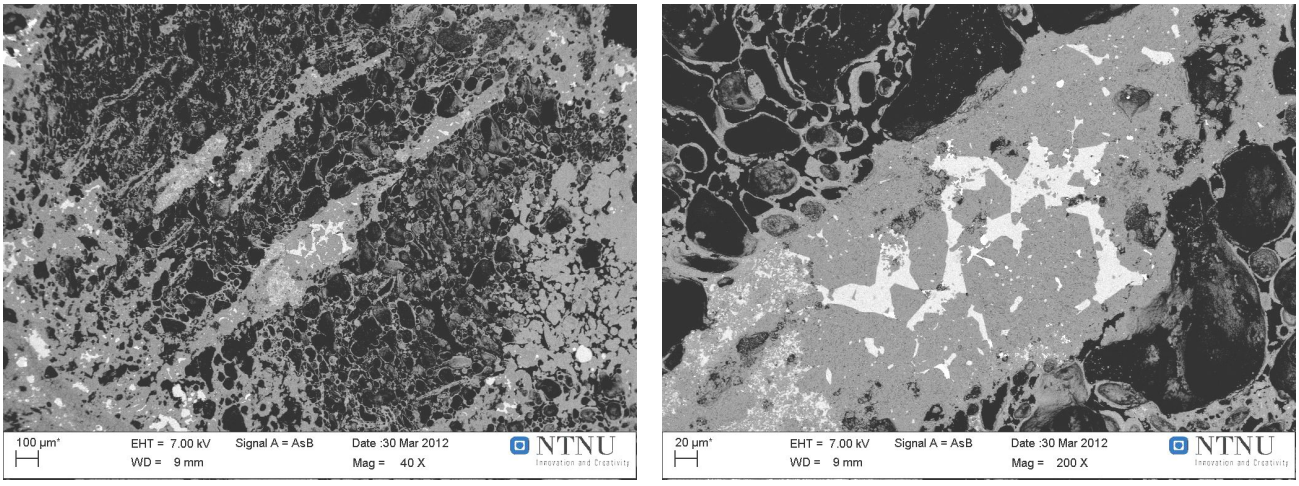

(a) 40X **(b)** 200X

Figure 4.25: Carbon particle partially converted to SiC and Si in sample position 7.

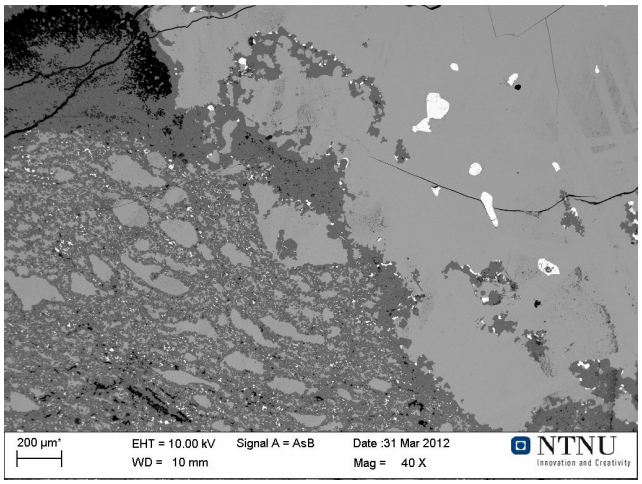

(a) 40X

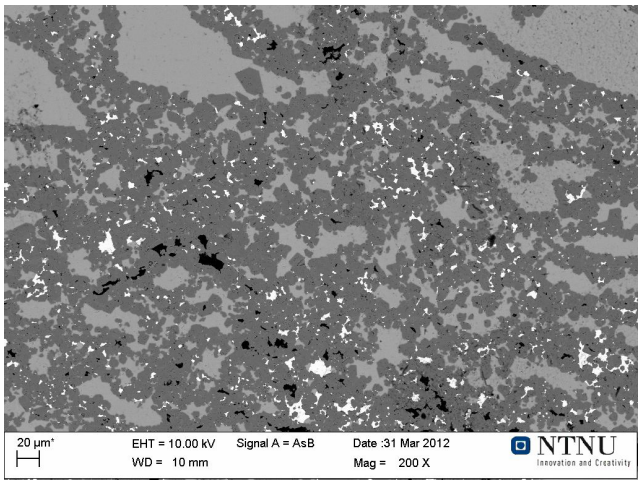

(b) 200X

Figure 4.26: Carbon particle partially converted to SiC and Si in sample position 8.

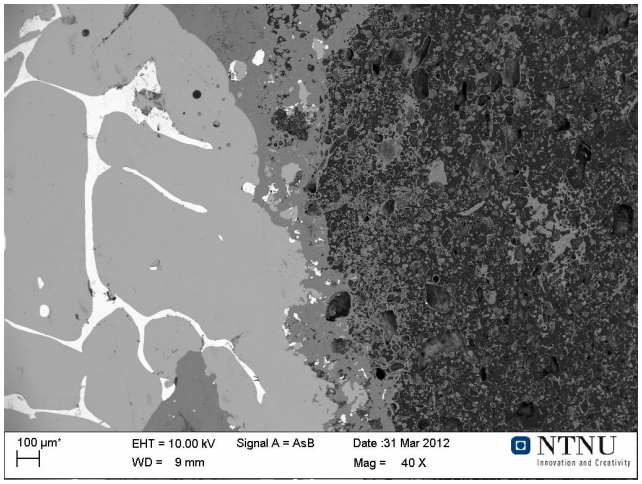

(a) 40X

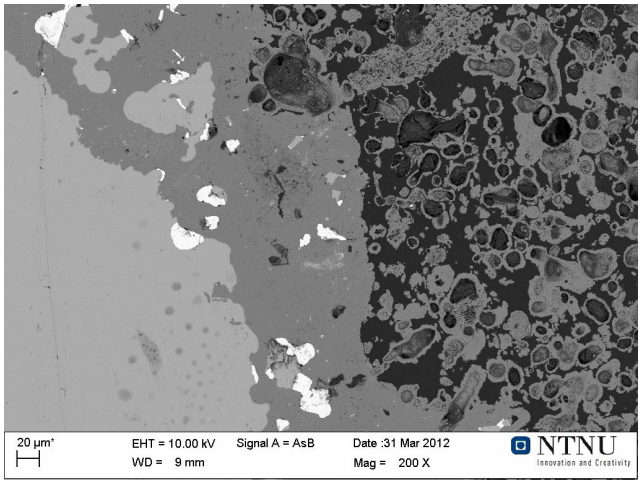

(b) 200X

Figure 4.27: Carbon particle partially converted to SiC and Si in sample position 9.

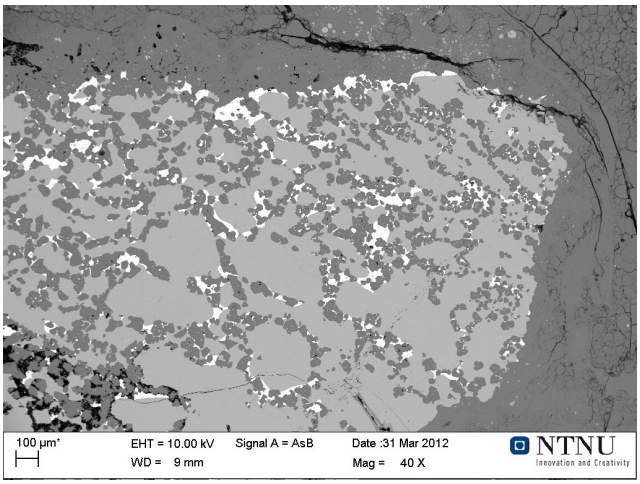

(a) 40X

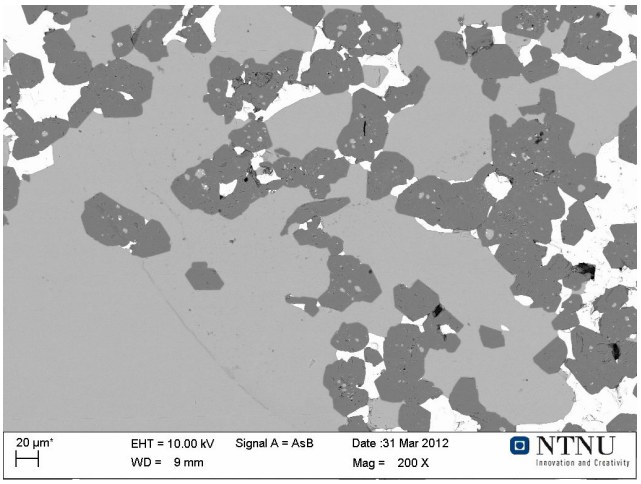

(b) 200X

Figure 4.28: SiC particle partially converted to Si in sample position 10.

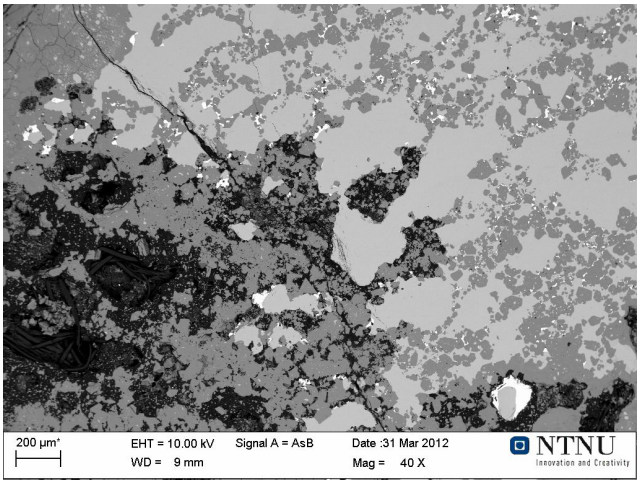

(a) 40X

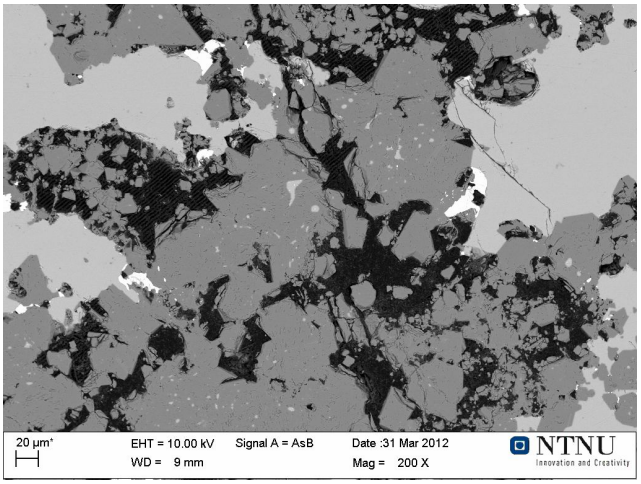

(b) 200X

Figure 4.29: SiC particle partially converted to Si in sample position 11.

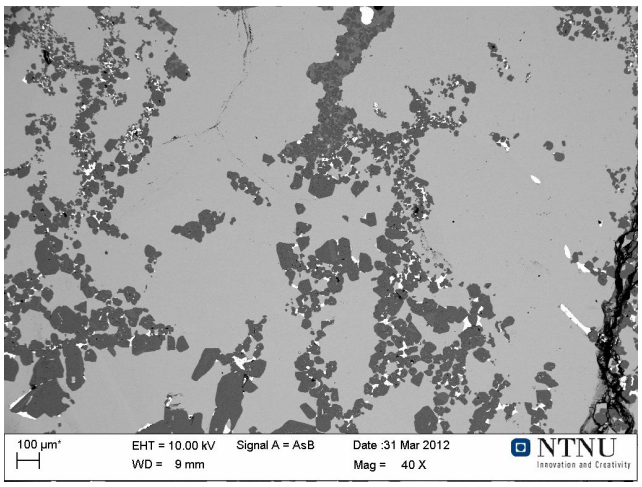

Figure 4.30: SiC particle almost fully converted to Si in sample position 12. - 40X

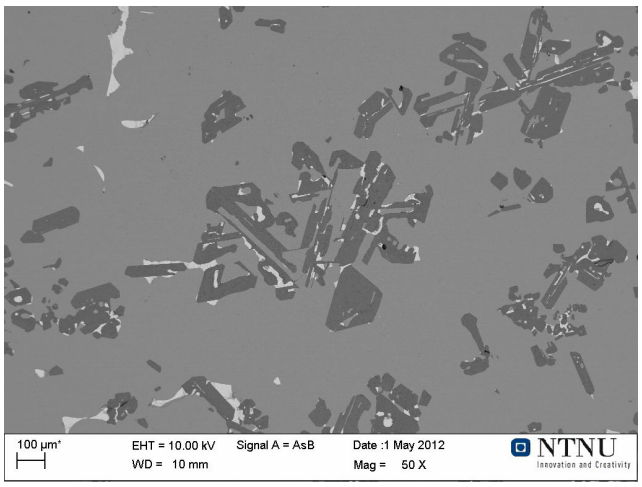

Figure 4.31: Silicon metal with SiC particles from position 13 (metal bath - upper phase). - 40X

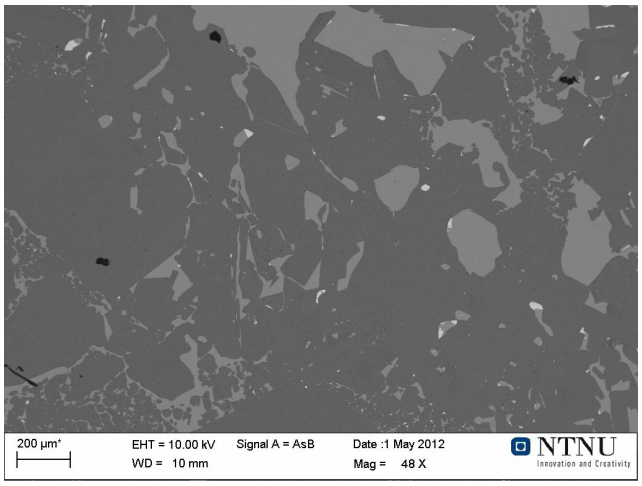

Figure 4.32: SiC rich phase with soaked with silicon metal in position 14 (metal bath - lower phase). - 40X

4.2 Induction furnace experiments (IF75)

In the following section the results from the IF75 experiments are presented. Observations from the furnace, mass balance, cross-sections from the crucibles as well as the samples taken from these are included. The condensate in the cavity roof has been investigated by microstructure analysis in the SEM as well as mechanical testing.

4.2.1 Experiment observations

Temperature data has been recorded for all five experiments. Type C thermocouples were positioned in the hot spot (T_{bottom}) as well as where the cavity roof was expected (T_{top}). Furnace power input was also listed during the experiments giving an impression on when the endothermic reaction occurs. The crucibles reached their target temperature after heating for about 45 minutes Experiment 1 through 4 was held at the target temperature for 60 minutes to obtain comparable results. The last experiment was held for 15 minutes, since this was sufficient to produce condensate in the upper charge layer.

No particular events were observed during experiment 1. No gas or flames could be seen at the crucible top. Furnace power was reduced after 30 minutes to stabilize the temperature atT_{bottom} ≃1790 °C (figure 4.33).

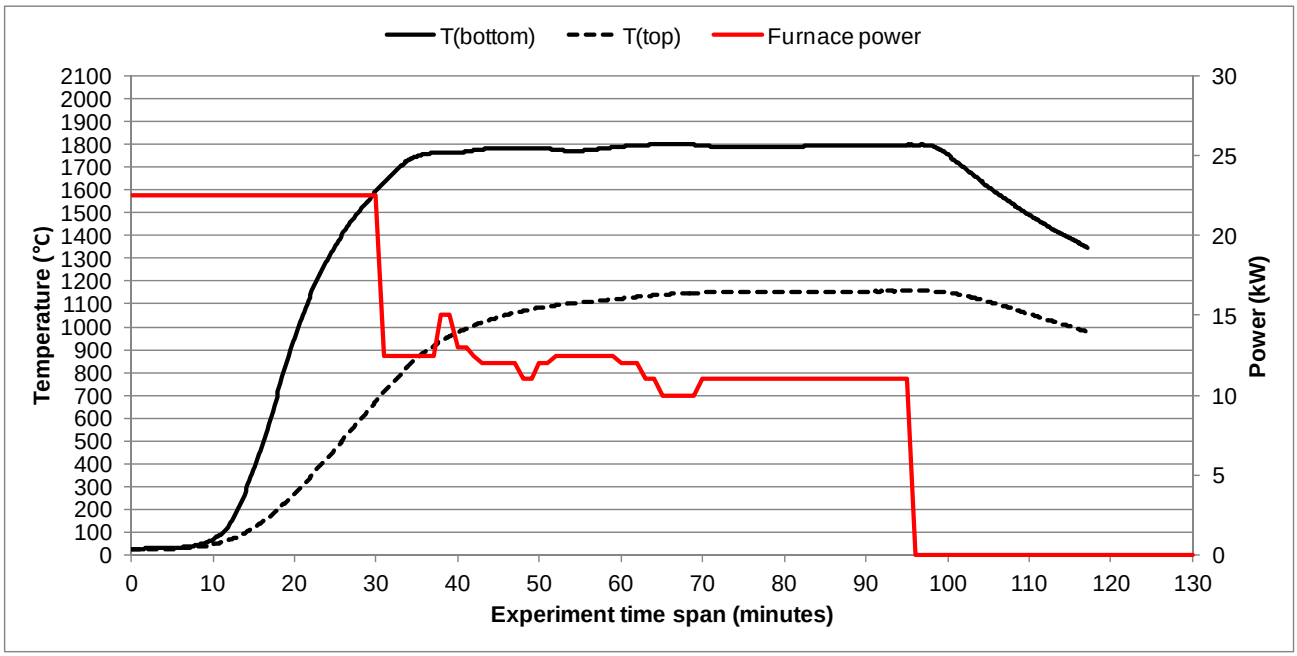

Figure 4.33: Time - temperature graph for experiment 1. T_{bottom} ≃1790 °C was held for 60 minutes. The furnace power output is displayed in the red line. $T_{top(max)}$ ≃1150 °C

The second experiment was held at T_{bottom} ≃1820 °C. Small gas flames appeared at T_{bottom} ≃1600 °C for experiment 2, 3 and 4 (figure 4.34, 4.35 and 4.36). Larger flames which stood 20 cm above the crucible top were observed in experiment 4 after ∼45 minutes. In experiment 5 (figure 4.37) where the upper third of the charge consisted of quartz and coke, the behavior on the charge top was significantly different. Black smoke emerged from the top after ∼20 minutes, but calmed down, disappeared and were replaced by the beforehand mentioned small gas flames at around 50 minutes.

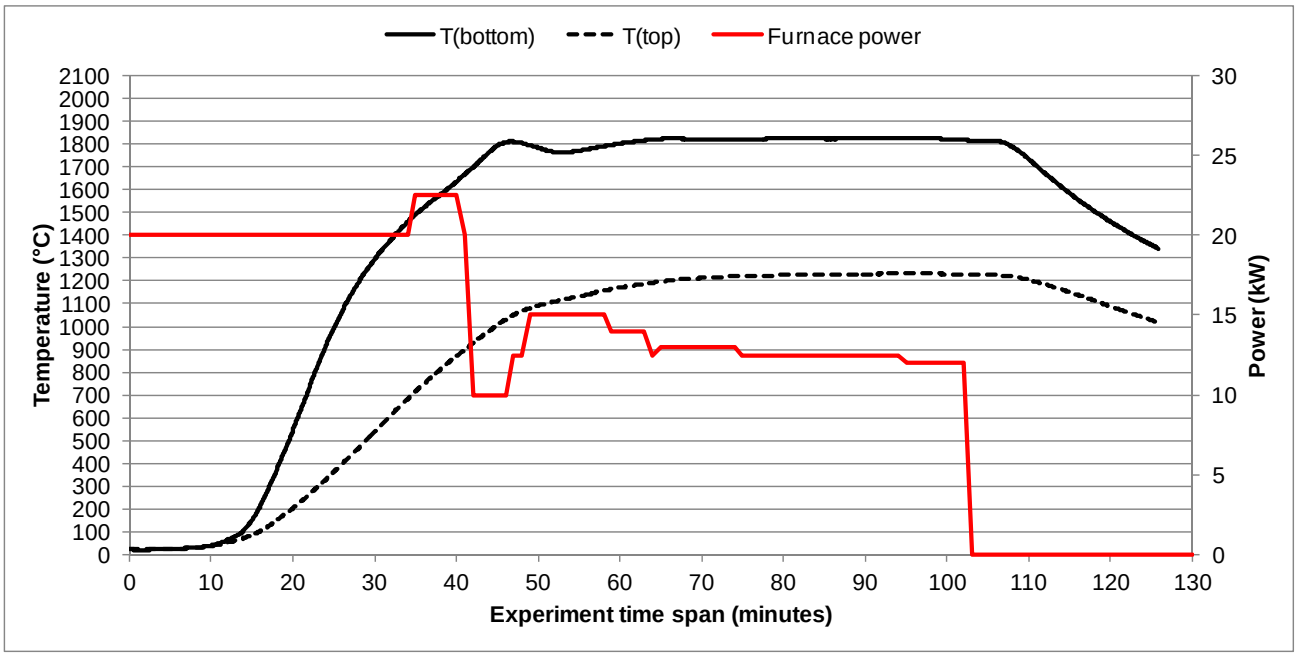

Figure 4.34: Time - temperature graph for experiment 2. T_{bottom} ≃1820 °C was held for 60 minutes. The furnace power output is displayed in the red line. $T_{top(max)}$ ≃1230 °C

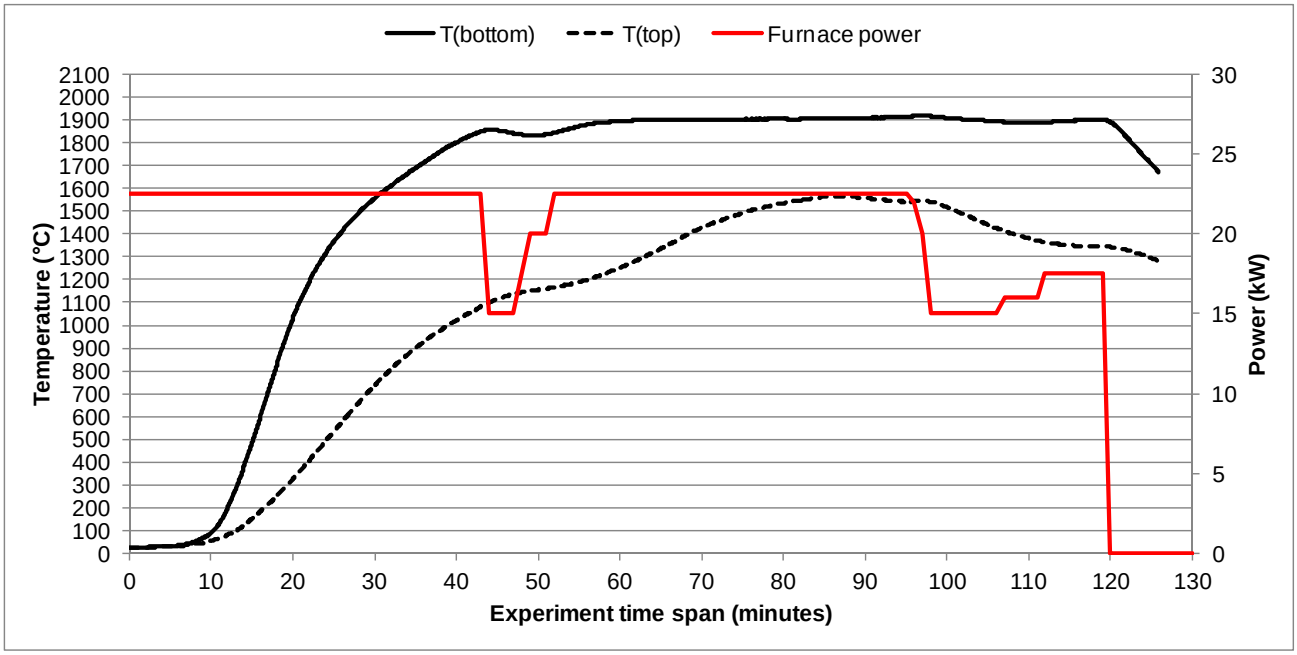

Figure 4.35: Time - temperature graph for experiment 3. T_{bottom} ≃1900 °C was held for 60 minutes. The furnace power output is displayed in the red line. $T_{top(max)}$ ≃1565 °C

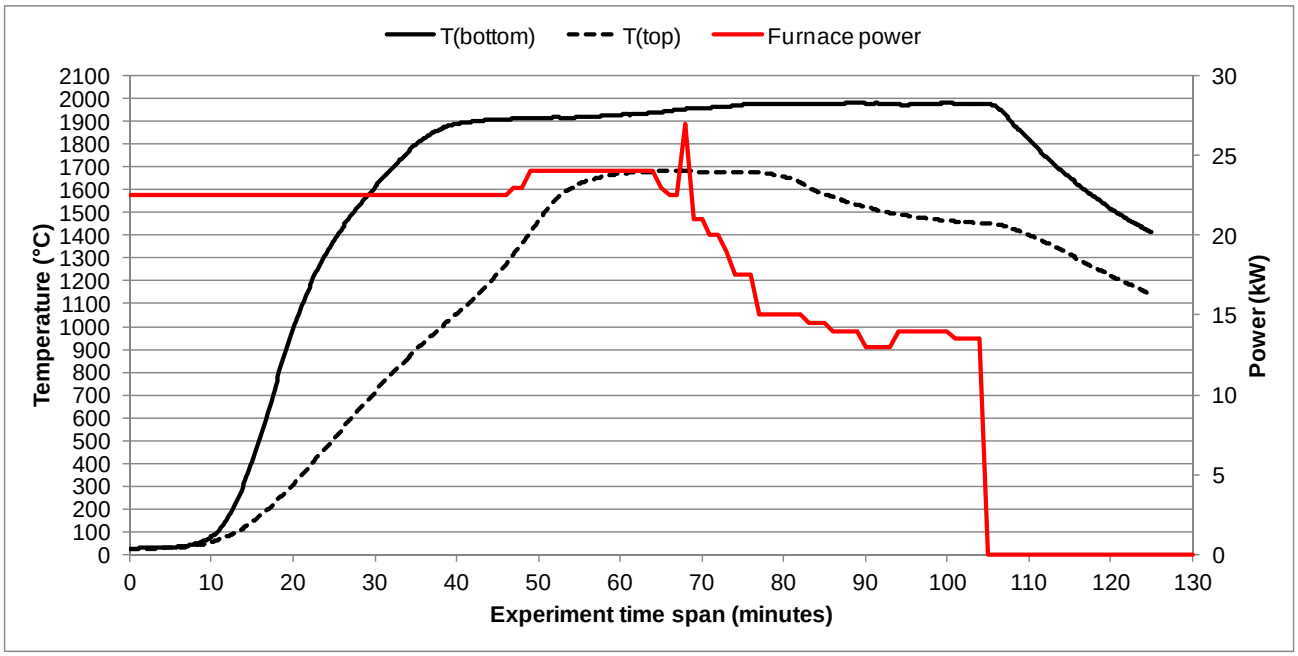

Figure 4.36: Time - temperature graph for experiment 4. T_{bottom} ≃1920→1980 °C was held for 60 minutes. The furnace power output is displayed in the red line. $T_{top(max)}$ ≃1680 °C

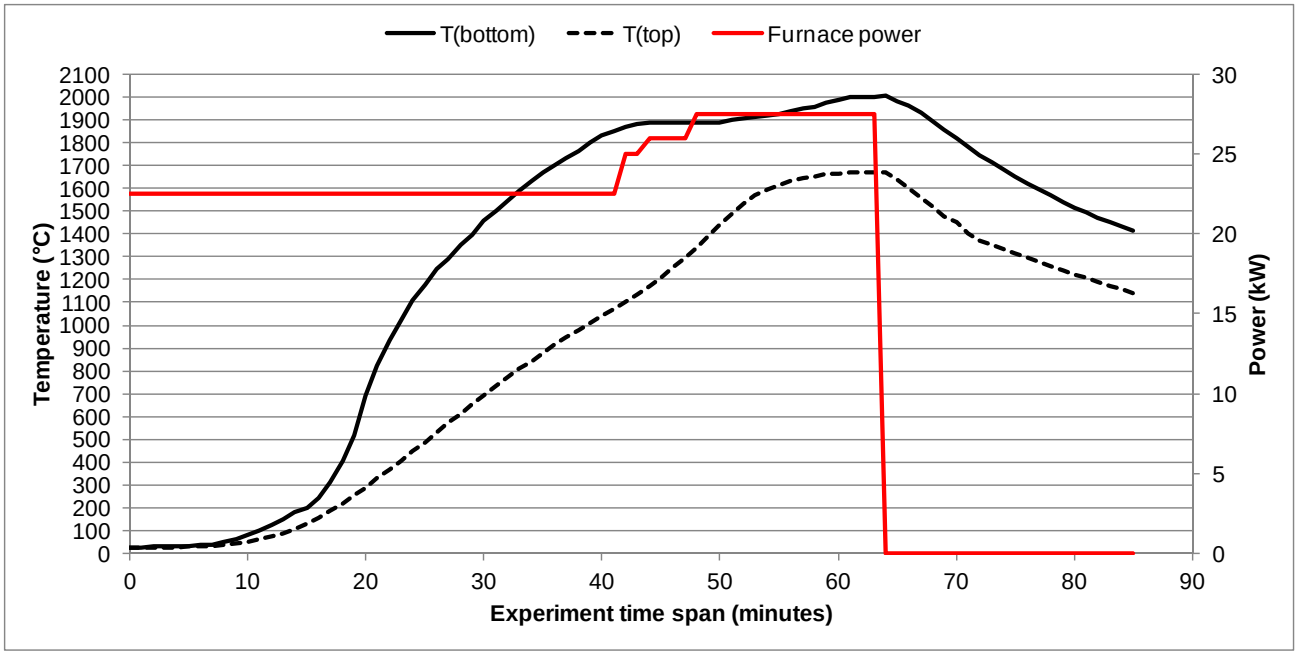

Figure 4.37: Time - temperature graph for experiment 5. T_{bottom} ≃1900→2000 °C was held for 15 minutes. The furnace power output is displayed in the red line. $T_{top(max)}$ ≃1670 °C

By calculating the integral under the power input graph, an indication on the total power comsumption for each experiment could be obtained. In table 4.1 the calculated energy consumptions are listed.

Table 4.1: Estimated power comsumptions for the IF75 experiments.

Experiment	Energy consumption [kWh]
1 (∼1790 °C)	24.23
2 (∼1820 °C)	27.31
3 (∼1900 °C)	41.91
4 (∼1980 °C)	35.49
5 (∼2000 °C)	25.65

4.2.2 Mass balance

The crucibles were weighed before and after the experiments, as well as after they were filled with epoxy. The weights can be seen in table 4.2. The difference in mass is due to gas escaping from the crucibles. Gas evolution is a result of the chemical reactions inside the crucible, and indicates the reaction rates for the different experiments.

Table 4.2: Weights from the IF75 experiments.

Experiment	Crucible(empty)	Crucible(full)	Charge	After exp.	Mass lost	$\frac{m_{lost}}{m_{charge}}$	Epoxy filled
1(∼1790 °C)	6004 g	11311 g	5307 g	11191 g	120 g	2.3%	1828 g
2(∼1820 °C)	6005 g	11320 g	5315 g	11177 g	143 g	2.7 %	1832 g
3(∼1900 °C)	6035 g	11352 g	5317 g	10840 g	512 g	9.6 %	599 g
4(∼1980 °C)	5981 g	11320 g	5339 g	10639 g	681 g	13.8 %	387 g
5(∼2000 °C)	6009 g	10920 g	4911 g	10181 g	739 g	15.0 %	0

4.2.3 Cross-sections of crucibles

Crucible 1 through 4 was filled with epoxy and cut in the vertical axis leaving the cross-sections shown in figure 4.38. Condensates produced in the upper part of crucible 3 and 4 obstructed the epoxy from flowing all the way down. A cavity can therefore be seen in these crucibles, while 1 and 2 was completely filled with epoxy. The cavity roof was positioned at approximately the same level for 3 and 4, although the brown condensate have penetrated further up in the crucible in number 4. This is also reflected in the high $T_{top(max)4}$ ≃1680 °C compared to $T_{top(max)3}$ ≃1565 °C for crucible 3, since the condensation reaction is exothermic.

Although the quartz had begun to melt in the first two crucibles, no condensate could found in these crucibles. The quartz inside crucible 2 had melted at a slightly higher level than in crucible 1 where the temperature was lower.

The material in the lower part of the cavity roof in crucible 3 and 4 was covered with a white layer of condensate, or brown condensate which had changed color after being exposed to high temperatures.

(a) Experiment number 1. T(bottom)≈1790°C.

(b) Experiment number 2. T(bottom)≈1820°C.

(c) Experiment number 3. T(bottom)≈1900°C.

(d) Experiment number 4. T(bottom)≈1980°C.

Figure 4.38: Cross-sections of the crucibles heated in the induction furnace (IF75). The crucibles width was 150 mm.

4.2.4 SEM images - condensate in IF75

Layers of brown condensate (SiO_2+Si) were deposited above the cavities in experiment 3 and 4. Samples from crucible 3 and 4 were extracted from the cavity roof region, and investigated in the SEM. The images in figure 4.39 shows the condensate when it is deposited at a fairly low temperature. The structure was fairly homogenous with small Si-spheres (d<1 μm). Figure 4.40, 4.41 and 4.42 was all from the same sample, but the microstructure varied somewhat. The structure was less homogenous, and the silicon was found as spheres with d<1 μm to bigger clumps larger than 10 μm.

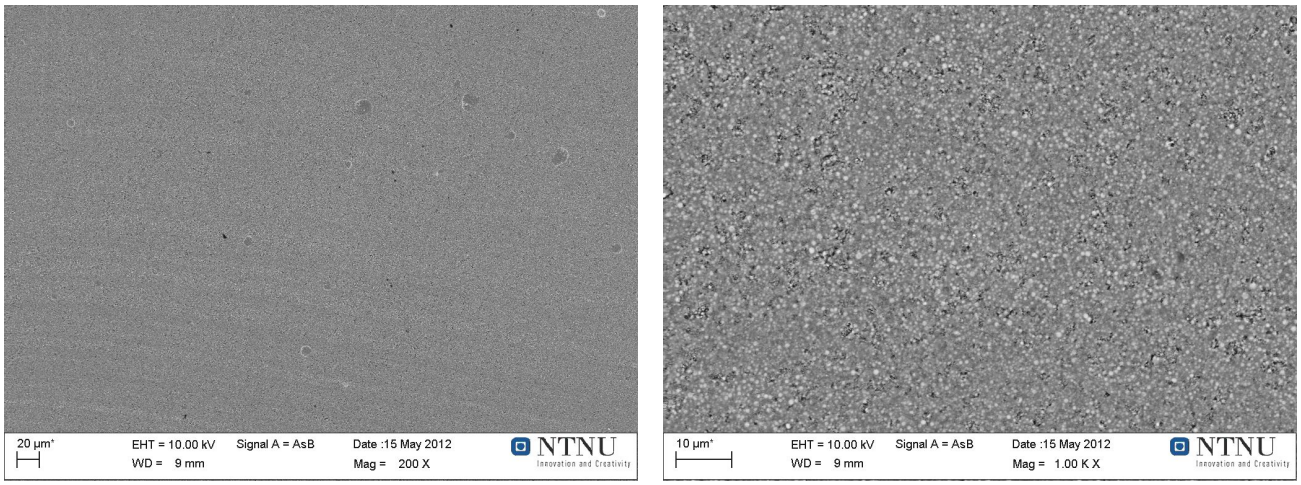

(a) 200X **(b)** 1000X

Figure 4.39: SEM images from the brown condensate in the cavity roof, exp. 3. $T_{bottom} \simeq 1565$ °C

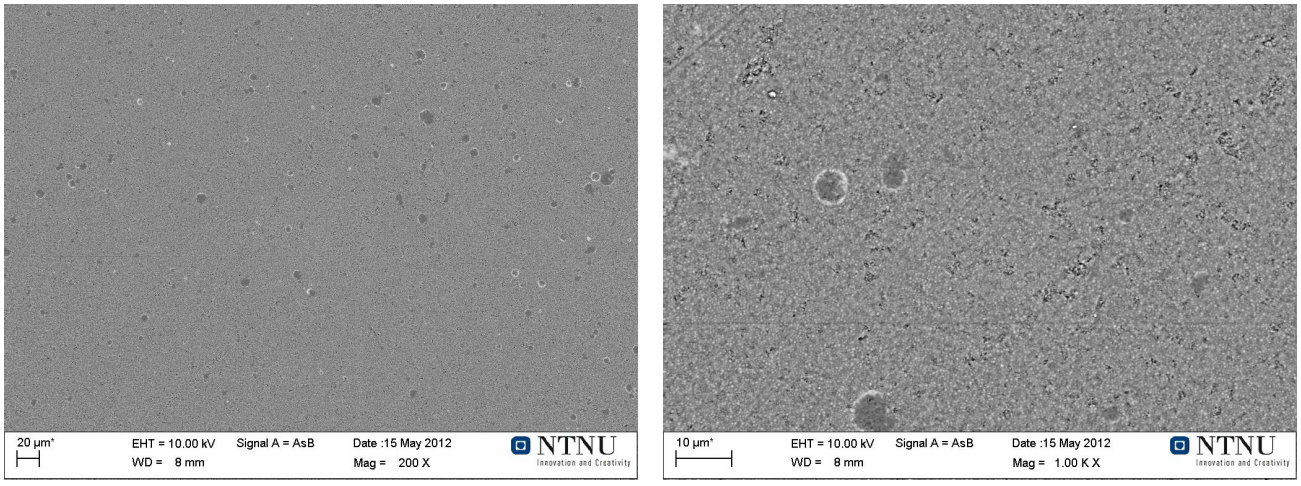

(a) 200X **(b)** 1000X

Figure 4.40: SEM images from the brown condensate in the cavity roof, exp. 4. $T_{bottom} \simeq 1680$ °C

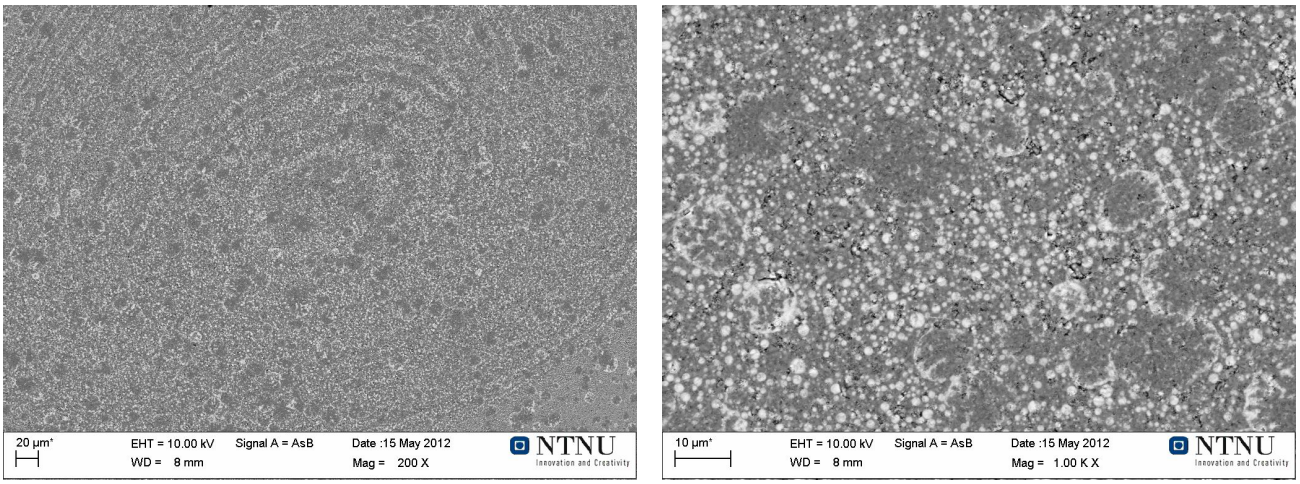

(a) 200X **(b)** 1000X

Figure 4.41: SEM images from the brown condensate in the cavity roof, exp. 4. $T_{bottom} \simeq 1680$ °C

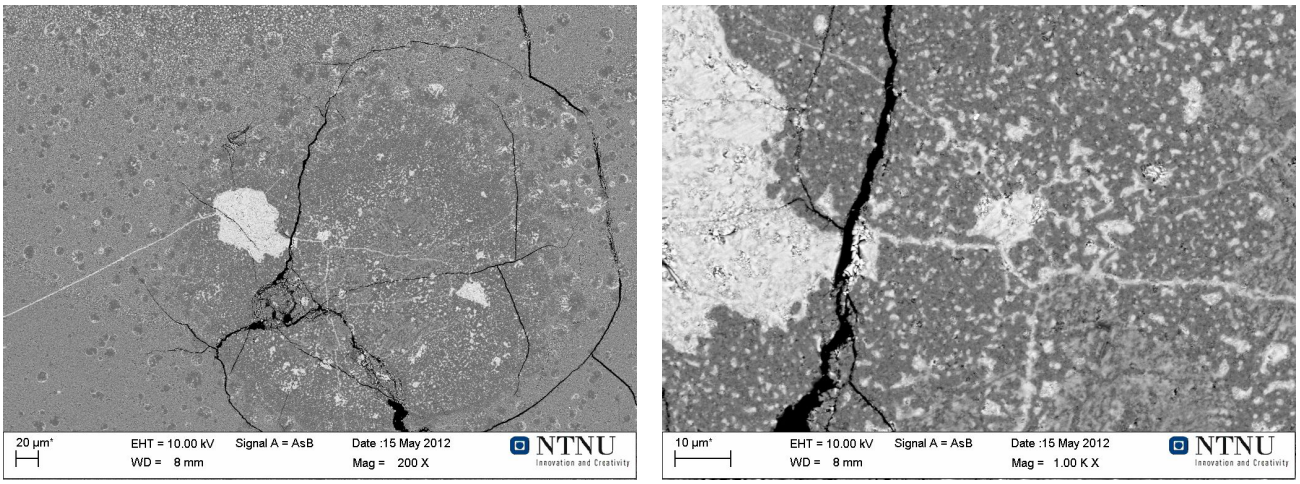

(a) 200X **(b)** 1000X

Figure 4.42: SEM images from the brown condensate in the cavity roof, exp. 4. $T_{bottom} \simeq 1680$ °C

4.3 Compression tests of cavity roof material

The purpose of experiment 5 was to create enough condensate in the upper part of the crucible which could subsequently be mechanically tested. Epoxy was not filled in the crucible, and samples were extracted. Compression tests were conducted, and the results are graphically presented in fig. 4.43, 4.44 and 4.45 as well as an overview in table 4.3. The tests showed that the samples exposed to low temperatures (T<1670 °C) had a higher compression strength than those exposed to higher temperatures (T>1670 °C).

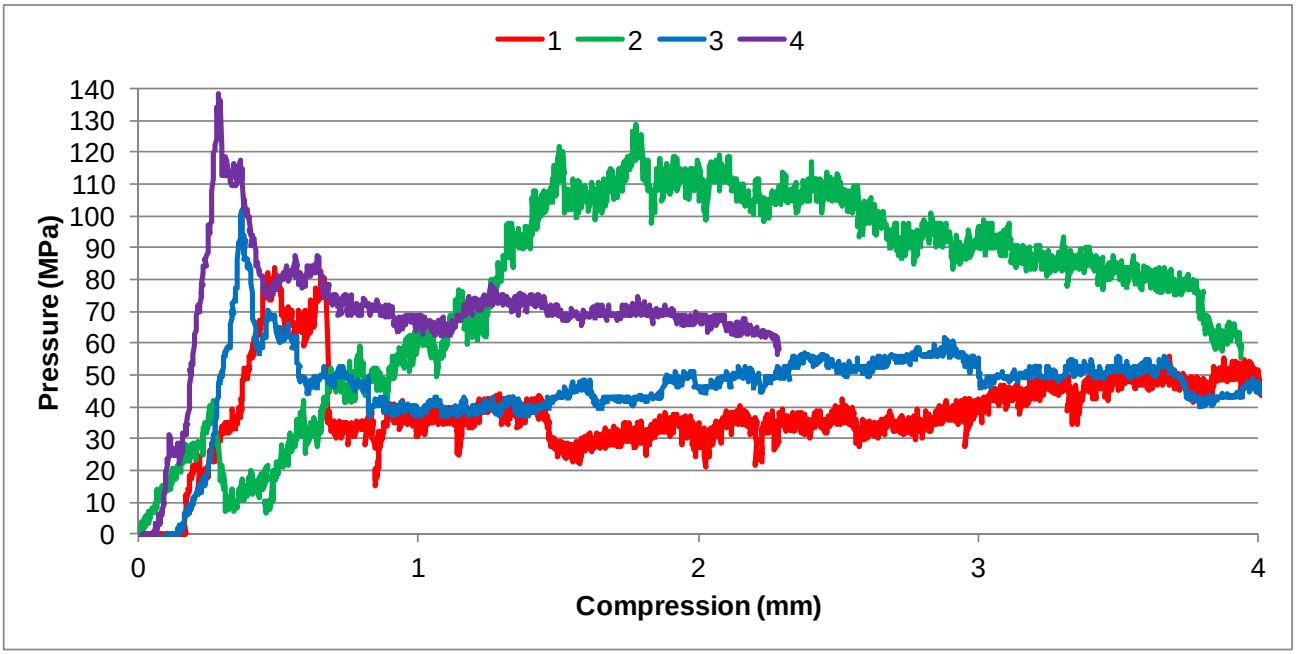

Figure 4.43: Compression tests of samples exposed to T>1670 °C

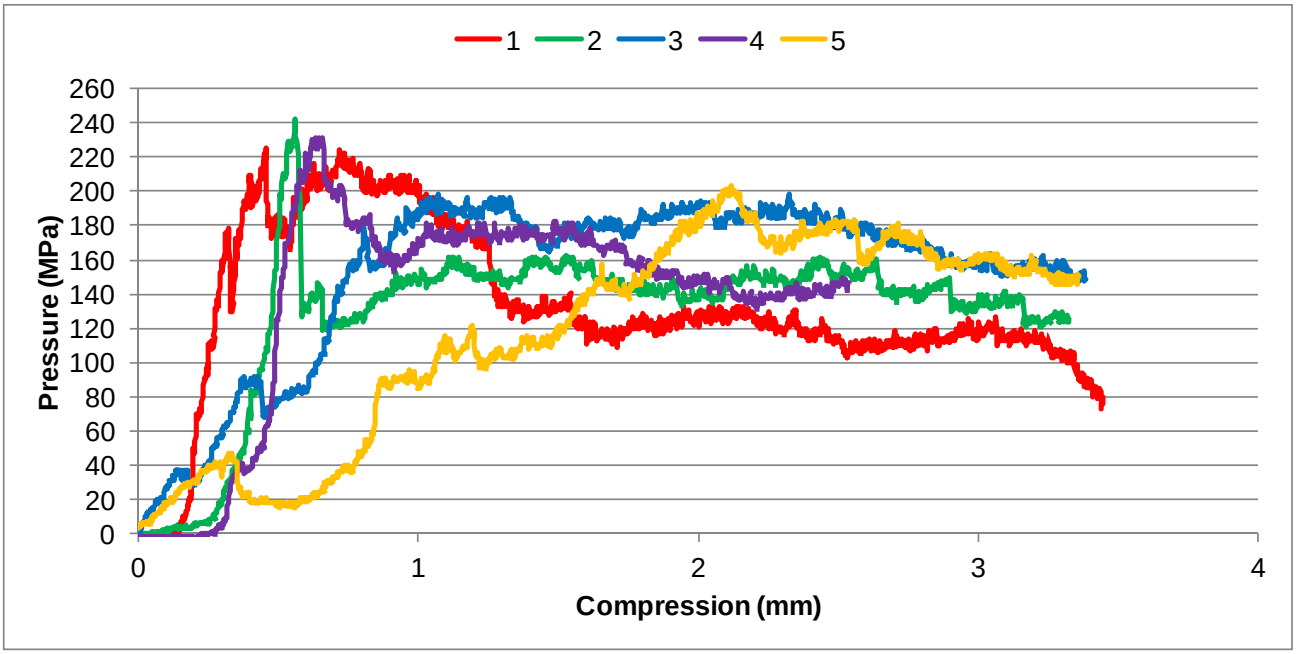

Figure 4.44: Compression tests of samples exposed to T≈1670 °C

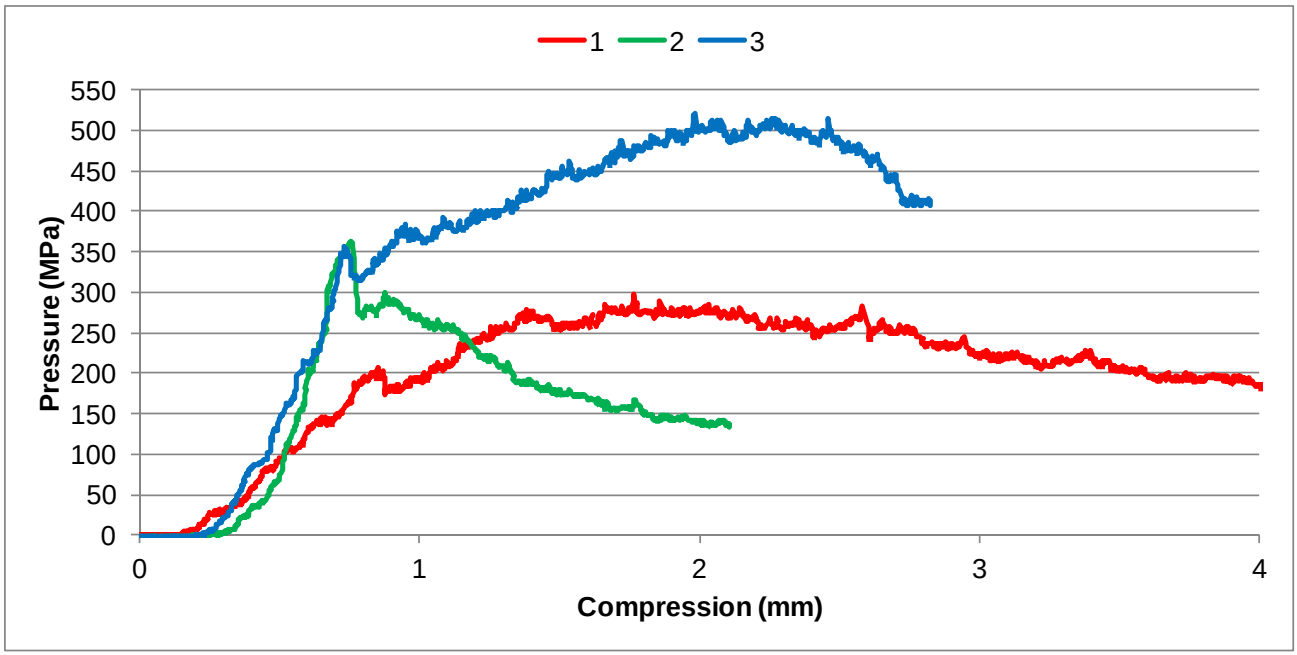

Figure 4.45: Compression tests of samples exposed to T<1670 °C

Table 4.3: Maximum Compressive strength for the samples from the IF75 experiments.

Temperature exposure	>1670 °C	~1670 °C	<1670 °C	Quartz reference, room temp.
Compressive strength (MPa)	84	226	299	~288
	130	243	364	~203
	105	200	524	~133
	139	234		~370
		203		
Av. compressive strength (MPa)	~115	~221	~396	~249

Chapter 5

Discussion

5.1 Silicon production in the IF 75 experiments

The mass balance from the IF75 experiments can tell us how much silicon there was in the metal, compared to the amount of silicon in the condensate. The mass decrease after each experiment was assumed to be CO gas escaping the crucible. The SiO gas was contained inside the crucible since no condensate were observed to reach the top of the crucible charge. Characteristic white smoke was also not observed under any of the experiments. If all mass lost is CO-gas, then the stoichiometry will be according to the total reaction $SiO_2 + 2SiC = 3Si + 2CO(g)$, since the molar ratio is $\frac{SiC}{SiO_2} = 2$. It is possible to calculate the theoretic amount of silicon produced through this reaction. For every mole of CO (n_{CO}) gas produced, there will be produced $n_{Si} = \frac{3}{2} \cdot n_{CO}$ moles of silicon metal. The according weight ratio becomes:

$\frac{m_{Si}}{M_{Si}} = \frac{3}{2} \cdot \frac{m_{CO}}{M_{CO}} \rightarrow m_{Si} = \frac{3M_{Si}}{2} \cdot \frac{m_{Si}}{M_{Si}} = \frac{3 \cdot 28.1 g/mol}{2} \cdot \frac{m_{CO}}{28 g/mol} = 1.505 \cdot m_{CO}$

Through this rough estimate we get the values for the different experiments in table 5.1. An estimate for how high a corresponding pool of molten silicon will reach in the crucible used in the IF75 experiments is also included in this table. A cylindrical shape for this pool was assumed, and the formula used was: $h = \frac{m_{Si}}{\rho_{Si} \cdot \pi \cdot r^2}$. The measured height of the silicon pool in experiment 4 was ∼2.4 cm, indicating that all the silicon cannot be found in a pool at the bottom. In this experiment, this equals ∼452 g silicon that should be found somewhere else. This silicon will most likely have been gasified into SiO through reaction (2) and (3) and then condensed in the upper part of the charge according to reaction (-3). This combination of reactions will result in heat being transported upwards in the furnace.

$$2SiO_2(s,l) + SiC(s) = 3SiO(g) + CO(g) \qquad \triangle H_{2000^\circ C} = 1364 \text{ kJ/mol} \qquad (2)$$

$$SiO_2(s,l) + Si(s,l) = 2SiO(g) \qquad \triangle H_{2000^\circ C} = 599 \text{ kJ/mol} \qquad (3)$$

$$2SiO(g) = SiO_2(s,l) + Si(s,l) \qquad \triangle H_{1800^\circ C} = \text{-}606 \text{ kJ/mol} \qquad (-3)$$

452 g of silicon will therefore probably be in the form as silicon droplets inside the condensate in the cooler parts of the crucible. This is a substantial amount of silicon, ∼44% of the total amount produced. One can say that recovery of silicon from the condensate is an important factor for the silicon process, and that this contributes as an important silicon producing mechanism.

The total energy consumption could also be estimated for experiment 4. The electrical consumption was ∼35.49 kWh, and ∼573 g Si was produced, this gave a power consumption of ∼62MWh per ton Si. This is very high compared to the industrial consumption which is around 11-13 MWh / ton Si.

Table 5.1: Estimate of silicon produced in the IF75 experiments.

Experiment	Mass lost (m_{CO})	m_{Si} estimated	height of silicon pool (estimate)	height of silicon pool (measured)	m_{Si} in pool	m_{Si} not in pool
1 (∼1790 °C)	120 g	181 g	0.76 cm	0		
2 (∼1820 °C)	143 g	215 g	0.90 cm	0		
3 (∼1900 °C)	512 g	771 g	3.2 cm			
4 (∼1980 °C)	681 g	1025 g	4.3 cm	∼2.4 cm	∼573 g	∼452 g
5 (∼2000 °C)	739 g	1112 g	4.7 cm			

5.2 Reaction rates in the IF75 experiments

When comparing the temperature graphs for the IF75 experiments (figure 5.1), it is evident that there is a resistance against further temperature increase between 1850 and 1900 °C. For the first two experiments the power was reduced around this point to be able to stabilize to the desired temperatures. This resistance against temperature increase is caused by the strongly endothermic reactions (2), (3) and (4). These reactions will have negative △G values at temperatures higher than those listed below. The $\triangle G$ values are also graphically presented in figure 5.2 for these reactions.

$$2SiO_2(s,l) + SiC(s) = 3SiO(g) + CO(g) \qquad \triangle G = 0 \text{ at } 1877\ ^\circ\text{C} \qquad (2)$$

$$SiO_2(s,l) + Si(s,l) = 2SiO(g) \qquad \triangle G = 0 \text{ at } 1870\ ^\circ\text{C} \qquad (3)$$

$$SiO(g) + SiC(s) = 2Si(s,l) + CO(g) \qquad \triangle G = 0 \text{ at } 1930\ ^\circ\text{C} \qquad (4)$$

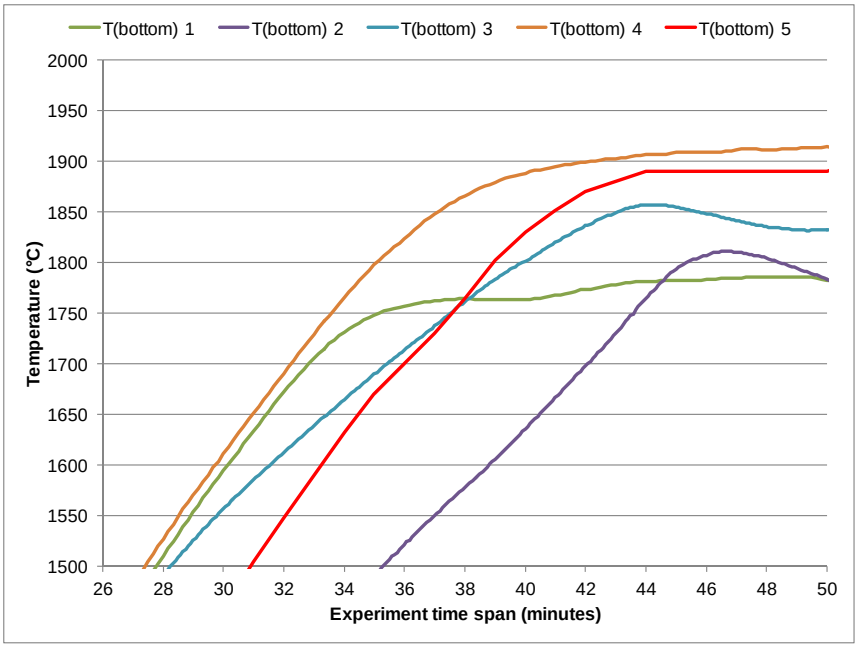

Figure 5.1: Comparison of the temperature graphs for the IF75 experiments. The graph is zoomed in on the area where the temperature increase is halted.

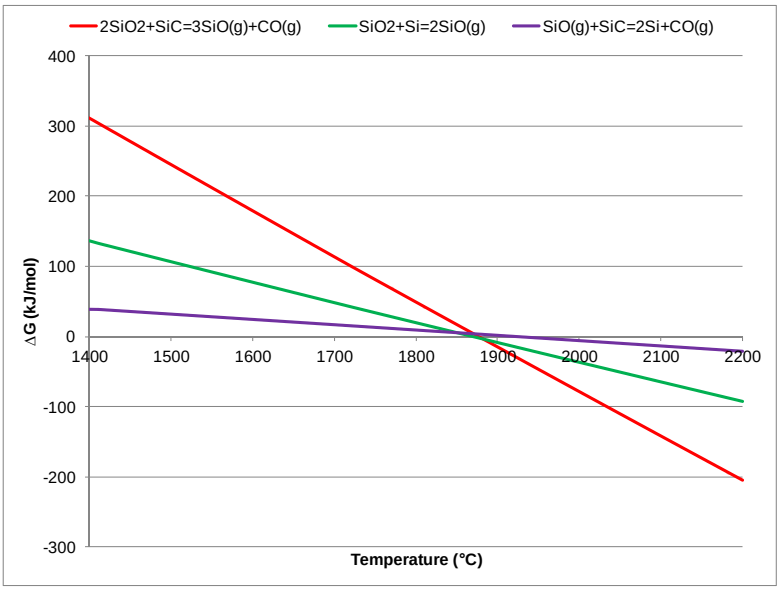

Figure 5.2: $\triangle G$ values for the strongly endothermic reactions in the silicon process.

By taking a closer look at experiment 4 a better understanding of the heat-consuming reactions can be obtained. This experiment had a stable energy input of 22.5 kW the first 46 minutes, and significant resistance against further temperature-increase occured when the temperature was between 1800 and 1900 °C. This corresponded well with reaction (2) and (3), and was an indication of high reaction rate for these reactions at this temperature level. The results from Andersen (2010) are also comparable in this case (figure 5.3). Maximum rate of conversion (reaction rate) was obtained at around 1840 °C for the powder mixture of SiO_2 and SiC. Reduction of heating rate under constant power input, is an indication that certain reaction occurs, and can be compared to reaction rate in a limited manner. The results from experiment 4 correlates well with Andersen's results. Since the raw materials used in the IF75 experiments were SiO_2 and SiC, it is also natural that reaction (2) would dominate.

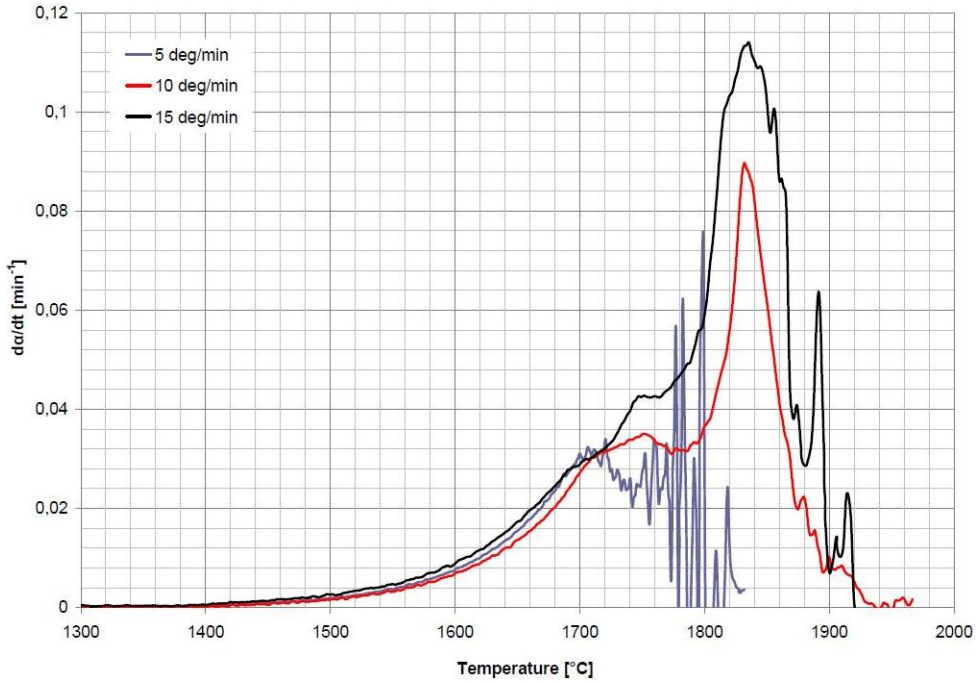

Figure 5.3: Rate of conversion of SiO_2 + SiC mixture versus temperature. (Andersen 2010)

Regarding the energy comsumption for the IF75 experiments (listed in table 5.2), it is interesting to see how the reaction rate is dependant on the temperature inside the furnace. The first two experiments had fairly low power consumption, as well as a not significant mass difference. This indicates that the reaction rate at temperatures around 1800 °C were fairly low. When the temperature was raised to ∼1900 °C (exp. 3) the mass lost was about four times higher than the first two experiments although the power consumption is only 1.5 times higher. Increasing the temperature to 1900 °C resulted in a significant increase in reaction rate. A more significant change in reaction rate could be seen for the last two experiments. The temperature was now around 2000 °C and the percentage mass lost was around 14 %. This charge consumption was 1.5 times higher than for the situation at ∼1900 °C. Interestingly the power consumption was lower for ∼2000 °C than for ∼1900 °C. The experiment at ∼1900 °C lasted somewhat longer, and operated at stable, high load. But the load was not high enough to raise the temperature significantly, and most of the energy used, was probably just spent heating the cooling water.

Raising the temperature slightly, from ∼1980 °C to ∼2000 °C had great impact on the rate of consumption. As can be seen in figure 4.36 and 4.37, the duration for exp 4 was ∼105 minutes, while exp 5 lasted ∼65 minutes, a whole 40 minutes shorter. This resulted in a lower power consumption and higher rate of consumption. The importance having sufficient temperature in the hot zone in the silicon furnace is a key aspect, and should always be kept in mind.

Table 5.2: Estimated power comsumptions and relative mass lost after the IF75 experiments.

Experiment	Energy consumption [kWh]	$\frac{m_{lost}}{m_{charge}}$
1 (∼1790 °C)	24.23	2.3%
2 (∼1820 °C)	27.31	2.7 %
3 (∼1900 °C)	41.91	9.6 %
4 (∼1980 °C)	35.49	13.8 %
5 (∼2000 °C)	25.65	15.0 %

SiO-gas formation is also a good indication on the rate of the reactions inside the furnace. The SiO-gas formation is tightly related to the condenate deposition in the upper part of the furnace which in turn raises the temperature in the cavity roof. A high temperature in the cavity roof region will thus be a sign that the SiO gas forming reactions are active. Maximum values in the cavity roof ($T_{top(max)}$) was for experiment 4 and 5 (fig. 4.36 and 4.37) measured to ∼1675 °C, which was significantly higher than for experiment 3 (∼1565 °C, see fig. 4.35). The first two experiments had $T_{top(max)} \simeq 1200$ °C (fig. 4.33 and 4.34). These temperature values indicated a high reaction rate for SiO production (reaction (2) and (3)) for crucible 4 and 5, which had bottom temperatures of ∼1980 °C and ∼2000 °C.

5.3 Condensate in the IF75 experiments

The condensate found in the IF75 experiments and in the pilot scale experiment was mainly the brown kind. This condensate was very distinct and easy to spot with its brown color. This type of condensate consisted of Si droplets in a SiO_2 matrix. Immediately after deposition, the Si-spheres were small and homogenously distributed in the the SiO_2 matrix. The SEM images representing the condensate under discussion can be seen in section 4.2.4. While the silicon spheres in the condensate taken from ∼1565 °C were homogenously distributed, the silicon in the sample taken from ∼1680 °C were varying a lot more in size. The SEM images was taken from the same sample, but showed big variation in microstructure. These variations can be explained by the fact that condensate will continously be deposited as long as the SiO pressure is sufficient. "Fresh" condensate will have the virgin homogenous structure with small Si-droplets, while the condensate exposed to the environment for a longer time period will probably agglomorate into larger units. This agglomoration will be faster when the temperature is increased.

There was no evidence of condensate formation in crucible 1 ($T_{bottom1}$ ≃1790 °C) and 2 ($T_{bottom2}$ ≃1820 °C), indicating that SiO gas will not be produced from reaction (2) and (3) at temperatures below 1820 °C. This is a fair assmuption since the driving force for these reactions are very low below this temperature. This is supported in the stability diagram (figure 2.2) as well as from Andersen's experiments (figure 2.3)

In experiment 4 the condensate formation had raised the temperature in the position indicated by figure 5.4 to 1680 °C. Below this position in the crucible where the temperature was higher, the silica changed appearence at the macrographical level. From being seemingly solid and unmelted above this point, the quartz particles changed to a more glassy and viscous look. The softening point of the quartz used was therefore ∼1680 °C. Above this level in crucible 4, the brown condensate dominated. Below the same level the condensate seemed to have changed color. From having a brown color below ∼1680 °C, the layer around the particles whitened when the temperature exceeded this temperature. This white layer can be seen in fig. 5.5b This is probably the same behavior as Vangskåsen (2011*a*) discovered. During heating of the brown condensate, the silicon perspired and gathered in a pool, leaving a white amorphous SiO_2 structure. Vangskåsen (2011*a*) also discovered that temperatures above 1700 °C will give rapid separation if Si in the condensate. The white color is probably an optical effect due to the relatively pure SiO_2 left behind. The brown condensate consists of silicon droplets in a SiO_2 matrix, and it would be reasonable to believe that heating of such a mixture would result in reaction (3) going to the right. This behavior was not confirmed by Vangskåsen (2011*a*), as the silicon escaped from the SiO_2 unreacted.

$$SiO_2(s,l) + Si(s,l) = 2SiO(g) \tag{3}$$

In crucible 3, the temperature at the same level was 1565 °C. Layers of brown condensate was found around this level. In the cavity walls the layer became grayish as seen in fig. 5.5a, due to the high temperature inside the cavity. The condensate in the cavity walls will be exposed to temperatures above 1565 °C, and since this is above the melting point of silicon T_m ≃1410 °C, the condensate will start to perspire liquid silicon leaving gray spots with low content of metallic silicon.

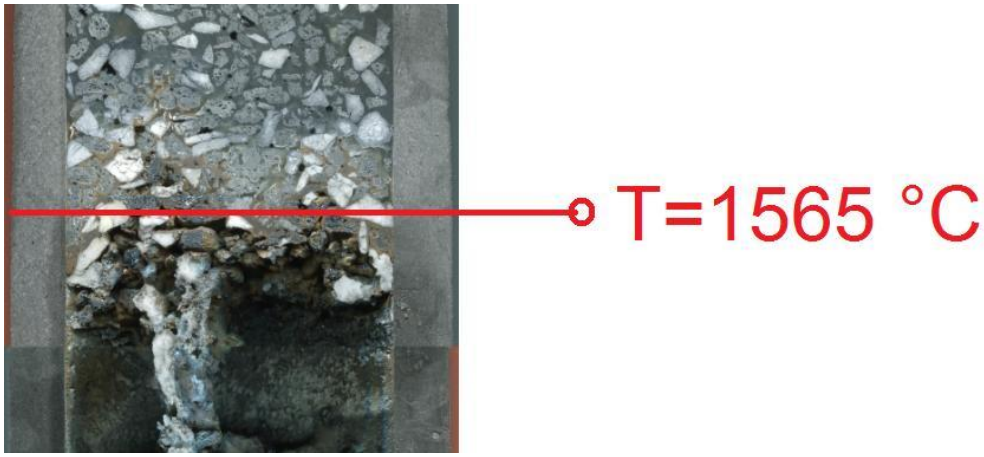

(a) IF75 experiment 3.

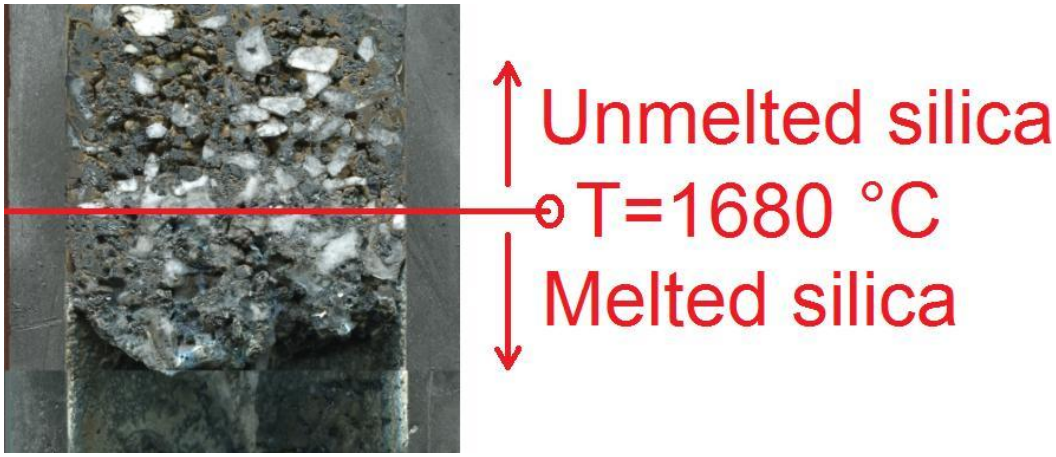

(b) IF75 experiment 4.

Figure 5.4: Maximum temperature obtained in the cavity roof regions. The crucible width is 150 mm.

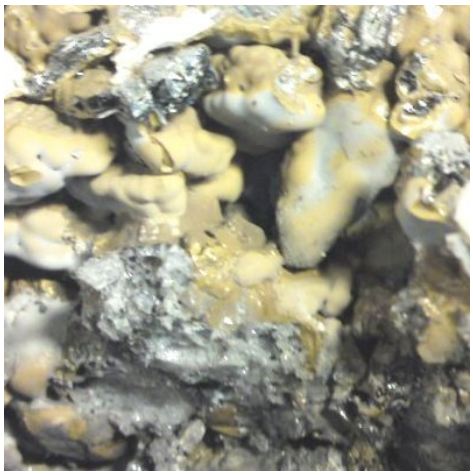

(a) Brown condensate with gray spots in crucible 3. $T_{bottom} > 1565$ °C.

(b) Condensate turned white in crucible 4.$T_{bottom} > 1680$ °C.

Figure 5.5: Pictures of the material underneath the cavity roof. The images covers an area approximately 25 x 25 mm.

5.4 Condensate in the pilot scale experiment

In the study of the condensate from the pilot experiment, samples were extracted from the top of the charge burden, and all the way down to the silicon bath underneath the electrode. By doing this, it was possible to say something about the behavior of the condensate as it was exposed to higher and higher temperatures downwards in the furnace. The SEM-images representing the condensate in the pilot furnace can be seen in section 4.1.2.

The microstructure of the condensate varied substantially as it slowly moved downwards in the furnace and became exposed to higher and higher temperatures. No temperature measurements were recorded, but from the appearence of the material it is possible to say something about how high the temperature must have been. Melting of the quartz particles occured below position 2 in fig. 4.1, and since the quartz is expected to melt above ∼1680 °C (discussed in sec. 5.3) the temperature at the top of the charge burden was at least below 1680 °C. The quartz used in the pilot experiment differs from the type used in the IF75 experiments, and will therefore not have the same melting point. After all quartz is not just quartz. Due to the cyclic behaviour of the silicon process, the temperature have probably varied a lot throughout the experiment which lasted for 44 hours. The pilot furnace was tapped 13 times, giving 87 kg of metal silicon.

The overall silicon yield in this experiment was 62%, meaning that 38% of the silicon has been lost to the off-gases. This is a relatively low yield compared to the industrial yield of 80-90% (Ringdalen & Tangstad 2012). The pilot furnace have probably been undercoked to produce enough gas to measure the emissions. This would result in periodically blowouts of SiO gas from the furnace top. A reasonable assumption would be that the temperature on top of the charge stayed below 1500 °C most of the time, but increased to around 1700 °C during these blowouts.

Condensate produced in the top of the pilot scale furnace was of the brown kind and consisted of Si particles in an SiO_2-matrix. The typical appeareance of the brown condensate can be seen in figure 5.6a. This sample consists of quartz and carbon particles, and the condensate can be found sticking on the surface of these particles. The material was embedded in epoxy, expaining the transparent yellow matter around the edge of the sample. The top of the furnace is defined as the area above the cavity roof and is represented by sample position 1, 2, 3 and 4 (see fig. 4.1). The cavity can be seen in this figure, to the left of the graphite electrode. The cross-section is representing half of the furnace body, and since the other half is more or less identical, it was not included due to pratctical considerations.

(a) Brown condensate in sample 4.

(b) Pale brown condensate in sample 5.

(c) Light brown condensate in sample 9.

Figure 5.6: Macrographical view of condensate in the samples from the pilot scale furnace. The samples have been polished and have a diameter of 25 mm.

Starting from sample position 1 and 2 the microstucture was relatively fine, but the particles have lost

their original spherical shape and the particles varied in size from 1 to 10 μm. Interconnecting lines of Si can slightly be seen between the particles, indicating that the Si in the condensate have melted and flowing together to make larger particles, hence explaining the size difference. Moving down in the furnace into sample position 3 and 4, the microstructure was composed of the same irregular structure as mentioned above. The size of the Si-particles varied from 1 to 10 μm and the shape reminded less of spheres but more of spots on a cow.

The microstructure of condensate in the upper part of the pilot scale furnace was coarser than the condensate found in the induction furnace experiments. This is probably due to the prolonged exposition of heat in the pilot furnace.

Raw material from the upper crust of the furnace were replaced by new material after stoking which was conducted after each tapping. The raw material in the upper section of the crucible would then be exposed to a certain environment for a specific time period. During this time period, the condensate would be heat treated making the microstructure coarser before the charge is broken down and sent towards the hot zone during stoking. The heat treated microstructure may change how the mixture reacts when it is sent down in the hot zone, and this could be subject for further investigation. For instance, will the condensate re-evaporate into SiO gas when directly exposed to temperatures above 2000 °C, or will the silicon separate and end up in the silicon pool? Previous reasearch (Vangskåsen 2011*a*) have found that the silicon will perspire when slowly heated up to temperatures above 1700 °C, but the behavior may be different when the condensate is suddenly heated to 2000 °C.

In the cavity side-walls in the pilot furnace (samples 5-12), the condensate looked different than the brown kind found right above the cavity. It had a pale brown color and the microstructure was less homogenous as seen in figure 5.6b. However, it consisted of the same phases, Si-particles in an SiO_2-matrix. In the samples 5 to 7, the Si-particles were more circular than those found above. This condensate have probably been exposed to high temperature for a konger duration than the condensate found in position 1 to 4, resulting in silicon droplets which have grown together and stabilized into circular particles. The droplets are generally less than 20 μm in diameter. The lines of silicon are more distinct and thicker, an they seem to go in the same direction, indicating that the silicon have flown down due to to gravity or some other force. The flow of silicon in the condensate can be compared to small raindrops running down a window, gathering into bigger drops of water.

From position 8 and below to 12, the microstructure are becoming even coarser. The same interconnecting lines of silicon can still be seen. Some particles have grown very large due to the elevated temperatures further down. Many particles are around 100 μm in diameter and can actually be seen with the bare eye in figure 5.6c. The scaly structure surrounding these large particles is probably condensate depleted on silicon. An EPMA map in fig. 4.4 which is taken from position 9 shows an silicon stream running into a large silicon droplet.

The image analysis made on the condensate revealed that the silicon content decreased when going down in the furnace. The values for silicon content as a funtion of sample position can be seen in figure 4.18. Sample 3 and 12 can be considered to be outliers, since they strongly differs from the overall falling trend. Variations from area to area can strongly affect the measured silicon content, but all images used in the analysis were taken from homogeneous areas to avoid this. Theoretically, the silicon content in a freshly depositet layer of brown condensate would be: $\frac{\rho_{Si}}{\rho_{Si}+\rho_{SiO_2}} = \frac{2.3g/cm^2}{2.3g/cm^2+2.6g/cm^2} = 47\%$. All sample positions gave silicon content lower than this. This may indicate that the silicon content measured is lower than the real silicon content in the condensate. One would believe that the silicon in condensate from position 1 was relatively close to 47%, but the measured value was 34%. The exposure to relatively high temperatures may explain why the silicon content was lower. The heat treatment may have caused silicon to escape from the condensate, and falling back down in the furnace. An other possibility to these low values are the experimental part. The sensitivity of the image analysis tool is crucial for the results, and may be a significant element of uncertainty.

The industrial excavation at Finnfjord AS (Tranell et al. 2010), found an almost pure silicon phase 40 cm below the charge top in the furnace. Tranell et al. were intrigued by finding silicon this high up in

the furnace. The origin of this might have been due to the condensation reaction or due to elevated temperatures higher up in the furnace due to relative high power input. Perspiration of silicon from the condensate is a interesting mechanism, and may contribute significantly to the overall production if silicon in a furnace. Silicon droplets could be seen in the pale brown condensate with the bare eye as high as position 5 in the pilot scale furnace. This silicon may have been produced by silicon perspiring from the condensate, since the droplets were found inside the condensate structure. The more well known Si producing mechanism is reaction 4: $SiO(g) + SiC(s) = 2Si(s,l) + CO(g)$ which will be discussed in the following section.

5.5 From carbon to silicon in the pilot scale experiment

The SEM-images representing the carbon materials way to silicon in the pilot furnace can be seen in section 4.1.3. Beginning from the top of the furnace, in sample position 1 to 4 (fig. 4.1), the carbon particles have reacted with the SiO gas and started to form SiC according to reaction 6: $SiO(g) + 2C(s) = SiC(s) + CO(g)$. The EPMA map in fig. 4.3 is showing this reaction unfolded in sample position 2. SiC have been formed in the channels of the carbon particle, which is most likely coke. Coke was the main carbon source for the pilot scale experiment, but som woodcips were also added to increase the permeability of the charge. Condensate was engulfing the particle, restricting more SiO gas to react with the carbon surface. Since SiC have been formed inside the particle before the condensate have had the oppurtunity to deposit, it is reasonable to believe that reaction 6 will go faster than the condensation reaction (-3): $2SiO(g) = SiO_2(s,l) + Si(s,l)$, at least in this case at position 2 in the furnace. This can also be supported by the stability diagram in fig. 2.2 where it is easy to see that reaction 6 will have the larger driving force than -3 at the same temperature.

Going further down, inside the cavity wall of the furnace, there is evidence of silicon as high as in position 5. This silicon is found as a small cluster inside the structure of C and SiC. This has most likely been produced through reaction 4: $SiO(g) + SiC(s) = 2Si(s,l) + CO(g)$. In position 6 the SiC is concentrated in the edges of the former carbon structure and no Si was found here. The SiC is dominating the area in position 7, but in position 8 almost half the area has been converted to silicon metal. The rate reaction 4 seem to speed up significantly at this point. Some other metal can also be seen in sample 8, most likely iron. In position 9, 10 and 11 the fraction of silicon is ever more increasing, eating up the SiC. In sample 12 the particle is almost completely converted to silicon metal. The iron phases are also becoming more visible and have probably been segragated from the silicon during solidification.

It was also interesting to see that the consumption of carbon in the particles did not necessarily follow the unreacted core model. In the unreacted core model, a core of carbon will be left while the outer part of the particle will become converted to SiC. This model is good theoretical assumption, but does not seem to apply for the randomness inside the silicon furnace. The pores inside the carbon particles will greatly increase the reaction rate with the SiO gas. There was also evidence of the particle being consumed from one side to the other. This can partly be seen in the EPMA map in fig. 4.5, where the reaction border of silicon and SiC was moving upwards (in the image) as more and more carbon was consumed. All in all it is very difficult to get a clear image of the process from carbon through SiC to Si, since a lot of areas representing different stages of the process can be found many places in the very same sample. The trend however, is easier to see when comparing samples from the top with those all the way at the bottom.

Below the elecrode the metal bath was found, with samples 12 and 13 representing this area. Two distinct phases dividing the metal bath can be seen in lower part of figure 4.1. Analysis of the metal bath revealed that the upper gray phase was mainly silicon metal with some SiC-particles. This is seen in the analysis of sample 12, while sample 13 which made from the darker gray phase was mainly SiC soaked with some silicon. This is the SiC sponge structure which the pure silicon metal flows through when its tapped.

SiC will be a solid at the temperatures below ~2830 °C and may disturb the flow of metal if the SiC is sufficiently accumulated. The SiC in the light gray phase have probably been solved in the silicon at the high temperatures. During solidification the solubilty of SiC in Si decreases and some SiC will therefore be deposited.

The phase diagram in figure 5.7 shows the solubilty of carbon in silicon. The deposition of these SiC particles at lower tremperatures may hinder the tapping. The border between the metal phases are radially aligned relative to the electrode tip. Decreased temperature with distance from the electrode, must have caused the SiC to deposit from the silicon metal. The low density of silicon (ρ_{Si} =2.3 g/cm^3) compared to SiC (ρ_{SiC} =3.2 g/cm^3)(Aylward & Findlay 2002), will force the silicon upwards relative to the SiC. The deposition of SiC at lower temperatures and the density difference will form this SiC sponge. Severe deposition of SiC may obstruct the taphole and thus complicate the tapping process.

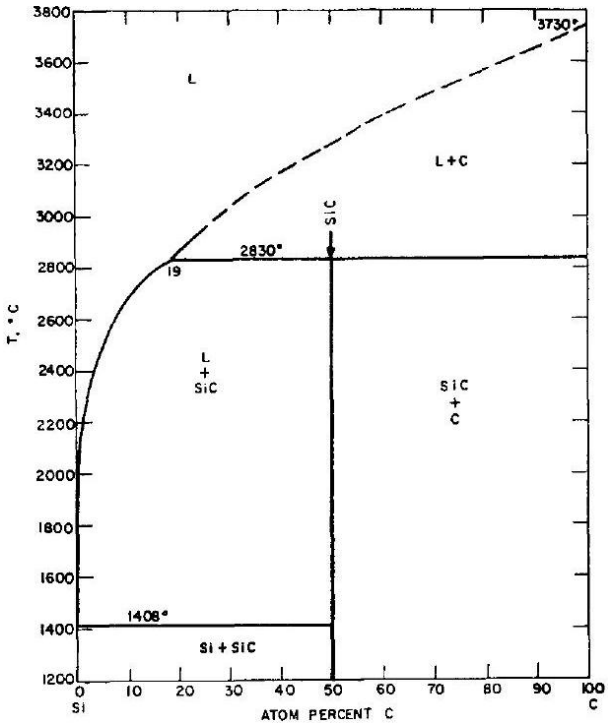

Figure 5.7: The phase diagram Si-C. (Scace & Slack 1959)

5.6 Description of the zones in the pilot scale furnace

There are some well defined zones in the pilot scale furnace and these are be graphically presented in figure 5.8. This cross-section shows the furnace right before it is ripe for stoking. The area above the cavity, is marked in the figure as zone 1. When the charge beneath this zone has been consumed, this upper part of the charge burden is broken down. This happens industrially every 30-75 minute, but the average stoking cycle for this pilot scale was 200 minutes. The material in this zone will then have been static for a while before it is sent downwards in the furnace to be consumed.

When the furnace is stoked, the cavity will be filled up, and the reactions will start to go. A crust will form due to the condensation of the SiO gas in the upper part, creating a new cavity roof. The consumption will proceed around the electrode, while material will melt and fall towards this hot zone. The dynamic of this process will probably be a lot like Vangskåsen (2011*b*) described in figure 2.12. The area of zone 3 will decrease in the direction of the arrow as shown in figure 5.8, as the consumption takes place. The last part of zone 3 will flow towards the hot zone.

Zone 2 represents a relatively inactive part of the furnace. SiO gas will condense in these cooler parts, and if the temperature is lower than normal, this zone may increase due to the sintering of the charge. This process is often called crust formation and can make the stoking of the furnace very difficult. The sintered mass of quartz, carbon and condensate (Si+SiO_2) is a hard mixture which and will be discussed in the next section. It is desired to avoid the crust formation, since the crust can decrease the ring shaped opening around the electrode (seen from above). Occasionally, this opening can become narrow and cause operational problems. If the crust formation gets good conditions, it will grow at the expense of zone 3, reducing the effective reaction volume in the furnace, also reducing the efficiency of the furnace.

The metal produced will end up in zone 4. Silicon will float above the sponge-like structure of SiC, since Si metal is less dense and the SiC is deposited at lower temperatures further down in the furnace.

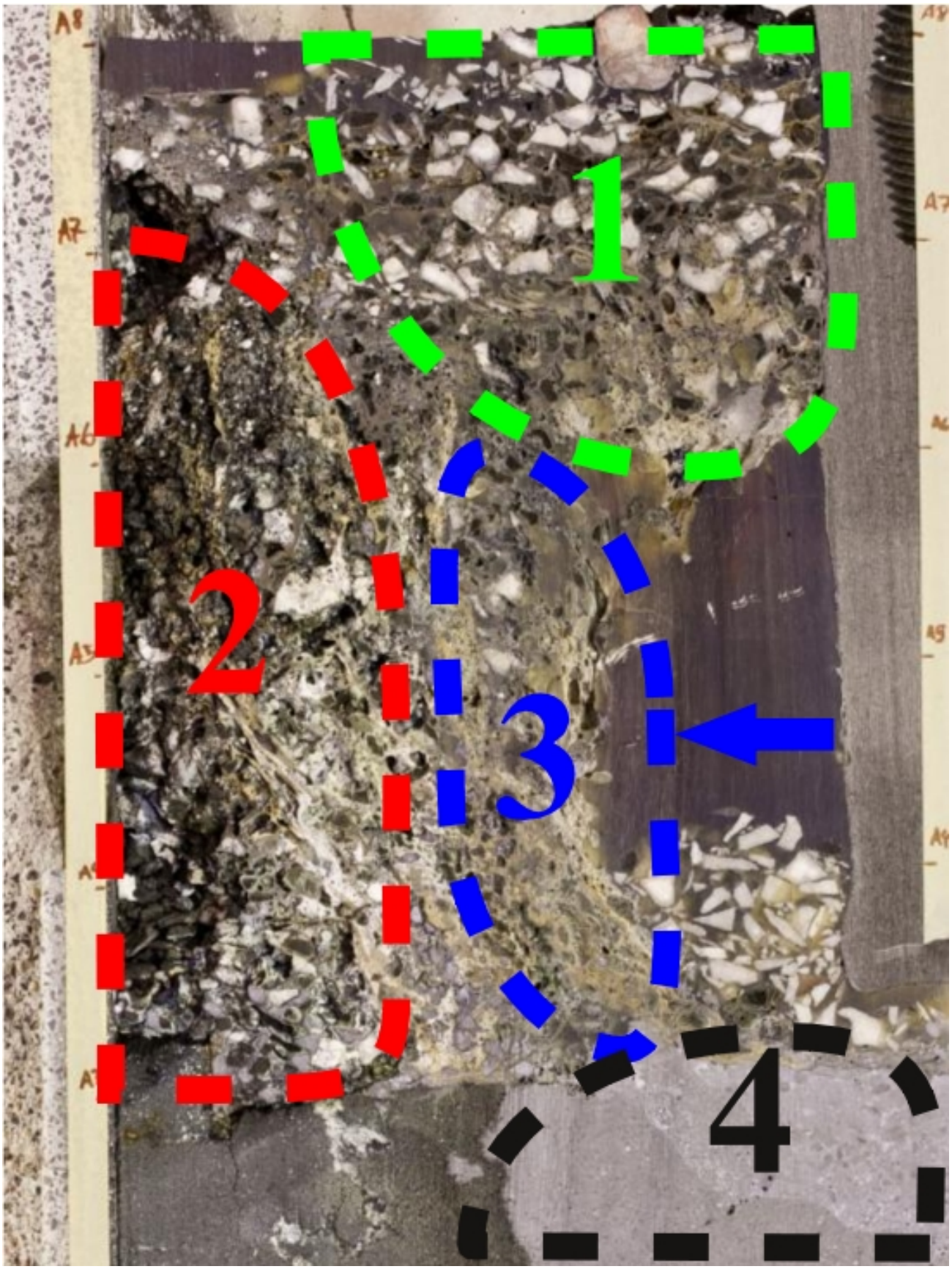

Figure 5.8: Reaction zones in the pilot scale furnace. 1: Periodically stoked zone (cavity roof). 2: Inactive crust formation zone. 3: Slow-flowing zone. 4: Metal bath.

5.7 Mechanical strength of cavity roof

The cavity roof is defined to be material in a silicon furnace which holds the upper part of the charge suspended over the cavity. The cavity roof consists of a sintered mixture of quartz (melted or not melted), carbon particles (coke, coal, charcoal or woodchips partially converted to SiC) and condensate (SiO_2+Si). The condensate is probably the main contributor to the strength of this cavity roof, but evidence is necesarry to prove this. No previous data can be found on the mechanical strength of the matter above the cavity inside a silicon furnace.

Schei et al. (2000) described the crust formation as a problem in the metallurgical silicon process. Normally the upper parts of the charge can be broken down during stoking. But if stoking have been carried out incompletely in the past, condensate may have been allowed to grow and sinter the charge together. The charge closest to the furnace walls will be sintered first since charge consumption is highest around the electrode. This will make stoking more difficult since this sintered mass of condensate and viscous silica is difficult to break. As this vicious circle continues, the passive volume of sintered mass will increase towards the electrode and decrease the charge permeability as well.

For very strong crusts blasting with explosives has been carried out to break them (Schei et al. 2000), and this is as an indication of the strength of this sintered mixture.

From the compression tests made on the material above the cavity in IF75 experiment number 5, some conclusions could be made. A summary of the compression reults are shown in table 5.3. For instance, samples experiencing temperatures above 1670 °C had significantly lower strength than the samples from cooler areas. This is probably due to the softening of silica. The silica from these samples was very porous and had a characteristic "melted look". As discussed in section 5.3 the melting of this quartz occur around 1680 °C.

For the samples exposed to temperatures below 1670 °C, the compressive strength was approximately doubled, and even matched the rough values estimated for the pure pieces of quartz rock. The strength of these samples were most likely provided by the condensate sticking the solid particles together.

Interestingly, the compression strength values were all higher than commercial grade portland cement concrete. These values should probably not be directly compared to each other, but they are giving an impression of the potential strength of the cavity roof. Experimental setup and the relatively small samples used for the compression tests may induce a high level of uncertainty.

Table 5.3: Maximum compressive strength for the samples from the IF75 experiments.

Temperature exposure	>1670 °C	~1670 °C	<1670 °C	Quartz reference, RT	Portland cement
Compressive strength (MPa)	~115	~221	~396	~249	~40 (PCA 2012)

5.8 Experimental setup

Some issues were observed with the thermocouples during the IF75 experiments, but not as bad as the author's previous experiences. Type C thermocouple is not designed for oxidizong atmospheres at high temperatures. A graphite tube was protecting the thermocouple and this worked well up to temperatures ∼1980 °C. Around this point, the metal sheet surrounding the thermocouple wires will melt. The thermocouple will then become stuck inside the graphite tube due to solidification at the walls, making it useless for later experiments. The thermocouple may still give the correct signal, but it becomes very vulnerable without the protective sheet. Exceeding 2000 °C is very risky since the probabilty of failure of the thermocouple is very high. Since the reactions inside the furnace for the silicon process is extremely endothermic at these temperatures, it is not easy to exceed 2000 °C in a controlled manner. But when the charge suddenly have been consumed, the heat consumption is gone, and the temperature can suddenly surpass 2000 °C and go even further. This is a very efficient way to kill a thermocouple.

The measuring incertainty for the thermocouple was listed to be 1% up to 2320 °C. A reasonable assumption for incertainty during the experiments would be like ±10 °C.

Chapter 6

Conclusions

Investigation of the small scale induction furnace experiments have shown that the material consumption (SiO_2+SiC) was very low for temperatures below 1820 °C as no SiO gas was produced. At 1900 °C, 9.6 % of the initial charge mass had been consumed. The consumption increased to 13.8 % when the temperature was raised to 1980 °C. A small increase from 1980 °C to 2000 ° had a great effect on the rate of consumption since the consumption increased (15.0 %) and the power consumption decreased. High consumption of the charge gave high production of SiO gas, which in turn deposited into large amounts of condensate (SiO_2+Si)

A typical experiment conducted in the induction furnace (holding temperature = 1980 °C) had a specific power consumption of roughly 62 MWh per ton silicon produced, far more than normal industrial power consumption of 11-13 MWh per ton Si produced. Mass balance demonstrated that just over half of the silicon produced were left in the silicon pool in the bottom of the crucible. ∼44% of the total amount silicon produced had to end up as Si-particles in the condensate deposited in the upper portion of the crucible.

Brown condensate exposed to temperatures above 1680 °C began to decompose and eventually changed color to pale brown and white. The microstructure became coarser and the relative amount of silicon within the condensate dropped as the temperature increased. The silicon in the condensate accumulated and separated from the SiO_2-matrix. Separation of silicon from the condensate is expected to play a signinficant role of the total production of silicon. Further investigation should be carried out to determine the proportion of silicon produced through this mechanism.

Deposition of condensate caused the charge to agglomerate which makes stoking difficult. Compression tests made on this agglomerated material exposed to different temperatures gave the following results:

Temperature exposure	Compressive strength (MPa)
>1670 °C	∼115
∼1670 °C	∼221
<1670 °C	∼396

Chapter 7

Further work

The following topics could be area for further investigation:

- Quantify the amount of silicon produced through melting of condensate. This can be done by producing large deposits of condensate at some inert surface, which then is heated to temperatures above 1700°C.
- Investigate the kinetics of the various reactions in the silicon process.

Bibliography

Andersen, V. (2010), Reaction mechanism and kinetics of the high temperature reactions in the silicon process, Master's thesis, NTNU.

Aylward, G. & Findlay, T. (2002), *SI Chemical Data*, Wiley.

Grådahl, S., Johansen, S. T., Ravary, B., Andresen, B. & Tveit, H. (2007), 'Reduction of emmisions from ferroalloy furnaces', *INFACON 11, New Dehli, India 2007* .

Hjartarson, H. (2009), Waste heat utilization at elkem ferrosilicon plant in iceland, Master's thesis, University of Iceland.

Hjelen, J. (1989), *Scanning elektron-mikroskopi*, NTH.

HSC (2012), 'Hsc chemistry 6.1'.

Kamfjord, N. E., Tveit, H. & Solheim, I. (2012), 'Pilot scale measurements of no-emissions from the silicon process', *TMS 2012, 3rd International Symposium on High-Temperature Metallurgical Processing* .

Kvande, R. (2008), 'Trial lecture, phd dissertation, ntnu, trondheim, norway'. Not published.

Mølnås, H. (2010), Investigation of sio-condensate formation in the silicon process, Project report in subject tmt 4500, NTNU.

PCA (2012), 'Portland cement association - cement basics'.
URL: *www.cement.org*

Ringdalen, E. & Tangstad, M. (2012), 'Reaction mechanisms in carbothermic production of silicon, study of selected reactions', *TMS 2012, International Smelting Technology Symposium* .

Scace, R. I. & Slack, G. A. (1959), 'Solubility of carbon in silicon and germanium', *The journal of chemical physics* **30**.

Schei, A., Tuset, J. & Tveit, H. (2000), *Production of High Silicon Alloys*, Tapir.

Solheim, I., Jensen, R. & Kamfjord, N. E. (2012), 'Equipment for pilot scale experiments of nox-emissions from the silicon process', *TMS 2012, 3rd International Symposium on High-Temperature Metallurgical Processing* .

Tangstad, M. & Ksiazek, M. (2010), Investigation of white and brown condensate, Technical report, SINTEF.

Tangstad, M., Ksiazek, M., Andersen, V. & Ringdalen, E. (2010), 'Small scale laboratory experiments simulating an industrial si furnace', *INFACON 12, Helsinki, Finland 2010* .

Tranell, G., Andersson, M., Ringdalen, E., Ostrovski, O. & Steinmo, J. J. (2010), 'Reaction zones in a fesi 75 furnace - results from an industrial excavation', *INFACON 12, Helsinki, Finland 2010* .

Vangskåsen, J. (2011*a*), Condensate formation in the silicon process, Student report resina project, NTNU.

Vangskåsen, J. (2011*b*), Investigation of the cavity formation in the silicon process, Student report resina project, NTNU.

Vangskåsen, J. & Høgsand, O. (2011), Investigation of cavity and condensate formation in the silicon process, Student report resina project, NTNU.

Appendix A

Inductotherm 75kW furnace (IF75). VIP POWER-TRAK

Operating procedure

- Preparation of the melt/crucible: If you want to go to temperatures above 1600 °C, use of graphite insulation around the crucible is recuired. This is to protect the furnace lining.
- Get protection clothes, fire resistant clothes are in the wardrobe.
- On the HSE boards outside on each door: Note date, name, number and special risks (if using flammable gas for example).
- Make sure the furnace is intact, clean and visually inspect the furnace hole.

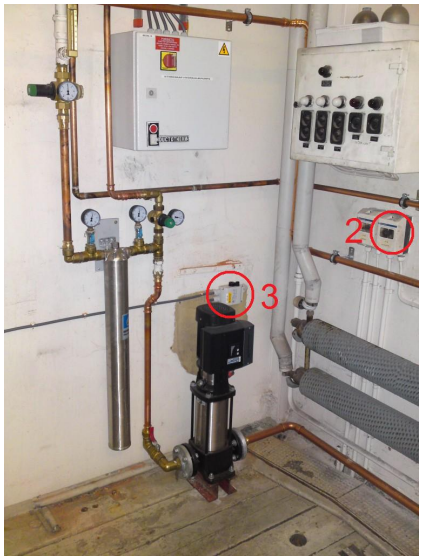

- Start of the unit:
    1. Turn on the warning light.
    2. Turn on the ventilation.
    3. Start the water pump (turn switch to left position).
    4. Open the furnace water inlet.

5. Switch on "Tilleggstrom".
6. When you hear a click, turn on the main power switch.
7. On the left hand side of the VIP, press the reset button on the black panel. The probe switch should be on "NORMAL", otherwise the furnace will not start.
8. On the right hand side of the VIP, make sure that the power wheel is on the lowest level.
9. Press the "STOPP/RESET" button.
10. Press the "START" button.
11. Increase the effect by using the power wheel.

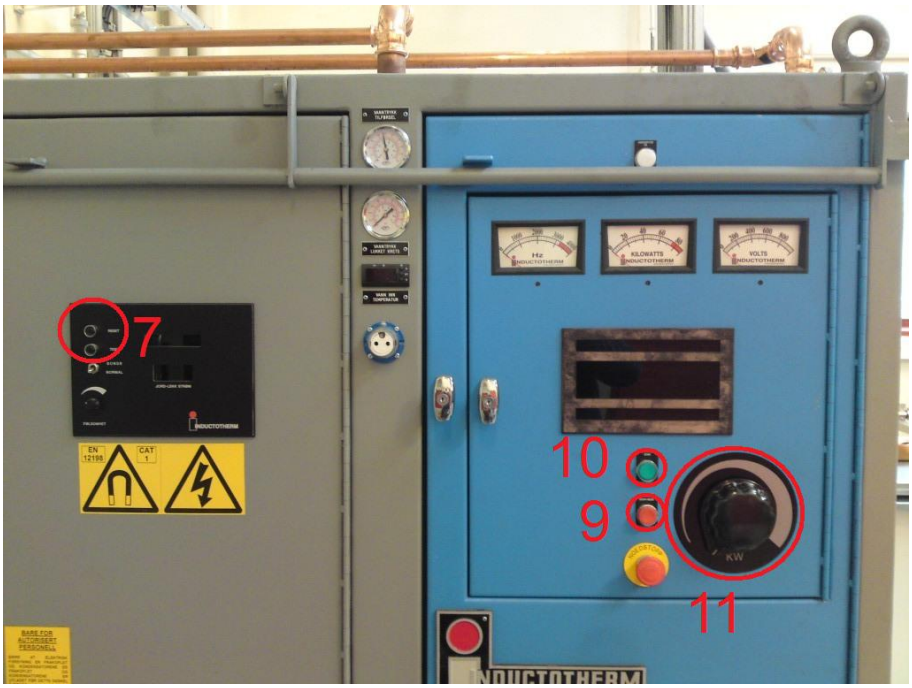

- Emergency stop:
  - There are two emergency interrupts on the furnace. One at the VIP panel, and one above the hydraulic pump for the tilting mechanism.
- Stop of the unit:
  1. Decrease the power to minimum.
  2. Press the "STOPP/RESET" button.
  3. Turn off main power switch (6).
  4. Turn off "Tilleggstrom" (5)
  5. Leave the warning light on as long as the casted metal or crucible is glowing hot. Put on the "hot" sign.
  6. Let the water run for at least three hours after the experiment. Then turn off (4) and (3).

Appendix B

Type C thermocouple

For C-type thermocouples the temperature (T) can be obtained from the potential-readings (E) using Hart Scientific readouts, model 1529. Temperatures are calculated from the conversion formula, with according constants shown in table B.1.

Conversion formula:	$T = \sum_{i=0}^{n}(C_i \cdot E_i)$

Table B.1: W5Re/W26Re thermocouple coefficients for Hart 1529.

Min T	0°C	631°C
Max T	631°C	2315°C
Std err	0.04°C	0.30°C
mV (25°C)	0.342	0.342
C0	0	411.025
C1	74.411468	-61.463789
C2	-4.5680255	14.651879
C3	0.60972079	-0.99683382
C4	-0.05588838	0.037141869
C5	0.002964559	-0.00070836
C6	-0.000065745	0.00000550127